Leibniz
Universität
Hannover

Function and Regulation of the Murine T-Box Genes *Tbx15* and *Tbx18*

Von der Naturwissenschaftlichen Fakultät
der Gottfried Wilhelm Leibniz Universität Hannover
zur Erlangung des Grades eines
Doktors der Naturwissenschaften
Dr. rer. nat.
genehmigte Dissertation
von Dipl.-Biol. Henner Farin
geboren am 26.09.1978, in Nordhorn

2009

Erstprüfer: Professor Dr. Andreas Kispert

Zweitprüfer: Frau Professor Dr. Rita Gerardy-Schahn

Drittprüfer: Professor Dr. Anaclet Ngezahayo

Tag der Promotion: 18.06.2009

Angefertigt am
Institut für Molekularbiologie
der Medizinischen Hochschule Hannover
unter der Betreuung von
Prof. Dr. A. Kispert

Meinen Eltern
und Jana.

Table of Contents

		Page
Summary		5
Zusammenfassung		6
Keywords		7
Introduction		8
Aim of this thesis		11
Part 1	“Transcriptional Repression by the T-Box Proteins Tbx18 and Tbx15 Depends on Groucho Corepressors”, Running title: **Repression by Tbx15 and Tbx18**	13
Part 2	“T-Box Protein Tbx18 Interacts with the Paired Box Protein Pax3 in the Development of the Paraxial Mesoderm”, Running title: **Tbx18 and Pax3 in somitogenesis**	26
Part 3	“TBX15 Mutations Cause Craniofacial Dysmorphism, Hypoplasia of Scapula and Pelvis, and Short Stature in Cousin Syndrome”, Running title: ***TBX15* mutations cause Cousin Syndrome**	36
Part 4	“Proximal-Distal Compartmentalization of the Developing Limb Bud by T-Box Transcription Factors Tbx15 and Tbx18 is Prerequisite for Formation of Stylopod and Zeugopod”, Running title: **Tbx15 and Tbx18 in limb development**	44
Concluding remarks		90
References		92
Acknowledgements		94
Curriculum vitae		96
Declaration		97

Tbx15 and *Tbx18* encode a closely related pair of T-box transcription factors that are characterized by a conserved DNA binding domain, the T-box. Loss-of-function studies in the mouse have revealed a critical requirement of Tbx15 and Tbx18 during the development of various organs. The molecular mechanisms, however that underlie the mutant phenotypes are poorly understood. The aim of this thesis was to gain insight into the embryological roles of Tbx15 and Tbx18 by a comprehensive biochemical and genetic analysis.

Biochemical analyses *in vitro* identified protein motives necessary for nuclear localization and co-repressor binding. Tbx18 repressed known T-box response promoters in a groucho-dependent manner by competition with activating members of the T-box family. This was exemplified by the competition of Tbx6-mediated activation of the *Delta-like 1* (*Dll1*) gene by Tbx18 that confers restriction of *Dll1*-expression to the posterior somite compartment.

Efficient DNA-binding of Tbx15/18 *in vitro* requires dimerization or the association with other classes of specific transcription factors. The paired type homeobox transcription factor Pax3 was identified as a novel protein interaction partner of Tbx15 and Tbx18 and co-operative functions during skeletal development were demonstrated by genetic interaction between mutant alleles of *Pax3* and *Tbx15/18 in vivo*.

The important function of Tbx15 for skeletal development is conserved in humans. In collaboration with a clinical research group this work contributed to the finding that the ‘Cousin syndrome’ is caused by mutations of the human *TBX15* gene.

Tbx15 and *Tbx18* are co-expressed in the early limb bud mesenchyme but loss of either gene alone does not cause major limb defects. Since both proteins share biochemical properties, redundancy may underlie this finding. Analysis of double mutant embryos indeed revealed a critical but redundant function of Tbx15 and Tbx18 in the generation of proximal (stylopod and zeugopod), while the distal skeletal elements (autopod) were unaffected. Tbx15/18 function controls a cellular adhesion/repulsion program that generates a proximal tissue compartment in the early limb bud mesenchyme. Eph/Ephrin molecules were identified as potential downstream mediators of Tbx15/18. Organ culture experiments uncovered regulatory mechanisms for restricted expression of *Tbx15/18* in the limb bud mesenchyme. In addition, using gain-of-function experiments it was possible to show that Tbx18 regulates a transcriptional repression program that is also sufficient to specify proximal limb identity.

Taken together, this study sheds new light on how tissue complexity is achieved during vertebrate development and substantially broadens our understanding of the molecular and cellular function of Tbx15 and Tbx18.

Tbx15 und *Tbx18* kodieren für zwei nahe verwandte Transkriptionsfaktoren der T-Box Familie, deren Mitglieder sich durch eine konservierte DNA-bindende Domäne (T-Box) auszeichnen. Verlustmutationen in der Maus belegten wichtige Funktionen von Tbx15 und Tbx18 in zahlreichen Entwicklungsprozessen. Molekulare Mechanismen, welche diese Phänotypen hinreichend erklären, waren bisher aber unbekannt. Ziel dieser Arbeit war deshalb, durch eine umfassende molekulare Charakterisierung, neue Einblicke in die Funktion beider Proteine zu gewinnen.

In biochemischen Experimenten konnten nukleäre Lokalisationssequenzen kartiert und funktionell charakterisiert werden. Die Existenz eines Korepressor-Bindungsmotivs wurde aufgezeigt, und die Bindung an groucho-Proteine und deren funktionelle Bedeutung für die Transkription geklärt. Tbx18 vermittelt die Repression von bekannten, T-Box abhängigen Promotoren durch Kompetition mit aktivierenden Mitgliedern der T-Box Familie. Kompetition mit Tbx6 um T-Box Bindelemente im *Delta-like 1* (*Dll1*)-Promotor wurde als Tbx18-abhängiger Mechanismus erkannt, die *Dll1*-Expression auf posteriore Somitenhälften zu beschränken. Protein-Interaktionen spielen für eine effiziente DNA-Bindung von Tbx15 und Tbx18 eine wichtige Rolle. Der paired-Typ Transkriptionsfaktor Pax3 wurde als neuer Bindungspartner von Tbx15/18 identifiziert. Genetische Interaktionsstudien konnte eine kooperative Funktion von Tbx15/18 und Pax3 in der Somitogenese und der Gliedmaßenentwicklung bestätigen.

In Zusammenarbeit mit einer klinischen Forschergruppe wurden Punktmutationen des humanen *TBX15* Gens als Auslöser des "Cousin-Syndroms" identifiziert und somit eine konservierte Funktion während der Skelettentwicklung belegt.

Während der Gliedmaßenentwicklung werden *Tbx15* und *Tbx18* in der proximalen Region der Gliedmaßenknospe koexprimiert, Einzelmutanten beider Gene weisen jedoch keine Gliedmassendefekte auf. Durch Analyse von *Tbx15/18* doppelmutanten Embryonen wurde eine essentielle redundante Funktion der beiden Proteine in der Entwicklung des proximalen Gliedmassenskeletts (Stylopod und Zeugopod) festgestellt, was in der Folge auf eine fehlerhafte Kompartimentierung der frühen Gliedmassenknospe zurückgeführt wurde. Dabei regulieren Tbx15 und Tbx18 ein zelluläres Adhäsionsprogramm, möglicherweise durch die Kontrolle der Expression des Ephrin-Signalsystems. Regulatorische Aspekte der *Tbx15/18* Expression wurden untersucht und Signale zur Etablierung dieses bisher unbekannten Zellkompartiments ermittelt. Schließlich konnte durch Missexpressions-Experimente gezeigt werden, dass Tbx18 nicht nur notwendig sondern auch hinreichend für die Spezifizierung der proximalen Zellidentität ist und *in vivo* eine Repressor-Funktion besitzt.

Die vorliegende Arbeit liefert somit neue Erkenntnisse zu Musterungsprozessen während der Organentwicklung und stellt einen wichtigen Beitrag zum Verständnis der molekularen und zellulären Funktion von Tbx15 und Tbx18 dar.

Keywords: Tbx15, Tbx18, mouse development
Schlagworte: Tbx15, Tbx18, Mausentwicklung

Introduction

Embryogenesis is a fascinating process that leads to the formation of a complex organism from a single cell, the fertilized oocyte. As an important mechanism to achieve tissue diversity, transcriptional regulation initiates diverse gene expression programs that allow the differentiation of distinct cell types.

T-box (*Tbx*) genes encode a multi-gene family of transcription factors that are involved in numerous developmental processes. Exhaustive searches have identified T-box genes in all metazoa ranging from hydra to man. The unifying feature of all family members is the highly conserved T-box, a region of 180 amino acid residues that confers specific DNA binding to conserved DNA-motifs, the T-box binding element (TBE), also known as T-half site. These elements are based on the consensus sequence 5'-AGGTGTGA-3' that was initially identified *in vitro* as binding site for Brachyury (T), the founding member of this gene family (1).

Among different T-box proteins considerable sequence diversity is found outside the T-box region, which reflects distinct molecular properties. Depending on the presence of activator or repressor domains, T-box proteins can differentially modulate target gene expression (2,3,4). In some cases it was found that the transcriptional role of T-box proteins also depends on the cellular and the promoter context (3,5). To date, a limited number of direct transcriptional target genes are known that preferentially contain several T-half sites in their upstream regulatory sequences, indicating that target selectivity is achieved by cooperative DNA binding (6-10). Furthermore, members of other transcription factor families have been recognized as T-box protein binding partners, which may also be involved in the generation of promoter specificity (11-15).

The vast majority of T-box genes studied to date exhibit highly specific expression patterns during development. Loss-of-function studies in the mouse but also in other model organisms have revealed functional requirements of T-box genes in a diverse array of developmental processes, including formation and patterning of the mesoderm and organogenesis (for a review 16). Notably, mutations in a number of T-box genes have been identified as underlying causes for human congenital disorders (17), illustrating the importance of this gene family in development and disease.

Mammalian genomes are known to harbor 17 family members that have been divided in five major subfamilies based on sequence conservation of the T-box. Focus of this study is *Tbx15* and *Tbx18*, a closely related pair of T-box genes that together with *Tbx22* form a subgroup of the *Tbx1* subfamily in vertebrates. During mouse development *Tbx18* expression is confined to anterior somite halves, pro-epicardial and epicardial cells, and the mesenchyme of the limb bud and the septum transversum (18). Additional expression domains include the mesenchymal precursor cells of the ureter and the otic fibrocytes (19,20).

Mice carrying a null allele of *Tbx18* die shortly after birth due to severe malformations of the axial skeleton, a phenotype that was traced back to the function of *Tbx18* in somitogenesis (21). During this process epithelial somites are generated as segmental units on both sides of the neural tube from the unsegmented paraxial mesoderm, also known as presomitic mesoderm. During development new somites are added posteriorly in a continuous manner, while the more mature somites start to differentiate into sclerotome and dermomyotome, which contain the precursors of the axial skeleton, and of muscles and dermis, respectively. Coupled to the process of segmentation, each somite becomes subdivided into a distinct anterior and posterior compartment, a process that is orchestrated by the interplay of Notch-signaling and the transcription factor Mesp2 in the anterior presomitic mesoderm (22,23). Somitic anterior-posterior polarity is required for the metameric structure of the axial skeleton since both somite halves differentially contribute to the axial skeleton. Cell fate mapping studies in the chick have shown that the vertebral pedicles and proximal ribs are exclusively formed by the posterior somite half, whereas the vertebral bodies, laminae with the spinal processes, the rib heads, and the distal ribs derive from both somite halves (24). *Tbx18*$^{-/-}$ mutants display multiple fusions of pedicles and proximal ribs. By analysis of *Uncx4.1* expression, that marks the posterior somite compartment (25), it was shown that loss of anterior *Tbx18* expression is accompanied with a progressive expansion of posterior somite identity, demonstrating that Tbx18 has a function in maintaining the anterior somite compartment. Interestingly, the homozygous loss of *Uncx4.1* causes an opposite phenotype characterized by ectopic *Tbx18* expression and a loss of skeletal structures derived from posterior somite halves (21,26). Misexpression experiments further demonstrated that Tbx18 is sufficient to confer anterior somite identity (21). These studies, thus, revealed a genetic circuit of two transcription factors, Tbx18 and Uncx4.1 that control the maintenance of anterior and posterior somite compartments in a mutually antagonistic fashion.

Additionally, Tbx18 plays an important role in a compartmentalization process during inner ear development (20). It was found that *Tbx18* expression in the inner region of the otic mesenchyme is required for the correct subdivision of the otic mesenchyme in an inner region of prospective otic fibrocytes and the surrounding precursors of the otic capsule. Loss of *Tbx18* resulted in a disturbed boundary between both compartments and was associated with a defective differentiation of otic fibrocytes. Otic fibrocytes failed to condense at the lateral side of the cochlear duct, which resulted in a disrupted formation of the stria vascularis, phenotypes that collectively caused deafness of *Tbx18* mutant mice (20).

Another patterning process that was shown to require Tbx18 function is the development of the ureter (19). The epithelium of ureter derives from an outgrowth of the Wolffian duct at the hindlimb level, known as ureteric bud. Guided by signals from the flanking metanephric mesenchyme the ureteric bud elongates and initiates branching morphogenesis at its proximal end. Branching, in concert with the induction of nephrogenesis in the metanephric mesenchyme, leads to the formation of the kidney. In the distal region of the ureteric bud branching morphogenesis is inhibited. The epithelium instead acquires a mesenchymal coating by condensation of periureteric cells that express *Tbx18*. Subsequently, mesenchymal and epithelial differentiation generates smooth muscle cells and the highly specialized 'urothelium', respectively, that together are required for the appropriate drainage of urine from the kidneys into the bladder. Phenotypic analysis of *Tbx18*-deficient mice revealed that periureteric cells dislocalize to the kidney surface instead of covering the ureter stalk. This defect was accompanied by disrupted smooth muscle differentiation and secondarily also resulted in defective differentiation of the urothelium. Failure in drainage of the urine then caused the emergence of hydroureter and hydronephrosis. Phenotypic analysis thus revealed a primary requirement for *Tbx18* in condensation of the periureteric mesenchyme.

During heart development *Tbx18* expression in the septum transversum region defines a mesenchymal precursor population of cardiomyocytes that later surround the sinus horns, which are the myocardial parts of the caval veins. Very similar to the defects during ureter development, *Tbx18* mutant embryos showed a defective recruitment of mesenchymal precursors that resulted in a failure of myocardial differentiation of the sinus horns (27).

Tbx15 (also known as Tbx8 or Tbx14) is the closest relative of Tbx18, as witnessed by more than 84% identity (87% similarity) of the amino acid sequences within the T-domain. The overall protein identity is 55% (67% similarity) and only extends to relatively short protein stretches outside the T-box region. Expression of *Tbx15* has been reported in mesenchymal cells of the craniofacial region, cartilaginous elements of the axial and appendicular skeleton, the skin, and overlapping with *Tbx18* in the limb bud mesenchyme during mouse development (28,29).

Mice homozygous for a targeted null allele of *Tbx15*, or for the spontaneous mutation *droopy ear*, in which *Tbx15* is deleted, exhibit a general reduction of bone size and show defects in skin pigmentation and craniofacial development (29,30). These studies have revealed a primary function of Tbx15 during dorso-ventral patterning of the mouse coat and endochondral bone formation. Already the cartilaginous preskeleton was reduced in size and mutant embryos showed a transient delay in ossification. Reduced proliferation of prehypertrophic chondrocytes as well as of mesenchymal precursor cells, suggested that Tbx15 plays an important role during skeletal development by controlling the number of mesenchymal precursor cells and chondrocytes (29).

Aims of this thesis

Loss-of-function analyses of *Tbx15* and *Tbx18* in mice and conservation of expression in other vertebrates (31-33) has revealed the importance of this closely related pair of T-box transcription factors in an impressive number of patterning and differentiation processes during vertebrate development (see above). In contrast, our current understanding of the molecular mechanisms underlying these phenotypes is scarce since neither protein interaction partners nor transcriptional targets for either factor have been identified. As a step towards this goal, the objective of my thesis was to study the molecular properties of Tbx15 and Tbx18 at multiple experimental levels.

Starting with a bioinformatic analysis I addressed, if the primary structures of the Tbx15/18 proteins contain motives that can be correlated with a biochemical function. One aim was the identification of nuclear localization signals and protein-protein interaction domains. Candidate motifs were subsequently characterized by deletion analysis in a cellular system. As mentioned above Tbx15/18 target genes are unknown. The characterization of the DNA binding properties of both proteins should therefore provide important insights, how target specificity is achieved. To approach this question, the *in vitro* DNA binding properties of Tbx15/18 were analyzed and compared to other T-box proteins. Furthermore, it is unknown how Tbx15 and Tbx18 proteins influence the transcription process. Using reporter gene assays the effect of Tbx15/18 expression on basal transcription was studied followed by mapping of activator or repressor domains. For other members of the T-box family it was shown that the association with transcription factors of other classes is important to achieve target promoter specificity (see above). Knowledge about protein interaction partners of Tbx15/18 may therefore improve the possibility to predict target genes. To identify potential protein-binding partners a yeast-two-hybrid screen was performed. Functional significance of candidate interactions was subsequently evaluated both *in vitro* in a cellular context as well as *in vivo* in a mouse model.

The development of the vertebrate limb subsequently served as a model system to study the cellular and molecular function of the proteins *in vivo*. Both genes are co-expressed in early limb buds, however *Tbx15* or *Tbx18* single mutants lack major limb defects. To investigate possible redundant functions of both proteins during limb development a double mutant analysis was performed. The resulting phenotypes were characterized on a morphological, cellular and molecular level to integrate the role of Tbx15/18 into known developmental pathways. As a complementary approach conditional misexpression of Tbx18 was initiated. To this end, transgenic mouse lines were generated that allow the induced expression of Tbx18 following cre-mediated recombination in any tissue of choice.

The highly specific expression patterns of *Tbx15* and *Tbx18* during mouse development (18,29) suggested a complex transcriptional regulation of both genes. However, activating or repressing signals that control *Tbx15/18* expression are still unknown. The limb model was used to address this issue, because it provides an accessible system to study gene regulatory aspects *in vitro*. Early limb rudiments were cultured and the influence of adjacent tissues and growth factors on the expression of *Tbx15* and *Tbx18* was studied using RT-PCR and whole mount *in situ* hybridization analyses.

This project thus represents a comprehensive experimental study that was aimed to provide important insights into the function and regulation of *Tbx15* and *Tbx18*.

Transcriptional Repression by the T-Box Proteins Tbx18 and Tbx15 Depends on Groucho Corepressors

Henner F. Farin, Markus Bussen, Martina K. Schmidt, Manvendra K. Singh, Karin Schuster-Gossler and Andreas Kispert[1]

From the Institute for Molecular Biology, Medizinische Hochschule Hannover, 30625 Hannover, Germany

[1] Address correspondence to: Andreas Kispert, Medizinische Hochschule Hannover, Institute for Molecular Biology, OE5250, Carl-Neuberg-Str. 1, D-30625 Hannover, Germany. Tel. +49 511 532 4017; Fax: +49 511 5324283; E-mail: kispert.andreas@mh-hannover.de

Published in The Jounal of Biological Chemistry, 282, NO. 35, pp. 25748 –25759, August 31, 2007.

Reprinted with permission (http://www.jbc.org/misc/Copyright_Permission.shtml).

Transcriptional Repression by the T-box Proteins Tbx18 and Tbx15 Depends on Groucho Corepressors*◆

Received for publication, May 4, 2007, and in revised form, June 21, 2007 Published, JBC Papers in Press, June 21, 2007, DOI 10.1074/jbc.M703724200

Henner F. Farin, Markus Bussen, Martina K. Schmidt, Manvendra K. Singh, Karin Schuster-Gossler, and Andreas Kispert[1]

From the Institute for Molecular Biology, Medizinische Hochschule Hannover, 30625 Hannover, Germany

***Tbox18* (*Tbx18*) and *Tbox15* (*Tbx15*) encode a closely related pair of vertebrate-specific T-box (Tbx) transcription factors. Functional analyses in the mouse have proven the requirement of *Tbx15* in skin and skeletal development and of *Tbx18* in the formation of the vertebral column, the ureter, and the posterior pole of the heart. Despite the accumulation of genetic data concerning the embryological roles of these genes, it is currently unclear how Tbx18 and Tbx15 exert their function on the molecular level. Here, we have initiated a molecular analysis of Tbx18 and Tbx15 proteins and have characterized functional domains for nuclear localization, DNA binding, and transcriptional modulation. We show that both proteins homo- and heterodimerize, bind to various combinations of T half-sites, and repress transcription in a Groucho-dependent manner. Competition with activating T-box proteins may constitute one mode of action as we show that Tbx18 interacts with Gata4 and Nkx2–5 and competes Tbx5-mediated activation of the cardiac Natriuretic peptide precursor type a-promoter and that ectopic expression of Tbx18 down-regulates Tbx6-activated Delta-like 1 expression in the somitic mesoderm *in vivo*.**

T-box (*Tbx*) genes encode a family of transcription factors that regulate a variety of developmental processes. The unifying and designating feature of all family members is a highly conserved region of 180 amino acid residues that confers DNA binding. To date, a limited number of direct target genes are known that all contain one or several T half-sites in their upstream promoter sequences. These elements are based on the consensus sequence 5′-AGGTGTGA-3′ that was initially identified *in vitro* as a DNA binding site for Brachyury (T), the founder of this gene family (1). Brachyury proteins preferentially bind as dimers to a palindromic repeat of two anti-parallel T half-sites. Orientation and spacing of T half-sites are likely to affect DNA binding of specific T-box proteins (1–3). Target gene specificity is additionally controlled by protein interaction partners. T-box proteins have been shown to bind to several classes of transcription factors including homeodomain and zinc finger proteins conferring synergism in binding to adjacent DNA binding elements (4–10).

Exhaustive searches have identified T-box genes in all metazoa ranging from hydra to humans. Mammalian genomes are known to harbor 17 family members that have been divided into five major subfamilies based on sequence conservation of the T-box. Loss-of-function studies in the mouse have revealed functional requirements of T-box genes in a diverse array of developmental processes in the post-implantation embryo including formation and patterning of the mesoderm and organogenesis (11). Notably, mutations in a number of T-box genes have been identified as underlying causes for human congenital disorders (12).

Tbx18 and *Tbx15* encode a closely related pair of T-box proteins that, together with Tbx22, form a subgroup of the Tbx1 subfamily in vertebrates. Mice carrying a null allele of *Tbx18* die shortly after birth due to severe malformations of the axial skeleton, a phenotype that was traced back to the function of *Tbx18* in maintaining anterior-posterior somite polarity (13). Additionally, *Tbx18* regulates the condensation of mesenchymal cells around the distal ureter stalk. Newborn $Tbx18^{-/-}$ mice display a prominent hydroureter and hydronephrosis phenotype due to the lack of the smooth muscle layer of the ureter (14). Finally, *Tbx18* is essential for the formation of the sinus horns from the mesenchyme of the pericardial wall and for their myocardial differentiation (15).

Mice homozygous for a targeted null allele of *Tbx15* or for the spontaneous mutation *droopy ear*, in which *Tbx15* is deleted, exhibit defects in skin pigmentation and in the skeleton. These phenotypic changes reveal a role for *Tbx15* in dorso-ventral patterning of the mouse coat and in mesenchymal aggregation that precedes endochondral bone formation (16, 17).

Loss-of-function analyses of *Tbx15* and *Tbx18* in mice and conservation of expression in other vertebrates has revealed the importance of this closely related pair of T-box transcription factors in an impressive number of patterning and differentiation processes during vertebrate development. In contrast, our current understanding of the molecular mechanisms underlying these phenotypes is scarce since neither protein interaction partners nor transcriptional targets for either factor have been identified. As a step toward this goal we initiated a molecular analysis of Tbx18 and Tbx15 proteins. We here characterize the subcellular localization, DNA binding specificities, protein interactions, and transcriptional properties and their structural prerequisites in the two proteins. We provide evidence that com-

---

* This work was supported by a grant from the European Union FP6 contract "HeartRepair" (LSHM-CT-2005-018630), by grants from the German Research Council (DFG) and by the DFG-funded cluster of excellence "REBIRTH." The costs of publication of this article were defrayed in part by the payment of page charges. This article must therefore be hereby marked "*advertisement*" in accordance with 18 U.S.C. Section 1734 solely to indicate this fact.

◆ This article was selected as a Paper of the Week.

[1] To whom correspondence should be addressed: Medizinische Hochschule Hannover, Institute for Molecular Biology, OE5250, Carl-Neuberg-Str. 1, D-30625 Hannover, Germany. Tel.: 49-511-5324017; Fax: 49-511-5324283; E-mail: kispert.andreas@mh-hannover.de.

petition with activating T-box proteins constitutes a possible mode of regulation of the promoters for *Nppa* (natriuretic peptide precursor type a) and *Dll1* (Delta-like 1) *in vitro* and *in vivo*.

EXPERIMENTAL PROCEDURES

Expression Constructs—cDNA fragments encoding full-length Tbx18 and Tbx15 and subregions thereof (see Fig. 1*A*) were PCR-amplified from mouse cDNA AF306666 and NM_009323, respectively. Full-length (aa[2] 1–436) and T-box region (aa 41–225) of Brachyury were amplified from mouse cDNA NM_009309. cDNA fragments encoding full-length protein (aa 1–767) and the WD40 domain (aa 445–767) of human TLE3 were amplified from the human cDNA BC043247 (kind gift from S. Stifani). For *in vitro* expression of proteins, cDNA fragments were cloned with C-terminal myc or HA tags in the vector pSP64 (Promega) that was modified to contain a 5′-β-globin leader and a 3′-β-globin trailer (1). For cytomegalovirus promoter/enhancer-driven expression in cells, the globin leader/cDNA/globin trailer cassette was shuttled into HindIII and EcoRI sites of pcDNA3 (Invitrogen). The Tbx18-VP16 fusion construct was generated by introduction of the Herpes simplex VP16 activator fragment (aa 419–490, kind gift of D. Kessler) in front of the stop codon of Tbx18. GAL4 fusions of Tbx18 and Tbx15 were generated by subcloning the coding sequences into the yeast-two hybrid vector pGBKT7 (Clontech) 3′ of the DNA binding domain of GAL4 (aa 1–147) followed by the SV40 nuclear localization signal (NLS). cDNA fragments encoding GAL4 fusion proteins were released with HindIII (5′) and SalI (3′) and directionally cloned into the HindIII and XhoI sites of pcDNA3. Expression plasmids encoding Gata4.HA, Nkx2–5.FLAG, Tbx5.HA, and Tbx2 cloned into pcDNA3 were a kind gift from V. Christoffels, and expression plasmids pcDNA3.Tbx6, pcDNA3.Tbx6-VP16, pCS2+.Tcf1e, and pCS2+.β-cateninS33A were provided by B. Herrmann and have been described previously (18, 19). Bacterial expression constructs were generated as N-terminal glutathione *S*-transferase (GST) fusions in pGEX-4T3 (Amersham Biosciences). All plasmids were sequenced, and expression was tested on Western blot. Details on cloning strategies and primer sequences are available upon request.

Site-directed mutagenesis was performed as described (20). Mutagenesis primers for the deletion of NLS sequences were 5′-GAGAAGCAGCAACAGCTTCAATTAATCACGGAAGAGGCGGCGGG-3′ (Tbx18) and 5′-GCCTTGATCGGCTCAAATATCGATTGGGAGGAGAAGGGGCTG-3′ (Tbx15), and primers for the generation of point mutants in the eh1 motif were 5′-CTAAGCCTCAAGGCGCACGCATTAATTGTGGAGGCACTGATCGGC-3′ (Tbx18) and 5′-GAGCTCCCGAGCACATGCATTAATCGTTGAAGCCTTGATCGGC-3′ (Tbx15).

Random Binding Site Selection and EMSA—Proteins used for binding site selection and electrophoretic mobility shift assay (EMSA) were generated from pSP64 expression constructs using the SP6-coupled TNT rabbit reticulocyte lysate (Promega) according to the supplier's instructions. The binding site selection was essentially carried out as described (1). After four rounds, the gel-eluted PCR products were subcloned in pBluescript and sequenced. Oligonucleotides used in EMSA were: BS.pF, 5′-GATCCGGTTTCACACCTAGGTGTGAAAGGA-3′; BS.pR, 5′-GATCTCCTTTCACACCTAGGTGTGAAACCG-3′; BS.invF, 5′-GATCCGGAGGTGTGAAATTTCACACCTGGA-3′; BS.invR, 5′-GATCTCCAGGTGTGAAATTTCACACCTCCG-3′; BS.dirF, 5′-GATCCGGAGGTGTGAAGGTGTGAAAGGA-3′; and BS.dirR, 5′-GATCTCCTTTCACACCTTCACACCTCCG-3′. Oligonucleotides were boiled for 5 min and cooled slowly down to room temperature to anneal. Double-stranded fragments were end-labeled with T4-PNK (New England Biolabs) in the presence of [γ-^{32}P]ATP. Binding reactions for gel shift assays contained 2–5 μl of *in vitro* translated myc-tagged protein in a total volume of 20 μl of Nonidet P-40 buffer (5 mM Tris, pH 7.5, 80 mM NaCl, 50 mM NaF, 1 mM $MgCl_2$, 0.1% Nonidet P-40) with 1× Complete protease inhibitor mixture (Roche Applied Science) and 1 μg of double-stranded poly(dI-dC). Reactions were preincubated for 20 min on ice before 10,000 counts of probe were added. For supershift experiments, 1 μl of anti-myc antibody (9E10, Sigma) was added to the lysate. Complexes were allowed to form at room temperature for 20 min, before the reactions were loaded on a native 4% polyacrylamide gel (0.5× Tris-borate-EDTA). Gels were run at 10 V/cm at 4 °C for 5 h before they were dried and exposed to autoradiography film.

Cell Culture, Transient Transfections, and Reporter Assays—HEK293 and HeLa cells were seeded at 20–30% confluency in Dulbecco's modified Eagle's medium supplemented with 10% fetal calf serum, grown overnight, and transfected using the calcium phosphate method. For reporter assays, HeLa cells were seeded in six-well dishes and transfected with constant amounts of reporter plasmids and 25 ng of pCMVβ (Clontech) for normalization. The total amount of expression plasmid was kept constant by adding empty pcDNA3. Per transfection, 250 ng of 5xGAL4$_{UAS}$-tk-luciferase reporter plasmid (a kind gift of J. Milbrandt), 75 ng of pGL3.Nppa-luciferase, containing a 0.7-kb fragment of the mouse *Nppa* promoter (a kind gift of V. Christoffels), or 75 ng of pKS.msd-luciferase (kindly provided by B. Herrmann) was used (18, 19); luciferase and β-galactosidase activities were measured 48 h after transfection. All transfections were performed in duplicates, and experiments were repeated at least three times. After normalization, the mean luciferase activities and standard deviations were plotted as "fold activation" when compared with the empty expression plasmid. *p* values were determined with the Student's *t* test.

Immunofluorescence—Experiments in HEK293 cells were performed according to standard protocols. Primary antibodies used were rat anti-HA (3F10, Roche Applied Science) and mouse anti-myc (9E10, Sigma), both at 1:200 dilutions, and secondary antibodies were donkey anti-rat IgG(H + L) fluorescein isothiocyanate and donkey anti-mouse IgG(H + L) rhodamine (both Dianova), at 1:200 dilutions. Immunofluorescent detection of proteins was repeated at least three times, and representative examples were photographed on a Leica DM5000 microscope with DFC300FX camera (Leica).

---

[2] The abbreviations used are: aa, amino acids; eh1, engrailed homology 1; NLS, nuclear localization sequence; TLE, transducin-like enhancer of split; HA, hemagglutinin; GST, glutathione *S*-transferase; EMSA, electrophoretic mobility shift assay; RT, reverse transcription; CtBP, C-terminal-binding protein; N, N-terminal domain; C, C-terminal domain; T, T-domain.

GST Pulldown and Co-immunoprecipitation Assays—GST and GST-Tbx18 fusion proteins were produced in the *Escherichia coli* strain BL21 and bound to glutathione-Sepharose 4T beads (Amersham Biosciences). HA- or myc-tagged prey proteins were produced in HEK293 cells that were lysed in pull-down buffer (20 mM HEPES, pH 7.9, 100 mM NaCl, 10 mM KCl, 5 mM $MgCl_2$, 0.5 mM EDTA, 5% glycerol, 0.05% Triton X-100, and 1 mM dithiothreitol). The binding reaction was performed as described (21). For co-immunoprecipitation assays, HEK293 cells were seeded in 10-cm dishes and either transfected with myc-tagged expression construct alone or transfected together with a HA-tagged bait construct. After 48 h, cells were lysed in 500 μl of Nonidet P-40 buffer, cellular debris was precipitated by centrifugation for 30 min at 4 °C, and the supernatant was precleared from nonspecific binding by incubation with 25 μl of protein A-agarose (Roche Applied Science). 5 μl of anti-HA antibody and 25 μl of protein A-agarose were added to the supernatant for 2 h at 4 °C, before the beads were washed three times with 500 μl of Nonidet P-40 buffer. Proteins eluted from the beads were analyzed by Western blot with anti-myc and anti-HA antibodies, and 5% of the input was loaded as a control.

Quantification of Endogenous Nppa Expression—The mouse atrial cardiomyocyte tumor cell line HL-1 was cultured as described (22). For transfections, 1.3×10^6 cells were seeded in 60-mm dishes. Transfections were performed on the following day using FuGENE HD (Roche Applied Science, 20 μl of each) according to the supplier's instructions. Each transfection was performed using 250 μl of OptiMEM (Invitrogen), 3 μg of expression plasmid, and 3 μg of pMACS4.1 (Miltenyi Biotech), which encodes a truncated CD4 cell surface marker. After 48 h, magnetic cell sorting of $CD4^+$ cells was carried out using anti-CD4 magnetic beads and MS columns (Miltenyi Biotech) following the manufacturer's instructions. In a control experiment, the transfection of pd1EGFP-N1 (Clontech) resulted in an approximate efficiency of 5% GFP^+ cells before and 50% GFP^+ cells after magnetic cell separation. From the eluted cells, total RNA was isolated with PeqGOLD (Peqlab), and cDNA was synthesized using 0.75 μg of RNA and avian myeloblastosis virus reverse transcriptase (Promega). Quantitative RT-PCR using an ABI Prism 7000 cycler and SYBR Green was performed in triplicates with primers specific for *Nppa* and *HPRT* as endogenous control. Primer sequences are available upon request. Mean relative gene expression levels and standard deviations were calculated from two independent transfections with the comparative threshold cycle (C_T) method following the ABI Prism user manual. Additionally, p values were determined from ΔC_T values using the Student's t test.

In Situ Hybridization Analysis—Embryos for expression analysis were derived from matings of mice heterozygous for a mutant allele of *Uncx4.1* (23). Genomic DNA prepared from yolk sac or tail biopsies was used for genotyping by PCR. For timed pregnancies, vaginal plugs were checked in the morning after mating; noon was taken as embryonic day 0.5. Fetuses were dissected in phosphate-buffered saline and fixed in 4% paraformaldehyde in phosphate-buffered saline. Whole-mount *in situ* hybridization was performed following a standard procedure with digoxigenin-labeled antisense riboprobes (24). Stained specimens were transferred into 80% glycerol prior to documentation on a Leica M420 microscope with a Fujix digital camera HC-300Z. All images were processed in Adobe PhotoShop 7.0.

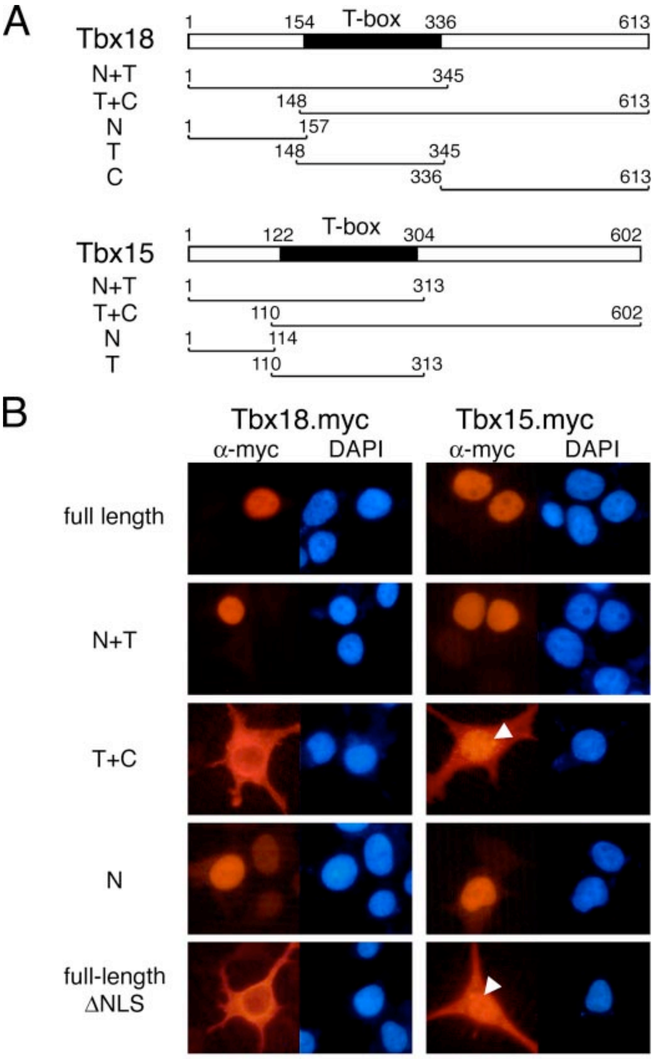

C Tbx18 NLS : 32-QQLQKKRRKLATEE-45

Tbx15 NLS : 24-IGSNKKRKLRDWEE-37

FIGURE 1. **Tbx18 and Tbx15 harbor a classical NLS close to the N terminus.** *A*, schematic representation of the primary structure of Tbx18 and Tbx15 and their deletion mutants used in this study; the T-box (T) is shaded in *black*, and the N- and C-terminal domains (N and C) are shown in *white*. The *numbers* indicate the length of the proteins and their domains, respectively. *B*, intracellular localization of myc-tagged Tbx18 and Tbx15 proteins and their deletion mutants in transiently transfected HEK293 cells as detected by anti-myc immunofluorescence. All proteins containing the N-terminal region are exclusively localized to the nucleus (compare nuclear staining with 4′,6-diamidino-2-phenylindole (*DAPI*)). Deletion of this region causes relocalization to the cytoplasm. Tbx15 T + C and full-length ΔNLS proteins are partially retained in the nucleus (*white arrowheads*). *C*, amino acid sequence of the identified NLS in Tbx18 and Tbx15. Basic residues are marked in *red*, and amino acid residues deleted in full-length ΔNLS constructs are *underlined*.

RESULTS

Tbx18 and Tbx15 Harbor a Classical Nuclear Localization Signal—To analyze the subcellular localization of Tbx18, we transfected a series of Tbx18 expression constructs (Fig. 1*A*) in

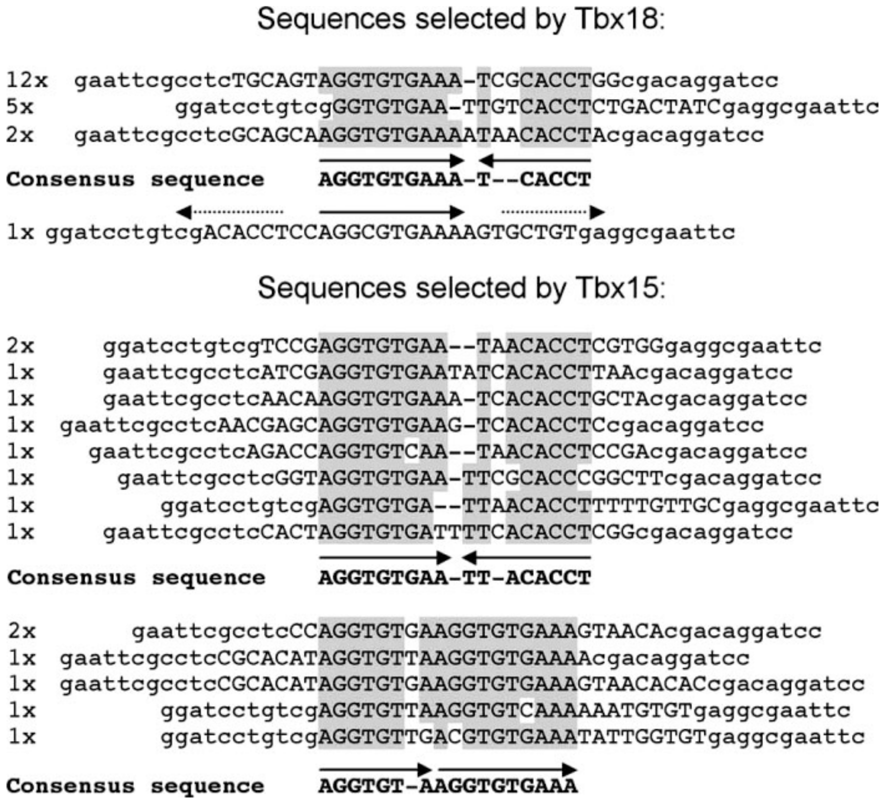

Sequences selected by Tbx18:

12x gaattcgcctcTGCAGTAGGTGTGAAA-TCGCACCTGGcgacaggatcc
5x ggatcctgtcgGGTGTGAA-TTGTCACCTCTGACTATCgaggcgaattc
2x gaattcgcctcGCAGCAAGGTGTGAAAATAACACCTAcgacaggatcc

Consensus sequence AGGTGTGAAA-T--CACCT

1x ggatcctgtcgACACCTCCAGGCGTGAAAAGTGCTGTgaggcgaattc

Sequences selected by Tbx15:

2x ggatcctgtcgTCCGAGGTGTGAA--TAACACCTCGTGGgaggcgaattc
1x gaattcgcctcATCGAGGTGTGAATATCACACCTTAAcgacaggatcc
1x gaattcgcctcAACAAGGTGTGAAA-TCACACCTGCTAcgacaggatcc
1x gaattcgcctcAACGAGCAGGTGTGAAG-TCACACCTCcgacaggatcc
1x gaattcgcctcAGACCAGGTGTCAA--TAACACCTCCGAcgacaggatcc
1x gaattcgcctcGGTAGGTGTGAA-TTCGCACCCGGCTTcgacaggatcc
1x ggatcctgtcgAGGTGTGA--TTAACACCTTTTTGTTGCgaggcgaattc
1x gaattcgcctcCACTAGGTGTGATTTTCACACCTCGGcgacaggatcc

Consensus sequence AGGTGTGAA-TT-ACACCT

2x gaattcgcctcCCAGGTGTGAAGGTGTGAAAGTAACAcgacaggatcc
1x gaattcgcctcCGCACATAGGTGTTAAGGTGTGAAAAcgacaggatcc
1x gaattcgcctcCGCACATAGGTGTGAAGGTGTGAAAGTAACACACcgacaggatcc
1x ggatcctgtcgAGGTGTTAAGGTGTCAAAAAATGTGTgaggcgaattc
1x ggatcctgtcgAGGTGTTGACGTGTGAAATATTGGTGTgaggcgaattc

Consensus sequence AGGTGT-AAGGTGTGAAA

FIGURE 2. **DNA binding sites of Tbx18 and Tbx15 contain variably arranged T half-sites.** Sequences of DNA fragments isolated after four rounds of PCR-assisted *in vitro* binding site selection are shown. In total, 20 bound fragments were analyzed for Tbx18 (*upper panel*), and 15 were analyzed for Tbx15 (*lower panel*), respectively; some fragments were isolated several times. Sequences were aligned at the invariant core 5′-AGGTG-3′ and grouped according to the orientation of the half-sites. Consensus sequences were derived for nucleotide positions that were found in >70% of the cases. All except one site selected by Tbx18 exhibit a palindromic orientation, whereas Tbx15 selected both direct repeats and palindromes. The *arrows* indicate the orientation of the half-sites. Conserved positions are marked in *gray color*, and linker sequences are shown in *lowercase letters*.

HEK293 cells and detected the myc tag by immunofluorescence (Fig. 1*B*). Full-length Tbx18 protein showed exclusive nuclear localization in HEK293 (Fig. 1*B*) and in NIH3T3 cells (data not shown). Deletion of the C-terminal region did not alter this distribution, whereas removal of the N-terminal region resulted in relocalization to the cytoplasm. The N-terminal region alone was found in the nucleus, demonstrating that it is not only necessary but also sufficient for nuclear import. Similar results were obtained for Tbx15. However, a truncation mutant of Tbx15 lacking the N-terminal region retained partial nuclear localization (Fig. 1*B*, *white arrowhead*). Inspection of the primary structure of Tbx18 and Tbx15 revealed a cluster of 5 basic amino acid residues resembling a classical NLS at a conserved position at the N terminus of the two proteins (Fig. 1*C*, marked in *red*). Deletion of this cluster resulted in exclusive (Tbx18) and predominant (Tbx15) cytoplasmic localization of the full-length proteins (Fig. 1*B*). Our results demonstrate that a classical NLS mediates constitutive nuclear localization of Tbx18. Tbx15 might possess additional sequences mediating nuclear localization as it has been previously seen in other DNA-binding proteins including T-box transcription factors (25, 26).

Tbx18 and Tbx15 Bind to Repeats of T Half-sites—To date, transcriptional targets of Tbx18 and Tbx15 have not been described. As a first step toward the identification and validation of potential target genes, we determined the DNA binding specificities of the two proteins using a PCR-based *in vitro* cyclic binding site selection protocol (1). DNA fragments recovered after four rounds of the selection protocol were isolated by molecular cloning and sequenced (Fig. 2). In each pool, some oligonucleotides were represented several times, indicating that the complexity of the selected pool had decreased at this stage in favor of strong binding sites. All oligonucleotides represented repeats of the core sequence 5′-AGGTGTGA-3′ (Fig. 2, *upper panel*) that is known as a common T half-site. A consensus target sequence for Tbx18 was identified through the compilation of 19 sequences. It constitutes an imperfect palindrome, composed of two anti-parallel T half-sites. The orientation of these half-sites is inversed with respect to the reported binding site of Brachyury (BS.p (see Ref. 1)) and was therefore designated BS.inv. For Tbx15, nine of fifteen selected oligonucleotide sequences matched the BS.inv consensus sequence (Fig. 2, *middle panel*). A smaller fraction (6 of 15 sequences) featured a direct repeat of the T half-site, indicating differences in binding specificity between the two proteins (Fig. 2, *lower panel*). The consensus of this directly repeated binding site was named BS.dir.

We next compared the DNA binding properties of Tbx18, Tbx15, and the distant family member Brachyury by EMSA. All three proteins failed to bind to DNA fragments harboring single T half-sites under our experimental conditions (data not shown). In contrast, DNA fragments with repeats of T half-sites supported protein-DNA binding of full-length, *in vitro* translated Tbx18, Tbx15, and Brachyury (Fig. 3). All three proteins formed specific complexes with the consensus sites BS.inv, BS.dir, and the palindromic binding site identified for Brachyury, BS.p (Fig. 3*A*). Brachyury was found to bind strongly to BS.p and BS.inv but weakly to BS.dir. In the case of Tbx18 and Tbx15, BS.inv and BS.dir sites supported stronger binding than the BS.p site (Fig. 3*C*, *open arrowheads*). The addition of specific antibody resulted in the generation of slower migrating complexes (supershifts), confirming the specificity of DNA binding (Fig. 3*C*, *black arrowheads*). We next determined whether the T-box region is sufficient to recapitulate the binding characteristics of the full-length proteins (Fig. 3*D*). T-box-containing peptides of Tbx18, Tbx15, and Brachyury exhibited strongly diminished DNA binding (Fig. 3*D*, *lanes 3*), indicating

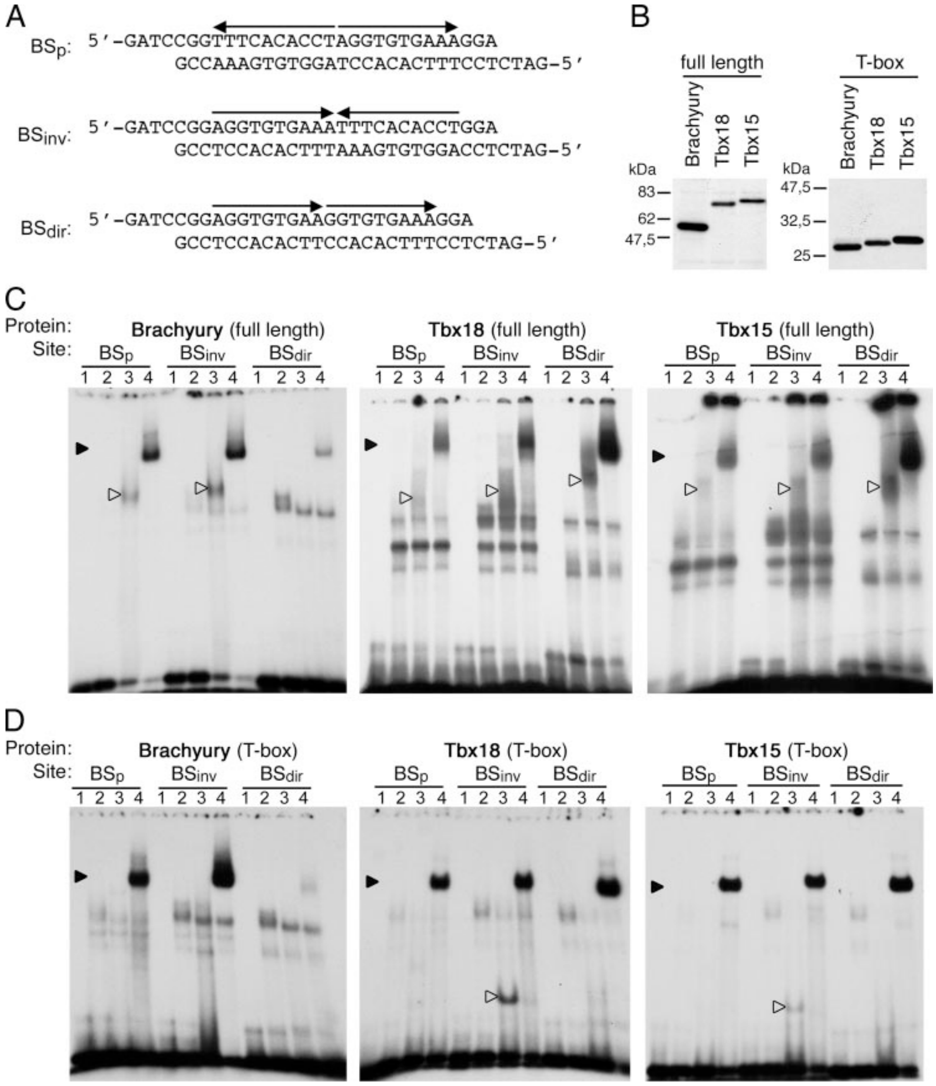
A
BSp: 5'-GATCCGGTTTCACACCTAGGTGTGAAAGGA
GCCAAAGTGTGGATCCACACTTTCCTCTAG-5'
BSinv: 5'-GATCCGGAGGTGTGAAATTTCACACCTGGA
GCCTCCACACTTTAAAGTGTGGACCTCTAG-5'
BSdir: 5'-GATCCGGAGGTGTGAAGGTGTGAAAGGA
GCCTCCACACTTCCACACTTTCCTCTAG-5'
B
full length
T-box
Brachyury
Tbx18
Tbx15
kDa
83
62
47,5
47,5
32,5
25
C
Protein:
Site:
Brachyury (full length)
Tbx18 (full length)
Tbx15 (full length)
BSp
BSinv
BSdir
1 2 3 4
D
Brachyury (T-box)
Tbx18 (T-box)
Tbx15 (T-box)

FIGURE 3. **Comparative DNA binding analysis of Tbx18, Tbx15, and Brachyury.** *A*, double-stranded oligonucleotides with different orientation of half-sites (*arrows*) were tested for binding in electrophoretic mobility shift assays. *B*, assays were performed with equal amounts of *in vitro* synthesized myc-tagged Tbx18, Tbx15, and Brachyury full-length proteins (*left*) and their T-boxes (*right*), respectively, as determined by anti-myc Western blot. *C*, Tbx18 and Tbx15 bind to composite sites irrespective of the orientation of the half-sites (*open arrowheads*). Specificity of binding is confirmed by the addition of anti-myc antibody that results in the formation of a supershifted complex (*black arrowheads*). Binding experiments were performed under the following conditions: *lane 1*, probe alone; *lane 2*, non-programmed lysate; *lane 3*, programmed lysate; *lane 4*, programmed lysate plus anti-myc antibody. *D*, T-box regions of Tbx18 and Tbx15 preferentially bind to BS.inv; experiments were performed as in *C*.

that the N- and C-terminal regions participate in protein-DNA complex formation. T-boxes of Tbx18 and Tbx15, but not of Brachyury, exclusively bound to the BS.inv site (Fig. 3*D*, *open arrowheads*), suggesting that the T-boxes of Tbx18 and Tbx15 possess an inherent binding specificity for this sequence. A strong increase in protein-DNA complex formation was observed for all truncated T-box peptides and full-length proteins after the addition of anti-myc antibody (Fig. 3, *C* and *D*, *black arrowheads*). Since this effect was not observed using a probe containing a single T half-site (data not shown), we assume that the divalent antibody may stabilize binding to composite sites as dimers.

Tbx18 and Tbx15 Dimerize—The composite nature of the DNA binding site of T-box proteins had previously suggested that dimerization of T-box proteins increases DNA binding specificity and/or affinity (27, 28). However, dimerization in the absence of DNA and in living cells had not been explored experimentally. To address the possibility that Tbx18 dimerizes *in vitro*, we performed pulldown assays using bacterially expressed GST-Tbx18 proteins that were incubated with lysates from HEK293 cells transfected with expression constructs for myc-tagged Tbx18, Tbx15, or Brachyury protein. Since GST-Tbx18 full-length protein could not be expressed in bacteria, we used a series of bacterially expressed fusion proteins of GST with the N- and C-terminal region and the T-box of Tbx18 instead (Fig. 4*A*, *left*). Tbx18 specifically bound to GST-Tbx18(N + T) and -Tbx18(T) but not to GST-Tbx18(N) or -Tbx18(C) (Fig. 4*A*, *right*), showing that dimerization via the T-box region occurred in the absence of DNA binding. A weaker interaction was observed with Tbx15 but not with Brachyury, indicating that related T-box proteins are able to form heterodimers.

To address whether dimerization occurs in cells, we analyzed the subcellular distribution of the myc-tagged Tbx18ΔNLS or Tbx15ΔNLS proteins (described above) by immunofluorescence in HEK293 cells upon coexpression of wild-type Tbx18 or Tbx15 (HA-tagged) proteins. Unlike for NLS mutants alone, we now detected nuclear localization of both Tbx18ΔNLS and Tbx15ΔNLS proteins (Fig. 4*B*), strongly suggesting that dimerization has occurred in these cells. The absence of nuclear recruitment upon coexpression of unrelated nuclear proteins confirmed the specificity of the interaction (data not shown).

Tbx18 and Tbx15 Are Potent Transcriptional Repressors—Members of the T-box gene family encode specific DNA-binding proteins that can activate or repress RNA polymerase II-mediated transcription (11). We performed luciferase reporter assays in HeLa cells to analyze how Tbx18 and Tbx15 modulate transcription. We used full-length Tbx18 and Tbx15 proteins fused to the GAL4-DNA binding domain cotransfected with a reporter plasmid containing five copies of the GAL4 binding site in front of the thymidine kinase minimal promoter ($5xGal4_{UAS}$-tk-luciferase, Fig. 5*A*). We observed a strong and

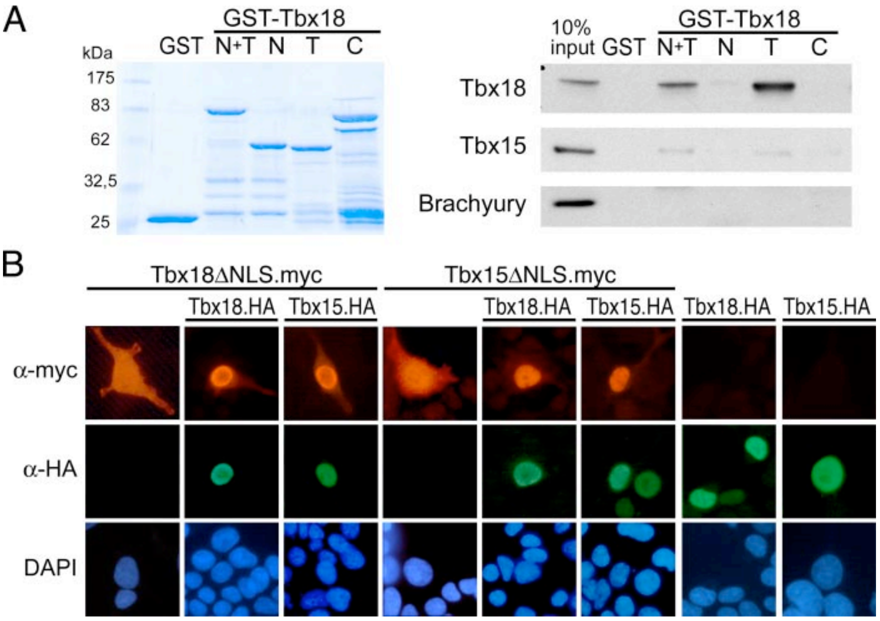

FIGURE 4. **Tbx18 and Tbx15 form homo- and heterodimers.** *A*, dimerization *in vitro*. *Left*, GST and fusion proteins of GST and N + T-, N-, T-, and C-domains of Tbx18 were purified from *E. coli* extracts and analyzed for integrity and quantity by Coomassie Brilliant Blue staining of SDS-polyacrylamide gels. *Right*, GST pulldown assays with protein extracts from HEK293 cells transfected with myc-tagged Tbx18, Tbx15, and Brachyury full-length expression constructs. *B*, dimerization in cells. HEK293 cells were transfected with expression constructs for myc-tagged Tbx18ΔNLS or Tbx15ΔNLS (*red*) in the presence or absence of HA-tagged wild-type Tbx18 or Tbx15 (*green*). Both NLS-deficient proteins are efficiently relocalized to the nucleus upon coexpression of wild-type Tbx18 or Tbx15 (compare 4′,6-diamidino-2-phenylindole (*DAPI*) nuclear counter staining).

dose-dependent repression of reporter gene activity by GAL4-Tbx18 with a maximal reduction of the basal activity to 5.5 ± 0.2% (Fig. 5*B*). The GAL4-DNA binding domain alone did not affect the transcription of the reporter gene. GAL4-Tbx15-mediated repression of the reporter to 8.4 ± 0.1% demonstrates that Tbx18 and Tbx15 do not only share similar DNA binding properties but also strong transcriptional repressor activities.

We then asked whether Tbx18 contains any identifiable domain that mediates this repression. GAL4-Tbx18(N + T), GAL4-Tbx18(N), and GAL4-Tbx18(C) proteins (data not shown) all repress 5xGal4$_{UAS}$-TK-luciferase reporter activity in HeLa cells, although more weakly than the full-length protein (Fig. 5*C*), suggesting that Tbx18 contains multiple regions capable of transcriptional repression.

Tbx18 and Tbx15 Interact with Groucho Corepressors—Transcriptional repression by tissue-specific transcription factors is mediated by binding to corepressor complexes that in turn modify chromatin structure. We wondered whether we could identify corepressors of Tbx18 by analyzing the primary structure of Tbx18 for motifs known to recruit such molecules. Near the N terminus of the protein, we identified an eh1 motif (engrailed homology 1) (Fig. 6*A*) that had also recently been noted in a genome-wide screen (29). The eh1 motif comprises a stretch of 7 amino acid residues that is present in a large number of transcription factors of various classes and is necessary for binding of Groucho proteins (30). Groucho proteins constitute a family of highly conserved corepressors, with the members Grg1–5 (Groucho-related genes) in mouse and TLE1–4 (Transducin-like enhancers of split) in humans (31). Interestingly, the eh1 motif is also found at a conserved N-terminal position in murine Tbx15, Tbx22, and Tbx20 proteins (Fig. 6*A*), suggesting that these members of the Tbx1 subfamily may also act as Groucho-dependent repressors.

To experimentally explore this possibility, we tested Tbx18 binding to Groucho proteins *in vitro*. Pulldown assays were performed using GST-Tbx18 fusions (compare Fig. 4*A*) that were incubated with lysates of HEK293 cells transfected with an expression construct for HA-tagged TLE3. Strong binding of TLE3 was observed with GST-Tbx18(N+T) and GST-Tbx18(N) but not with GST-Tbx18(T) or GST-Tbx18(C), indicating that the eh1-containing N-terminal domain is necessary and sufficient for an interaction with Groucho proteins (Fig. 6*B*). Co-immunoprecipitation experiments in HEK293 cells cotransfected with expression constructs for myc-tagged Tbx18 alone or together with HA-tagged TLE3 confirmed the presence of a Tbx18-TLE3 complex in a cellular environment

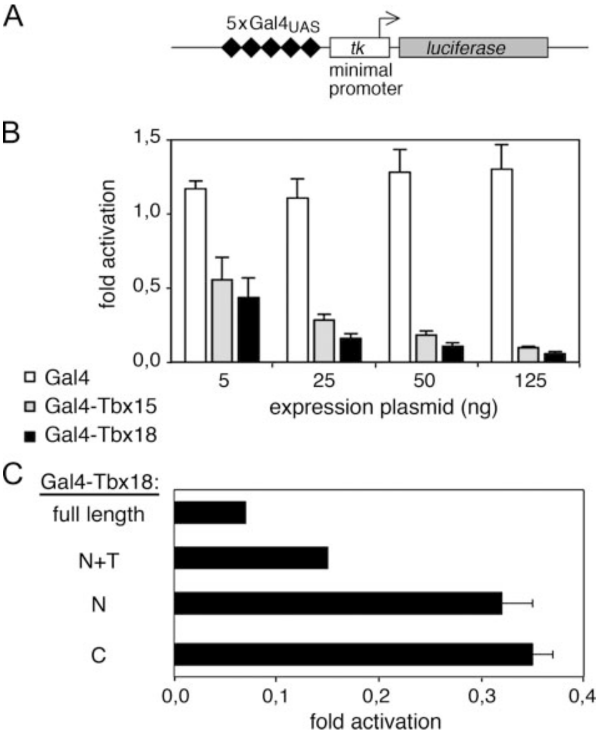

FIGURE 5. **Tbx18 and Tbx15 act as transcriptional repressors.** *A*, schematic representation of the 5xGal4$_{UAS}$-tk-luciferase-reporter plasmid containing a pentamer of the GAL4 binding site, the minimal promoter of the thymidine kinase gene (*tk*), and the luciferase reporter gene. *B*, HeLa cells were cotransfected with the reporter plasmid and increasing amounts of GAL4, GAL4-Tbx18, or GAL4-Tbx15 expression constructs. Tbx18 and Tbx15 dose-dependently repress luciferase reporter gene activity. *C*, full repression activity of Tbx18 requires N- and C-terminal regions as well as the T-box. HeLa cells were cotransfected with GAL4-Tbx18 deletion constructs (each 25 ng) and the 5xGal4$_{UAS}$-tk-luciferase reporter plasmid.

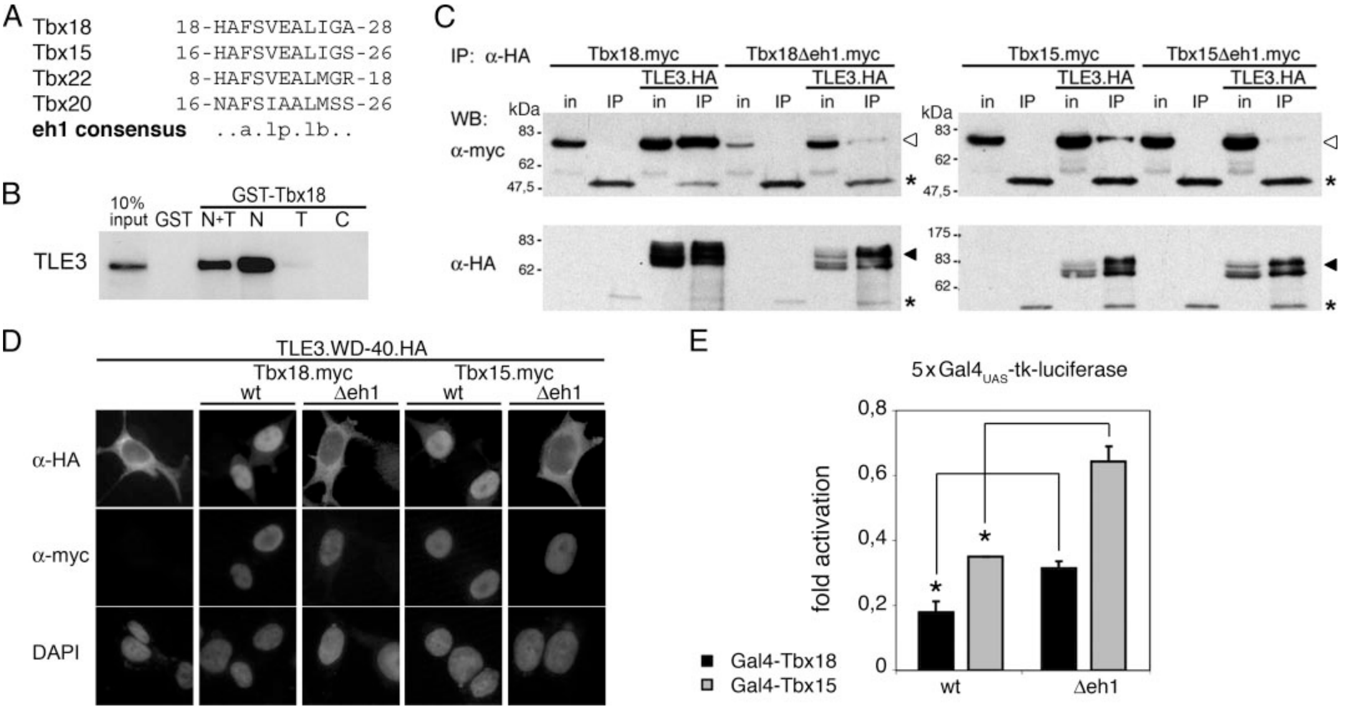

FIGURE 6. **Tbx18 and Tbx15 interact with the corepressor Groucho.** *A*, sequence alignment of mouse Tbx18 (AF30666), Tbx15 (NM_009323), Tbx22 (NM_145224), and Tbx20 (NM_194263) demonstrates the presence of an N-terminal eh1 motif; the *numbers* refer to the position within the protein. The eh1 consensus sequence (*a*, aromatic, *l*, aliphatic, *p*, polar, *b*, bulky amino acids (see Ref. 29)) is shown. *B*, interaction of Tbx18 with Groucho protein (TLE3) *in vitro*. Pulldown assays with GST-Tbx18 deletion mutants were carried out as outlined in the legend for Fig. 4 with extracts from HEK293 cells transfected with a TLE3.HA expression construct. *C* and *D*, interaction of Tbx18 and Tbx15 with Groucho *in vivo* requires the eh1 motif. *C*, HEK293 cells were transfected with expression constructs for wild-type (*wt*) or eh1-deleted (*Δeh1*) myc-tagged Tbx18 (*left*) and Tbx15 (*right*), respectively, either alone or in combination with a construct encoding HA-tagged TLE3. Lysates were immunoprecipitated with anti-HA antibody followed by Western blot (*WB*) analysis of input (*in*) and immunoprecipitated fractions (*IP*) with anti-myc and anti-HA antibodies. Signals for Tbx18 and Tbx15 (*open arrowheads*), TLE3 (*black arrowheads*), and IgH-bands (*asterisk*) are highlighted. *D*, nuclear recruitment assay. Coexpression of myc-tagged Tbx18 or Tbx15 (*middle row*) translocates the cytoplasmic WD40 domain of TLE3 (HA-tagged, *upper row*) to the nucleus as shown by immunofluorescence in HEK293 cells after cotransfection. *DAPI*, 4′,6-diamidino-2-phenylindole. *E*, repression activity of Tbx18 and Tbx15 partially depends on the presence of the eh1 motif. Expression constructs for fusion proteins of GAL4 with wild-type Tbx18 or Tbx15 and eh1 mutants (25 ng), respectively, were transfected in HeLa cells together with the 5xGal4$_{UAS}$-thymidine kinase-luciferase reporter plasmid. *, $p < 0.05$.

(Fig. 6*C*, *left*). Site-directed mutagenesis of the eh1 motif by replacing the amino acids phenylalanine and serine by leucine and isoleucine (Tbx18Δeh1) abolished complex formation. Not unexpectedly, Tbx15 also showed eh1-dependent binding to TLE3 (Fig. 6*C*, *right*). Groucho proteins are known to bind the eh1 motif with their C-terminal WD40 domain (32). To delineate the region in TLE3 that mediates interaction with the eh1 motif in Tbx18 and Tbx15, we performed immunofluorescence experiments in HEK293 cells expressing the HA-tagged WD40 domain of TLE3 in the presence or absence of myc-tagged Tbx18 or Tbx15. When expressed alone, the WD40 domain of TLE3 is distributed in the cytoplasm as it lacks a functional NLS. Coexpression of Tbx18 or Tbx15 led to nuclear translocation of the WD40 domain (Fig. 6*D*), an effect that was not observed following coexpression of Tbx18 or Tbx15 protein with a mutant eh1 motif, confirming the specificity of the interaction. Next, we determined whether the interaction of Tbx18 or Tbx15 with Groucho is required for transcriptional repression. Therefore, we compared the repression activities of wild-type and eh1 mutant versions of GAL4-Tbx18 and GAL4-Tbx15 on the 5xGal4$_{UAS}$-tk-luciferase-reporter in HeLa cells. Wild-type and eh1 mutant proteins were expressed at equal levels (data not shown). Both eh1 mutant proteins exhibit an approximate 50% reduction of repressor activity (Fig. 6*E*) with a release of repression from 17.8 ± 3.4 to 31.4 ± 2.1% for GAL4-Tbx18 and 35.0 ± 0.0 to 64.3 ± 4.7% for GAL4-Tbx15. We conclude that a major part of the repression activity of Tbx18 and Tbx15 is mediated through the eh1 motif. Overexpression of Groucho protein failed to increase repression by Tbx18 and Tbx15 wild-type proteins (data not shown), indicating that abundant endogenous expression in mammalian cell lines was sufficient to saturate the repression (33).

Tbx18 Interacts with Gata4 and Nkx2–5 and Represses the Nppa Promoter by Competition with Tbx5—Cooperativity between transcription factors in DNA binding plays a crucial role in target promoter specificity. For T-box proteins, this may be achieved by dimerization on multiple T half-sites and/or through interaction with other proteins (10, 28, 34–36). A well established paradigm for the latter is the interaction of Tbx2, Tbx5, and Tbx20 with the transcription factors Gata4 and Nkx2–5 to regulate cardiac expression of *Nppa* (natriuretic peptide precursor type a, also known as atrial natriuretic factor, *Anf*) (4–7, 18, 37, 38). The 700-bp upstream region of *Nppa* contains all the necessary control elements to confer correct spatial expression in the developing heart (18). Binding of Tbx5, Tbx20, NK-type homeodomain proteins, and GATA proteins to their respective recognition sequences synergistically activates this promoter, whereas binding of Tbx2 releases activa-

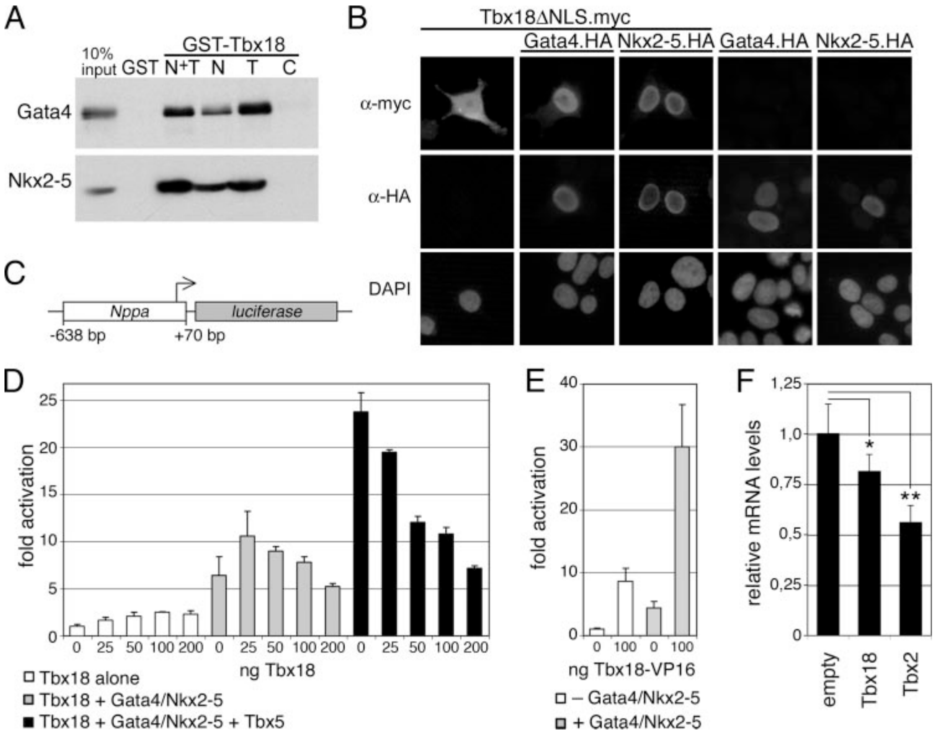

FIGURE 7. **Tbx18 binds Gata4 and Nkx2–5 and represses the *Nppa* promoter by competition with Tbx5.** *A*, interaction of Tbx18 with Gata4 and Nkx2–5 *in vitro*. Pulldown assays with GST-Tbx18, as described in the legend for Fig. 4, with lysates of HEK293 cells transfected with expression constructs for HA-tagged Gata4 or Nkx2–5, were performed. Bound protein was detected by anti-HA Western blot. *B*, nuclear recruitment of Tbx18ΔNLS by Gata4 or Nkx2–5. Immunofluorescence in HEK293 cells transfected with an expression construct for myc-tagged Tbx18ΔNLS either alone or in the presence of HA-tagged Gata4 or Nkx2–5. *DAPI*, 4′,6-diamidino-2-phenylindole. *C*, schematic diagram of the *Nppa* luciferase reporter (pGL3.Nppa-luciferase). The *numbers* indicate the genomic positions relative to the transcription start site. *D*, Tbx18 counteracts the transcriptional activation of the *Nppa* promoter mediated by Tbx5. HeLa cells were transfected with increasing amounts of an expression construct for Tbx18 (0–200 ng), alone (*white bars*), together with constant amounts of Gata4 and Nkx2–5 expression constructs (100 ng of each, *gray bars*), or with expression constructs for Gata4, Nkx2–5, and Tbx5 (100 ng of each, *black bars*). *E*, the expression of Tbx18-VP16 (*white bars*) activates the *Nppa* promoter and causes a synergistic activation in combination with Gata4 and Nkx2–5 (*gray bars*). *F*, forced expression of Tbx18 or Tbx2 decreases *Nppa* mRNA levels in HL-1 cardiomyocytes. Transfected cells were enriched, and endogenous *Nppa* expression was measured by quantitative RT-PCR. Mean relative mRNA expression levels were derived from two independent transfections and triplicate RT-PCR measurements. *, $p < 0.02$; **, $p < 10^{-4}$.

tion. Although Tbx2, Tbx5, and Tbx20 belong to different T-box subfamilies, they share several interacting partners. We therefore decided to investigate whether Tbx18 was also capable of interacting with GATA zinc finger and NK-type homeodomain proteins. Indeed, we found in GST pulldown assays that HEK293-expressed Gata4 strongly binds to GST-Tbx18(N+T) and GST-Tbx18(T), binds slightly more weakly to GST-Tbx18(N), but does not bind to GST-Tbx18(C) (Fig. 7*A*). A similar binding pattern was observed with Nkx2–5, indicating that both transcription factors either bind to two different sites in the T-box and N-terminal region or bind within the short stretch of overlapping amino acids present in both fusion proteins of Tbx18 (aa 148–157, Fig. 1*A*). We confirmed the interaction of Gata4 and Nkx2–5 with Tbx18 by a nuclear recruitment assay with Tbx18ΔNLS protein in HEK293 cells (Fig. 7*B*).

Binding of Tbx18 to Nkx2–5 and Gata4 as well as coexpression of *Gata4*, *Tbx5*, and *Tbx18* in the sinus horn mesenchyme (15, 39) suggest that failure of *Nppa* activation in this region of the developing heart might at least partly be caused by the repressive activity of Tbx18. We tested this hypothesis by analyzing the effect of Tbx18 in an *Nppa*-luciferase reporter assay (pGL3.Nppa-luciferase, Fig. 7*C*). Low concentrations of Tbx18 alone had little effect on the activity of the reporter. Coexpression of Gata4 with Nkx2–5 caused a moderate activation, in agreement with previous observations (40). Low concentrations of Tbx18 caused further activation when constant amounts of Gata4 and Nkx2–5 were present, suggesting that Tbx18 efficiently recruited the activators Gata4 and Nkx2–5 to the *Nppa* promoter. However, at higher doses of Tbx18, this activation was reversed to base line levels, indicating the dominance of Tbx18-mediated repression. Coexpression of Gata4 and Nkx2–5 with Tbx5 led to strong activation, demonstrating synergism of the three transcription factors in activating the *Nppa* promoter (4–6, 18). This activation was efficiently repressed in a dose-dependent manner upon the addition of Tbx18, suggesting that Tbx18 repressed the *Nppa* promoter by competition with the activator Tbx5 (Fig. 7*D*). An activator form of Tbx18 (Tbx18-VP16) caused transcriptional activation, which was synergistically increased when Gata4 and Nkx2–5 were coexpressed (Fig. 7*E*), demonstrating cooperative binding of Tbx18, Gata4, and Nkx2–5 proteins to DNA binding sites in the *Nppa* promoter.

To address whether Tbx18 is also sufficient to repress endogenous *Nppa* expression, we performed overexpression experiments in HL-1 cardiomyocytes (22). Since we achieved only low transfection efficiency of these cells, we enriched transfected cells by coexpression of a cell surface marker followed by magnetic cell separation. Endogenous *Nppa* expression levels were measured by quantitative RT-PCR. As shown in Fig. 7*F*, transfection of Tbx18 resulted in a weak but significant decrease of *Nppa* mRNA to 81.5 ± 8.4% of the control. As a positive control, we expressed the known repressor of *Nppa*, Tbx2 (18, 38), which resulted in a stronger repression of *Nppa* mRNA expression (56.1 ± 8.4%).

Tbx18 Represses Delta-like 1 Expression in Somites—Tbx6, in cooperation with canonical Wnt signaling, directly activates the presomitic expression of the Notch ligand *Delta-like 1* (*Dll1*) (19, 41, 42). After segmentation, the expression of *Dll1* is confined to the posterior halves of epithelialized somites, which is complementary to *Tbx18* expression that is

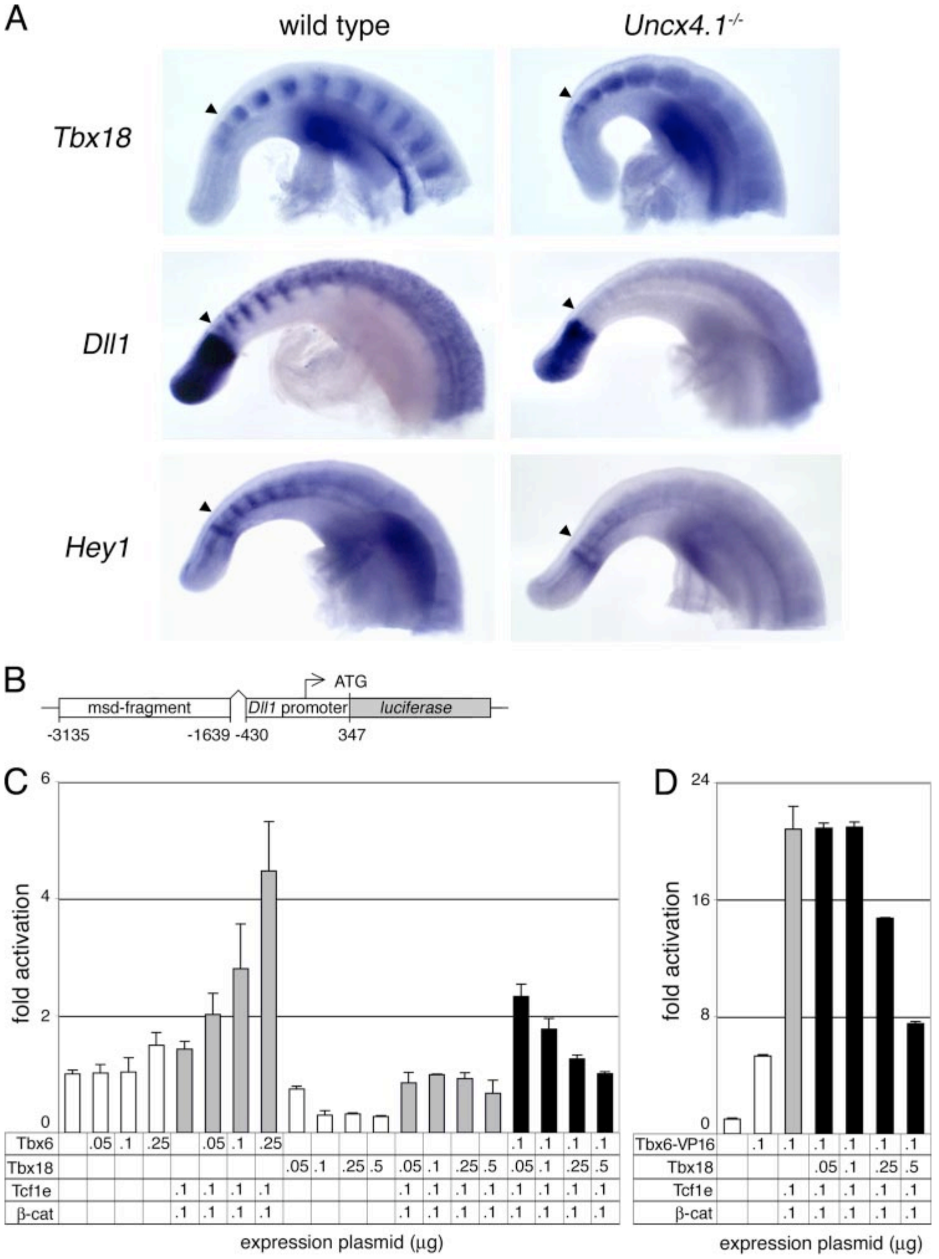

FIGURE 8. **Tbx6/Wnt-mediated activation of *Dll1* promoter activity is antagonized by Tbx18.** *A*, overexpression of *Tbx18* in somites coincides with the down-regulation of *Dll1* and *Hey1* expression in the posterior trunk region. Whole mount *in situ* hybridization of mouse embryonic day 10.5 wild-type and *Uncx4.1*$^{-/-}$ embryos. Genotypes and probes are as indicated in the figure. The *arrowheads* denote onset of segmentation. *B*, schematic representation of the pKS.msd-luciferase reporter plasmid containing the *Dll1* msd upstream enhancer fused to the *Dll1* minimal promoter (as described in Ref. 19); the *numbers* indicate genomic positions relative to the transcription start site. *C* and *D*, the transcriptional effects of Tbx18 and Tbx6 (*C*) or Tbx6-VP16 (*D*) alone (*white bars*) or in combination with Wnt mediators Tcf1e and β-catenin (*gray bars*) on msd-luciferase reporter activity. Tbx18 causes a repression of the basal activity and abolishes the activation caused by cotransfection of Tcf1e and β-catenin (*β-cat*) together with Tbx6 (*C*) or Tbx6-VP16 (*D*) expression constructs (*black bars*).

restricted to anterior somite halves. We therefore hypothesized that Tbx18 antagonizes Tbx6-mediated activation to restrict the expression of *Dll1* to the posterior somite compartment. We failed to detect ectopic expression of *Dll1* in anterior somite halves in *Tbx18*$^{-/-}$ embryos; however, coexpression of the closely related *Tbx22* gene in newly formed somites may compensate for the loss of Tbx18 function in this context (43). Restriction of *Tbx18* expression to anterior somite halves is achieved by the transcription factor *Uncx4.1* in posterior somite halves (13). In *Uncx4.1* mutant embryos, *Tbx18* expression is found throughout the somites, providing a natural situation to study the effect of ectopic *Tbx18* on *Dll1* somitic expression. Indeed, we found a down-regulation of *Dll1* expression and of the Notch target gene *Hey1* (44) in *Uncx4.1*$^{-/-}$ somites (Fig. 8*A*), suggesting that Tbx18 represses *Dll1*, and thus, Notch signaling in this tissue. To confirm this possibility at the molecular level, we performed reporter assays in HeLa cells using a luciferase reporter under control of the *Dll1* msd upstream enhancer fused to the *Dll1* minimal promoter (pKS.msd-luciferase (Fig. 8*B*) (Ref. 19)). The 1.4-kbp msd fragment is sufficient to direct *Dll1* transcription to the presomitic mesoderm, the somites, and the dermomyotome (45) and contains six T half-sites as well as four Tcf/Lef binding sites that are required to mediate this activity *in vivo* (19). Neither expression of Tbx6 at various concentrations (0–250 ng) nor of Tcf1e together with β-catenin (both 100 ng) stimulated the activity of the msd-luciferase reporter in our experiments. Cotransfection of Tbx6 and Tcf1e/β-catenin dose-dependently activated the reporter (Fig. 8*C*) in accordance with previous data (19). In contrast, Tbx18 alone repressed the basal reporter activity moderately and was unable to synergistically activate the msd reporter when coexpressed with Tcf1e/β-catenin (Fig. 8*C*). In addition, Tbx18 efficiently antagonized the activation mediated by Tbx6 together with Tcf1e and β-catenin (Fig. 8*C*) and was also able to compete with an even stronger synergistic activation caused by an activator form of Tbx6 (Tbx6-VP16) in combination with Tcf1e and β-catenin (Fig. 8*D*). An activator form of Tbx18 (Tbx18-VP16) caused transcriptional activation of the reporter gene, arguing that the effects of Tbx18 on the *msd* promoter are caused by competitive binding to T half-sites and not merely by protein interactions (data not shown).

DISCUSSION

Genetic analyses have shown that the closely related T-box genes *Tbx18* and *Tbx15* are crucial players in the formation of the heart, the ureter, the vertebral column, and the skin during mouse development. As a first step toward understanding the molecular pathways regulated by these two proteins, it is critical to define their molecular properties and the mode of regulation of direct transcriptional targets. Here, we have shown that Tbx15 and Tbx18 act as transcriptional repressors that may exert their function by antagonizing transcriptional activators of the same family. During cardiac development, Tbx18 may counteract Tbx5-mediated activation of the *Nppa* promoter and Tbx6-mediated activation of *Dll1* during somitogenesis. Interaction with Groucho corepressors is at least partially responsible for transcriptional repression. DNA binding specificity and protein interaction partners are likely to dictate target specificity of Tbx15 and Tbx18. Finally, we show that Tbx15 and Tbx18 are biochemically equivalent, suggesting redundant function in embryogenesis.

Repression by Tbx18 through Antagonizing T-box Activators in Somite and Heart Development—Mice carrying a null allele of *Tbx18* die shortly after birth due to severe malformations of the axial skeleton, a phenotype that was traced to the function of *Tbx18* in maintaining anterior-posterior somite polarity (13). Anterior-posterior somite polarity is established in the anterior presomitic mesoderm by the combined action of Mesp2 and Notch-Delta signaling (46). The latter induces expression of *Uncx4.1* in posterior somite halves (47) that is required to restrict the expression of *Tbx18* to anterior somite halves (13). In *Tbx18*$^{-/-}$ embryos, *Uncx4.1* expression gradually expands into anterior somite halves, suggesting inhibition of *Uncx4.1* activation by Tbx18 (13). To date, the lack of clarity on the mode of target gene regulation by Tbx18 has made it difficult to hypothesize on the molecular pathways controlled by Tbx18 in the somitic mesoderm. Our studies have now shown that Tbx18 is likely to act as a transcriptional repressor *in vivo*. Expansion of *Uncx4.1* expression in *Tbx18*$^{-/-}$ somites is therefore compatible with a direct transcriptional repression of *Uncx4.1*, and alternatively, with an indirect inhibition of *Uncx4.1* activation by repression of components of the Delta/Notch signaling pathway. The first possibility seems unlikely given the relatively slow expansion of *Uncx4.1* expression in *Tbx18*$^{-/-}$ somites. However, coexpression of *Tbx22*, a closely related *Tbx* gene, in anterior somite halves of newly formed somites (43) might prevent an immediate derepression of *Uncx4.1* transcription. The second possibility gains support from our data on the transcriptional control of the *Dll1* promoter *in vitro* and from analysis of molecular changes accompanying *Tbx18* overexpression in *Uncx4.1*$^{-/-}$ embryos. Tbx18 abrogates the Tbx6-mediated activation of the *Dll1* promoter, most likely by competition for T half-sites *in vitro*, and ectopic expression of Tbx18 in posterior somites coincides with the down-regulation of *Dll1* and Notch-Delta signaling *in vivo*. Expression of *Tbx6* mRNA and protein is restricted to the presomitic mesoderm (42), arguing for a role of Tbx6 in activating rather than maintaining somitic expression of *Dll1*. Tbx18 might therefore counteract Tbx6 to restrict *Dll1* expression to posterior stripes in the anterior presomitic mesoderm and/or might antagonize an as yet unidentified somitic activator to restrict *Dll1* to posterior somite halves. As a third possibility, expansion of *Uncx4.1* expression in *Tbx18*$^{-/-}$ embryos may merely reflect immigration of cells from posterior into anterior somite halves due to loss of adhesion or repulsion mechanisms.

The *Nppa* promoter is subject to a spatially complex pattern of regulation in which both activating and repressing T-box proteins may bind and compete for the same set of binding sites. *Nppa* expression in the chamber myocardium of the heart is established by synergistic action of Nkx2–5, Gata4, and Tbx5 transcriptional activators (4 – 6). Exclusion of *Nppa* expression from regions of the primary myocardium in the atrioventricular canal and the outflow tract is achieved by binding of the Tbx2 repressor to T half-sites in the *Nppa* promoter, competing Tbx5 activation (18, 38). Our studies show that Tbx18 might play a similar role in the sinus horn mesenchyme that is also devoid of *Nppa* expression. However, repression of *Nppa* expression in the posterior pole of the heart does not exclusively depend on the presence of Tbx18 but also on the absence of Nkx2–5 (15), providing an additional level of safety to exclude *Nppa* expression from this area.

Our analysis of *Nppa* repression by Tbx18 sheds light onto the molecular control of target site specificity of T-box genes. Tbx5 and Tbx18 are members of distantly related Tbx subfamilies, arguing for diverse modes of DNA and protein interactions. However, regulation of the same promoter clearly indicates that both proteins bind to the same DNA binding sites, a situation that is similarly found for Tbx6 and Tbx18 in the *Dll1* promoter. To date, all T-box proteins analyzed, including Tbx15 and Tbx18 tested here, recognize DNA binding sites containing a T half-site 5′-AGGTGT-GAA-3′. Earlier reports and this study suggest that *in vitro* selected (strong) binding sites are not necessarily present in the genome as such but that combinations of two or more (less conserved) T half-sites including their particular orientation and spacing influence DNA binding specificity *in vivo* (1–3, 28, 34). Along this line, we failed to detect the selected perfect binding sites of Tbx15 and Tbx18 in the mouse genome. Since binding affinities of Tbx18 and Tbx15 for paired T half-sites was considerably higher than for a single half-site, a cooperative mode of DNA binding seems mandatory. Indeed, we found that Tbx15 and Tbx18 are able to dimerize in the absence of DNA *in vitro* and in cells, providing a mechanism to stabilize weak monomer-DNA interactions. Moreover, the enhanced dimerization by the addition of antibody greatly increased the DNA binding affinity, an effect that was previously reported for other T-box proteins (1, 3). The available DNA-protein co-crystal structure of the *Xenopus* Brachyury homolog Xbra together with the palindromic binding site has implicated critical residues of the T-domain that mediate dimerization (27). Most of these residues are conserved in Tbx18 and Tbx15 (data not shown). However, the binding to paired T half-sites of inverted or directly repeated orientations implies an alternative quaternary structure of the protein dimer-DNA-complex, arguing for additional dimerization interfaces in Tbx18 and Tbx15 proteins. Furthermore, our finding that flanking N- and C-terminal protein regions confer high affinity DNA binding suggests that regions outside the T-box participate in dimer formation.

An additional level of target specificity might be achieved by protein-protein interaction with other DNA binding transcription factors. Our study has shown that Tbx18 can directly bind to the homeodomain transcription factor Nkx2–5 and the zinc finger protein Gata4 *in vitro* as well as in mammalian cells, two proteins that were previously identified as binding partners of Tbx1, Tbx2, Tbx5, and Tbx20 (4–7, 10). During heart development, transcription factors of all three families cooperatively regulate cardiac gene expression programs.

We found that the binding to Nkx2–5 and Gata4 is mediated by the T-box and (more weakly) by the N-terminal region, indicating that both transcription factors either bind to two different sites in the T-box and N-terminal region or bind within the short stretch of overlapping amino acids present in both fusion proteins of Tbx18 (aa 148–157). This is in line with previous studies that have shown that interaction of Tbx5 and Nkx2–5 proteins is mediated both by the N-terminal region outside the T-box as well as by the N-terminal part of the T-box (4). The high conservation of the T-box domain of different family members might thus not only be a prerequisite for shared DNA binding specificity but also for conserved binding to protein interaction partners. Nonetheless, it is likely that specific protein interaction domains are present in the regions outside the T-box, providing an additional level of specificity in target gene recognition by T-box transcription factors.

Repression by Recruitment of Corepressors—Transcription factors of various classes including basic helix-loop-helix, Tcf/HMG (high mobility group), homeodomain, runt domain, and zinc finger domain proteins have previously been reported to function as Groucho-dependent repressors (31). Groucho proteins are known to recruit histone deacetylases (48, 49) that remove acetyl groups from histone tails, thus rendering the chromatin inaccessible for transcriptional activation. Our analysis provides the first evidence that this mode of repression also extends to members of the T-box family of transcription factors. The eh1 motif that mediates binding to the WD40 domain of Groucho was not only identified at a conserved N-terminal position within the vertebrate homologues of Tbx18, Tbx15, Tbx22, and Tbx20 but also in the ancestral *Amphioxus* Tbx15/18/22 protein as well as in the *Drosophila* Tbx20 homologues Midline and H15 (data not shown). This evolutionary conservation strongly implies that all T-box proteins within the Tbx18/15/22/20 branch of the Tbx1 subfamily act as Groucho-dependent repressors. Widespread expression of vertebrate Groucho proteins is compatible with a corepressor function for these T-box proteins in diverse developmental contexts. However, it will be important to determine the functional significance of this interaction *in vivo* since Groucho recruitment might be tissue-specific as shown for the transcription factor Runx3 (50).

Mutation of the eh1 motif resulted in only partial loss of Tbx18 and Tbx15 repression activities, indicating the presence of additional repression domains, *i.e.* interfaces for recruitment of other corepressors. In the case of Tbx15, a recruitment motif for C-terminal-binding protein (CtBP) is present at amino acid positions 39–43. Two members of this corepressor family in the mouse, CtBP1 and CtBP2, also interact with histone deacetylase (HDAC) (51), suggesting an additional mode of gene silencing by Tbx15 that can be experimentally explored in the future. The mode of repression exerted by Tbx15 and Tbx18 is clearly distinct from that of the T-box factors Tbx2 and Tbx3 since the C-terminal motif that mediates repression by direct binding to HDAC1 is not found in Tbx15 and Tbx18 (52). Restriction of Tbx15 and Tbx18 function to transcriptional repression is clearly precocious at this point. The close relative Tbx20 was reported to contain both activation and repression domains, arguing for a more complicated context-dependent transcriptional modulation by T-box proteins (7).

Functional Redundancy of Tbx15 and Tbx18—Tbx15 and Tbx18 form a pair of structurally related T-box proteins. Sequence conservation between Tbx18 and Tbx15 amounts to 92% in the T-box region and extends to short stretches in the less well conserved N- and C-terminal domains, suggesting conservation of important functional interfaces for DNA and protein binding. Indeed, our biochemical analysis of Tbx15 and Tbx18 has demonstrated identical DNA binding properties, subcellular localization, and Groucho-dependent transcriptional repression activities. Together with our finding that Tbx18 and Tbx15 hetero- and homodimerize, this indicates that the two proteins are likely to regulate a similar set of targets when coexpressed in one tissue. Although *Tbx15* and *Tbx18* show highly specific and largely non-overlapping expression during mouse development (39, 53), they are coexpressed in the proximal region of the developing limb bud. Lack of defects in the appendicular skeleton of *Tbx18*$^{-/-}$ mice and mild phenotypic changes in *Tbx15*$^{-/-}$ limbs might thus indicate functional redundancy in the development of this structure.

This biochemical equivalence group is likely to include Tbx22, the third member of the Tbx15/18/22 subgroup in the Tbx1 subgroup of murine T-box genes. The T-box of Tbx22 is highly related to those of Tbx15 and Tbx18, exerting similar DNA binding preference to T half-sites, and also acts as a transcriptional repressor in reporter assays (54). Coexpression of *Tbx18* and *Tbx22* in anterior halves of epithelial somites suggests functional redundancy in anterior-posterior somite patterning and may explain the delayed expansion of posterior somite fates in *Tbx18*$^{-/-}$ embryos (13, 39, 43). Phenotypic characterization of compound mutants of *Tbx15*, *Tbx18*, and *Tbx22* will clarify functional redundancy of these T-box family members *in vivo*.

As a single copy representative of the subgroup is present in urochordates (*Tbx15/18/22* of *Ciona intestinalis*) and in cephalochordates (*Branchiostoma floridae Tbx15/18/22*) (55, 56), the three vertebrate genes probably arose from a chordate-specific precursor by two gene duplication events. Evidence suggests that basic transcriptional properties of the members of this subgroup have been preserved throughout vertebrate evolution. Functional specificity may have been acquired by unique expression domains and by new protein interactions outside the T-box region.

Acknowledgments—We thank Philip Stanier (London) for critical reading of the manuscript and Jeffrey Milbradt (St. Louis), Stefano Stifani (Montreal), Daniel S. Kessler (Philadelphia), Bernhard G. Herrmann (Berlin), and Vincent Christoffels (Amsterdam) for providing plasmids, William C. Claycomb (New Orleans) for the HL-1 cell line, Christoph Klein (Hannover) for help with cell sorting, and Silke Sperling (Berlin) and the Sperling team for supporting the quantitative RT-PCR experiments.

REFERENCES

1. Kispert, A., and Hermann, B. G. (1993) *EMBO J.* **12,** 3211–3220
2. Conlon, F. L., Fairclough, L., Price, B. M., Casey, E. S., and Smith, J. C. (2001) *Development* (*Camb.*) **128,** 3749–3758
3. Sinha, S., Abraham, S., Gronostajski, R. M., and Campbell, C. E. (2000) *Gene* (*Amst.*) **258,** 15–29
4. Hiroi, Y., Kudoh, S., Monzen, K., Ikeda, Y., Yazaki, Y., Nagai, R., and Komuro, I. (2001) *Nat. Genet.* **28,** 276–280
5. Bruneau, B. G., Nemer, G., Schmitt, J. P., Charron, F., Robitaille, L., Caron, S., Conner, D. A., Gessler, M., Nemer, M., Seidman, C. E., and Seidman, J. G. (2001) *Cell* **106,** 709–721
6. Garg, V., Kathiriya, I. S., Barnes, R., Schluterman, M. K., King, I. N., Butler, C. A., Rothrock, C. R., Eapen, R. S., Hirayama-Yamada, K., Joo, K., Matsuoka, R., Cohen, J. C., and Srivastava, D. (2003) *Nature* **424,** 443–447
7. Stennard, F. A., Costa, M. W., Elliott, D. A., Rankin, S., Haast, S. J., Lai, D., McDonald, L. P., Niederreither, K., Dolle, P., Bruneau, B. G., Zorn, A. M., and Harvey, R. P. (2003) *Dev. Biol.* **262,** 206–224
8. Leconte, L., Lecoin, L., Martin, P., and Saule, S. (2004) *J. Biol. Chem.* **279,** 47272–47277
9. Takeuchi, J. K., Mileikovskaia, M., Koshiba-Takeuchi, K., Heidt, A. B., Mori, A. D., Arruda, E. P., Gertsenstein, M., Georges, R., Davidson, L., Mo, R., Hui, C. C., Henkelman, R. M., Nemer, M., Black, B. L., Nagy, A., and Bruneau, B. G. (2005) *Development* (*Camb.*) **132,** 2463–2474
10. Nowotschin, S., Liao, J., Gage, P. J., Epstein, J. A., Campione, M., and Morrow, B. E. (2006) *Development* (*Camb.*) **133,** 1565–1573
11. Naiche, L. A., Harrelson, Z., Kelly, R. G., and Papaioannou, V. E. (2005) *Annu. Rev. Genet.* **39,** 219–239
12. Packham, E. A., and Brook, J. D. (2003) *Hum. Mol. Genet.* **12,** R37–R44
13. Bussen, M., Petry, M., Schuster-Gossler, K., Leitges, M., Gossler, A., and Kispert, A. (2004) *Genes Dev.* **18,** 1209–1221
14. Airik, R., Bussen, M., Singh, M. K., Petry, M., and Kispert, A. (2006) *J. Clin. Investig.* **116,** 663–674
15. Christoffels, V. M., Mommersteeg, M. T., Trowe, M. O., Prall, O. W., de Gier-de Vries, C., Soufan, A. T., Bussen, M., Schuster-Gossler, K., Harvey, R. P., Moorman, A. F., and Kispert, A. (2006) *Circ. Res.* **98,** 1555–1563
16. Singh, M. K., Petry, M., Haenig, B., Lescher, B., Leitges, M., and Kispert, A. (2005) *Mech. Dev.* **122,** 131–144
17. Candille, S. I., Van Raamsdonk, C. D., Chen, C., Kuijper, S., Chen-Tsai, Y., Russ, A., Meijlink, F., and Barsh, G. S. (2004) *PLoS Biol.* **2,** 30–42
18. Habets, P. E., Moorman, A. F., Clout, D. E., van Roon, M. A., Lingbeek, M., van Lohuizen, M., Campione, M., and Christoffels, V. M. (2002) *Genes Dev.* **16,** 1234–1246
19. Hofmann, M., Schuster-Gossler, K., Watabe-Rudolph, M., Aulehla, A., Herrmann, B. G., and Gossler, A. (2004) *Genes Dev.* **18,** 2712–2717
20. Ke, S. H., and Madison, E. L. (1997) *Nucleic Acids Res.* **25,** 3371–3372
21. Wissmuller, S., Kosian, T., Wolf, M., Finzsch, M., and Wegner, M. (2006) *Nucleic Acids Res.* **34,** 1735–1744
22. Claycomb, W. C., Lanson, N. A., Stallworth, B. S., Egeland, D. B., Delcarpio, J. B., Bahinski, A., and Izzo, N. J. (1998) *Proc. Natl. Acad. Sci. U. S. A.* **95,** 2979–2984
23. Leitges, M., Neidhardt, L., Haenig, B., Herrmann, B. G., and Kispert, A. (2000) *Development* (*Camb.*) **127,** 2259–2267
24. Wilkinson, D. G., and Nieto, M. A. (1993) *Methods Enzymol.* **225,** 361–373
25. Kispert, A., Koschorz, B., and Herrmann, B. G. (1995) *EMBO J.* **14,** 4763–4772
26. Sudbeck, P., and Scherer, G. (1997) *J. Biol. Chem.* **272,** 27848–27852
27. Muller, C. W., and Herrmann, B. G. (1997) *Nature* **389,** 884–888
28. Kusch, T., Storck, T., Walldorf, U., and Reuter, R. (2002) *Genes Dev.* **16,** 518–529
29. Copley, R. R. (2005) *BMC Genomics* **6,** 169
30. Smith, S. T., and Jaynes, J. B. (1996) *Development* (*Camb.*) **122,** 3141–3150
31. Fisher, A. L., and Caudy, M. (1998) *Genes Dev.* **12,** 1931–1940
32. Tolkunova, E. N., Fujioka, M., Kobayashi, M., Deka, D., and Jaynes, J. B. (1998) *Mol. Cell. Biol.* **18,** 2804–2814
33. Brantjes, H., Roose, J., van De Wetering, M., and Clevers, H. (2001) *Nucleic Acids Res.* **29,** 1410–1419
34. Casey, E. S., O'Reilly, M. A., Conlon, F. L., and Smith, J. C. (1998) *Development* (*Camb.*) **125,** 3887–3894
35. Lamolet, B., Pulichino, A. M., Lamonerie, T., Gauthier, Y., Brue, T., Enjalbert, A., and Drouin, J. (2001) *Cell* **104,** 849–859
36. Davidson, B., Shi, W., and Levine, M. (2005) *Development* (*Camb.*) **132,** 4811–4818
37. Plageman, T. F., Jr., and Yutzey, K. E. (2004) *J. Biol. Chem.* **279,** 19026–19034
38. Harrelson, Z., Kelly, R. G., Goldin, S. N., Gibson-Brown, J. J., Bollag, R. J., Silver, L. M., and Papaioannou, V. E. (2004) *Development* (*Camb.*) **131,** 5041–5052
39. Kraus, F., Haenig, B., and Kispert, A. (2001) *Mech. Dev.* **100,** 83–86
40. Shiojima, I., Komuro, I., Oka, T., Hiroi, Y., Mizuno, T., Takimoto, E., Monzen, K., Aikawa, R., Akazawa, H., Yamazaki, T., Kudoh, S., and Yazaki, Y. (1999) *J. Biol. Chem.* **274,** 8231–8239
41. Beckers, J., Schlautmann, N., and Gossler, A. (2000) *Mech. Dev.* **95,** 35–46
42. White, P. H., and Chapman, D. L. (2005) *Genes. J. Genet. Develop.* **42,** 193–202
43. Bush, J. O., Lan, Y., Maltby, K. M., and Jiang, R. (2002) *Dev. Dyn.* **225,** 322–326
44. Leimeister, C., Dale, K., Fischer, A., Klamt, B., Hrabe de Angelis, M., Radtke, F., McGrew, M. J., Pourquie, O., and Gessler, M. (2000) *Dev. Biol.* **227,** 91–103
45. Beckers, J., Caron, A., Hrabe de Angelis, M., Hans, S., Campos-Ortega, J. A., and Gossler, A. (2000) *Mech. Dev.* **95,** 23–34
46. Aulehla, A., and Herrmann, B. G. (2004) *Genes Dev.* **18,** 2060–2067
47. Barrantes, I. B., Elia, A. J., Wunsch, K., Hrabe de Angelis, M. H., Mak, T. W., Rossant, J., Conlon, R. A., Gossler, A., and de la Pompa, J. L. (1999) *Curr. Biol.* **9,** 470–480
48. Chen, G., Fernandez, J., Mische, S., and Courey, A. J. (1999) *Genes Dev.* **13,** 2218–2230
49. Choi, C. Y., Kim, Y. H., Kwon, H. J., and Kim, Y. (1999) *J. Biol. Chem.* **274,** 33194–33197
50. Yarmus, M., Woolf, E., Bernstein, Y., Fainaru, O., Negreanu, V., Levanon, D., and Groner, Y. (2006) *Proc. Natl. Acad. Sci. U. S. A.* **103,** 7384–7389
51. Chinnadurai, G. (2002) *Mol. Cell,* **9,** 213–224
52. Vance, K. W., Carreira, S., Brosch, G., and Goding, C. R. (2005) *Cancer Res.* **65,** 2260–2268
53. Agulnik, S. I., Papaioannou, V. E., and Silver, L. M. (1998) *Genomics* **51,** 68–75
54. Andreou, A. M., Pauws, E., Jones, M. C., Singh, M. K., Bussen, M., Doudney, K., Moore, G. E., Kispert, A., Brosens, J. J., and Stanier, S. (2007) *Am. J. Hum. Gen.*, in press
55. Beaster-Jones, L., Horton, A. C., Gibson-Brown, J. J., Holland, N. D., and Holland, L. Z. (2006) *Evol. Dev.* **8,** 119–129
56. Takatori, N., Hotta, K., Mochizuki, Y., Satoh, G., Mitani, Y., Satoh, N., Satou, Y., and Takahashi, H. (2004) *Dev. Dyn.* **230,** 743–753

T-Box Protein Tbx18 Interacts with the Paired Box Protein Pax3 in the Development of the Paraxial Mesoderm

Henner F. Farin[1], Ahmed Mansouri[2] , Marianne Petry[1], and Andreas Kispert[1,3]

[1]From the Institute for Molecular Biology, Medizinische Hochschule Hannover, 30625 Hannover, Germany

[2]From the Department of Molecular Cell Biology, Max-Planck-Institute of Biophysical Chemistry, 37077 Göttingen

[3]Address correspondence to: Andreas Kispert, Medizinische Hochschule Hannover, Institute for Molecular Biology, OE5250, Carl-Neuberg-Str. 1, D-30625 Hannover, Germany. Tel. +49 511 532 4017; Fax: +49 511 5324283; E-mail: kispert.andreas@mh-hannover.de

Published in The Jounal of Biological Chemistry, Vol. 283, No. 37, pp. 25372–25380, September 12, 2008.

Reprinted with permission (http://www.jbc.org/misc/Copyright_Permission.shtml).

T-box Protein Tbx18 Interacts with the Paired Box Protein Pax3 in the Development of the Paraxial Mesoderm*

Received for publication, April 8, 2008, and in revised form, June 27, 2008 Published, JBC Papers in Press, July 21, 2008, DOI 10.1074/jbc.M802723200

Henner F. Farin‡, Ahmed Mansouri§1, Marianne Petry‡, and Andreas Kispert‡2

From the ‡Institute for Molecular Biology, Medizinische Hochschule Hannover, OE5250, Carl-Neuberg-Strasse 1, D-30625 Hannover, Germany and the §Department of Molecular Cell Biology, Max-Planck-Institute of Biophysical Chemistry, 37077 Göttingen, Germany

The compartmentalization of somites along their anterior-posterior axis is crucial to the segmental organization of the vertebral column. Anterior-posterior somite polarity is generated in the anterior presomitic mesoderm by Mesp2 and Delta/Notch signaling and is further maintained by two transcriptional regulators, Uncx4.1 and Tbx18, acting in the posterior and anterior somite compartment, respectively. Here, we report that the paired box transcription factor Pax3 cooperates with the T-box protein Tbx18 in maintaining anterior somite half identity. Our findings that both genes are co-expressed in the anterior presomitic mesoderm and in early somites, that Pax3 and Tbx18 proteins physically interact, and that the loss of *Pax3* gene function enhances the vertebral defects (*i.e.* the gain of vertebral elements derived from posterior somite halves in *Tbx18* mutant mice) suggests that the two proteins cooperatively regulate the gene expression program necessary for maintaining anterior-posterior somite polarity. Genetic interaction of *Pax3* with *Tbx18* and the closely related T-box gene *Tbx15* was also observed in the development of the scapula blade, indicating an additional cooperative function for these genes in the paraxial mesoderm.

The metameric organization of the vertebral column derives from the somites, segmentally repeated units in the paraxial mesoderm. Somites form in a highly periodic and synchronized fashion by condensation and subsequent epithelialization of groups of mesenchymal cells at the anterior end of the presomitic mesoderm (PSM)[3] on both sides of the neural tube. Under the influence of signals from surrounding tissues, somites start to differentiate along their dorso-ventral axis. The ventral part undergoes an epithelial-mesenchymal transition to form the sclerotome, which contains precursors of the vertebral column and parts of the ribs. The dorsal part remains epithelial and generates the dermomyotome, from which skeletal muscles and the dermis of the skin will develop. In addition to differentiation along the dorso-ventral axis, somites become subdivided into distinct anterior and posterior compartments. Anterior-posterior (AP) polarization of somites underlies the segmental arrangement of the peripheral nervous system, since trajectories of neural crest and spinal nerves are confined to anterior somite halves. On the level of the sclerotome, the differential contribution of either compartment to the forming vertebra affects the structure of the axial skeleton. Vertebral bodies, laminae with the spinal processes, the rib heads, and the distal ribs derive from both somite halves, whereas pedicles with their transverse processes and proximal ribs derive from posterior somite halves only (1–3).

Establishment of somitic AP polarity is closely coupled to the segmentation process. Work from a variety of vertebrate model systems has shown that somite formation is governed by an oscillator known as the segmentation clock that operates in the PSM (4, 5). It is now believed that synchronized oscillations of a number of signaling pathways, including Wnt, fibroblast growth factor, and Notch signaling, are involved in the mechanism of the segmentation clock. Gradients of secreted signaling molecules cooperatively define the segmentation border within the anterior PSM. In this region, Notch oscillation is stabilized to a narrow domain, in which cells with a high Notch pathway activity will constitute the posterior half of a newly forming somite. In an adjacent stripe of cells, Notch signaling is suppressed by the action of the basic helix-loop-helix transcription factor Mesp2. The expression domain of *Mesp2* thereby defines the anterior somite half, and its anterior limit demarcates the next segmental border to be formed (6). Correspondingly, loss of Mesp2 activity leads to posteriorization of somites, whereas loss of *Delta-like1* (*Dll1*) gene function and Notch signaling results in somites that bear only features of anterior halves (7).

Molecular players required for the further maintenance of somitic AP polarity have recently surfaced. Genetic evidence from both loss- and gain-of-function studies in the mouse suggest that this process is controlled by the combined action of a pair of transcription factors, the T-box (Tbx) protein Tbx18 and the paired type homeobox protein Uncx4.1, which are expressed in anterior and posterior somite halves, respectively (8, 9). *Uncx4.1* is specifically required for the development of pedicles and proximal ribs (10, 11), elements exclusively derived from the posterior lateral sclerotome. In contrast, loss of *Tbx18* function results in expansion of pedicles and proximal ribs in the cervical and thoracic region of the axial skeleton (12). Notably, the forced misexpression of *Tbx18* in posterior somite

---

* This work was supported by grants from the German Research Council (Deutsche Forschungsgemeinschaft (DFG)) and by the DFG-funded cluster of excellence "REBIRTH" (to A. K.). The costs of publication of this article were defrayed in part by the payment of page charges. This article must therefore be hereby marked "*advertisement*" in accordance with 18 U.S.C. Section 1734 solely to indicate this fact.

[1] Supported by the Dr. Helmut Storz Stiftung and the Max-Planck-Society.

[2] To whom correspondence should be addressed. Tel.: 49-511-5324017; Fax: 49-511-5324283; E-mail: kispert.andreas@mh-hannover.de.

[3] The abbreviations used are: PSM, presomitic mesoderm; aa, amino acids; AP, anterior-posterior; E*n*, embryonic day *n*; NLS, nuclear localization sequence; GST, glutathione *S*-transferase; HA, hemagglutinin.

halves results in reduction of pedicles and proximal ribs (12), suggesting that Tbx18 is sufficient to specify anterior *versus* posterior somite fates. Opposing phenotypic consequences of loss of either factor are based on molecular cross-regulation. In *Uncx4.1* mutants, *Tbx18* expression is derepressed in posterior somite halves, whereas in *Tbx18* mutants, expression of *Uncx4.1* progressively expands in anterior somite halves (12). On the molecular level, Uncx4.1 may therefore act as transcriptional repressor of *Tbx18*, whereas Tbx18 may regulate *Uncx4.1* indirectly by controlling expression of the Notch ligand Dll1 (13). To get further insight into the molecular function of Tbx18, thus into the control of AP-somite compartmentalization, we sought to identify and characterize protein binding partners of Tbx18. This may also help to define transcriptional targets of Tbx18 and their molecular regulation.

Here, we report on the identification of the paired box (Pax) transcription factor Pax3 as a protein binding partner of Tbx18. We characterize this interaction on the biochemical level and define genetically that both transcription factors synergize in the development of the paraxial mesoderm, including anterior-posterior somite compartmentalization and scapula development.

EXPERIMENTAL PROCEDURES

Expression Constructs—Bacterial expression constructs were generated as N-terminal glutathione *S*-transferase (GST)-fusions in pGEX-4T3 (GE Healthcare). Generation of GST-Tbx18 fusion proteins has been described (13), and constructs covering the T-box region of mouse Tbx15 (aa 110–313), human TBX22 (aa 96–291), and mouse Brachyury (aa 41–225) were PCR-amplified from the cDNAs NM_009323, NM_016954, and NM_009309, respectively.

For *in vitro* expression of proteins, cDNA fragments were cloned with C-terminal Myc or HA tags in the vector pSP64 (Promega) that was modified to contain a 5′-β-globin leader and a 3′-β-globin trailer. Fragments encoding Pax3 partial (Fig. 1*D*) and full-length (aa 1–479) proteins were amplified from the mouse cDNA NM_008781. Expression plasmids of full-length Pax1 (aa 1–361), Pax7 (aa 1–503), and Pax9 (aa 1–342) were amplified from mouse cDNAs NM_008780, NM_011039, and NM_011041, respectively. For cytomegalovirus promoter/enhancer-driven expression in cells, the globin leader/cDNA/globin trailer cassette was shuttled into EcoRI and HindIII sites of pcDNA3 (Invitrogen). The expression vector for Tbx18ΔNLS has been described (13). All plasmids were sequenced; details on cloning strategies and primer sequences are available upon request.

Yeast Two-hybrid Screen—The construct for the generation of a fusion protein between the DNA binding domain of GAL4 and Tbx18 (aa 1–345) was cloned into pGBKT7 (Clontech). This bait vector was transformed into the yeast strain AH109 (Clontech), that was subsequently mated to the yeast strain Y187 that was pretransformed with a prey library of poly(T)-primed mouse embryonic day 11.5 (E11.5) whole embryo cDNAs (Clontech) following the manufacturer's instructions. Clones were selected on plates lacking leucine, tryptophan, histidine, and alanine. After this selection step, prey plasmids were isolated, amplified in *Escherichia coli*, and sequenced.

GST Pull-down, Immunofluorescence, and Co-immunoprecipitation Assays—These assays were performed as described (13).

Mice and Genotyping—Mice carrying a null allele of *Pax3* (*Pax3^{lacZ}*) (14), *Tbx18* (*Tbx18^{tm2Akis}* (12) (synonym: *Tbx18^{GFP}*), and *Tbx15* (*Tbx15^{tm1Akis}*) (15) (synonym: *Tbx15^{lacZ}*) were maintained on an outbred (NMRI) background. For the generation of compound mutants, double heterozygous mice were intercrossed. Genomic DNA prepared from yolk sacs or tail biopsies was used for genotyping by PCR (details on PCR strategies are available upon request). For timed pregnancies, vaginal plugs were checked in the morning after mating, and noon was taken as E0.5.

Skeletal Preparations—Skeletal preparations of E14.5 embryos and newborns were prepared essentially as previously described (12). Embryos were fixed in 95% ethanol overnight, and cartilaginous elements were then stained for 2 days in Alcian blue solution (150 mg/liter Alcian blue 8GX in 80% ethanol, 20% acetic acid). Embryos were transferred in methanol and cleared in benzylbenzoate/benzylalcohol (2:1).

In Situ Hybridization Analysis—Whole mount *in situ* hybridization analysis was performed with digoxigenin-labeled antisense riboprobes following a standard procedure (16). Stained specimens were transferred into 80% glycerol prior to documentation on a Leica M420 microscope with a Fujix digital camera HC-300Z. Images were processed in Adobe Photoshop CS. Details about probes are available upon request.

RESULTS

T-box and Pax Proteins Interact in Vitro—In order to identify protein interaction partners of Tbx18, we performed a yeast two-hybrid screen. We initially tested a number of fusion constructs of the GAL4-DNA-binding domain with subregions of Tbx18 protein for their quality as bait. A construct encoding a fusion protein with the N terminus and the T-domain of Tbx18, which was expressed and lacked autoactivation in yeast, was transformed into yeast, and the resulting bait strain was mated to a strain pretransformed with a mouse cDNA library from E11.5 whole embryos. One of the clones identified by the yeast two-hybrid screen harbored a partial cDNA for *Pax3*, a member of the gene family encoding paired box transcription factors (data not shown).

To validate and further investigate the interaction between Tbx18 and Pax3, we performed a series of *in vitro* binding assays using bacterially expressed subregions of Tbx18 fused to GST and *in vitro* expressed HA-tagged Pax3 protein (Fig. 1, *A* and *B*). In GST pull-down assays, Pax3 was specifically bound to GST-Tbx18 fusion proteins harboring the N-terminal domain and the T-box region (GST-Tbx18(N+T)) and the T-box region alone (GST-Tbx18(T)), respectively. Binding was observed neither with GST nor with GST-Tbx18(N) or GST-Tbx18(C), indicating that the T-domain of Tbx18 mediated the binding to Pax3 (Fig. 1*C*).

We next generated a series of deletion mutants of the *Pax3* cDNA for expression *in vitro* as HA-tagged peptides to determine which region of Pax3 confers interaction with Tbx18 (Fig. 1, *D* and *E*). Pax proteins are characterized by the presence of a conserved N-terminal DNA-binding region, the paired domain. Some of the eight murine family members, including

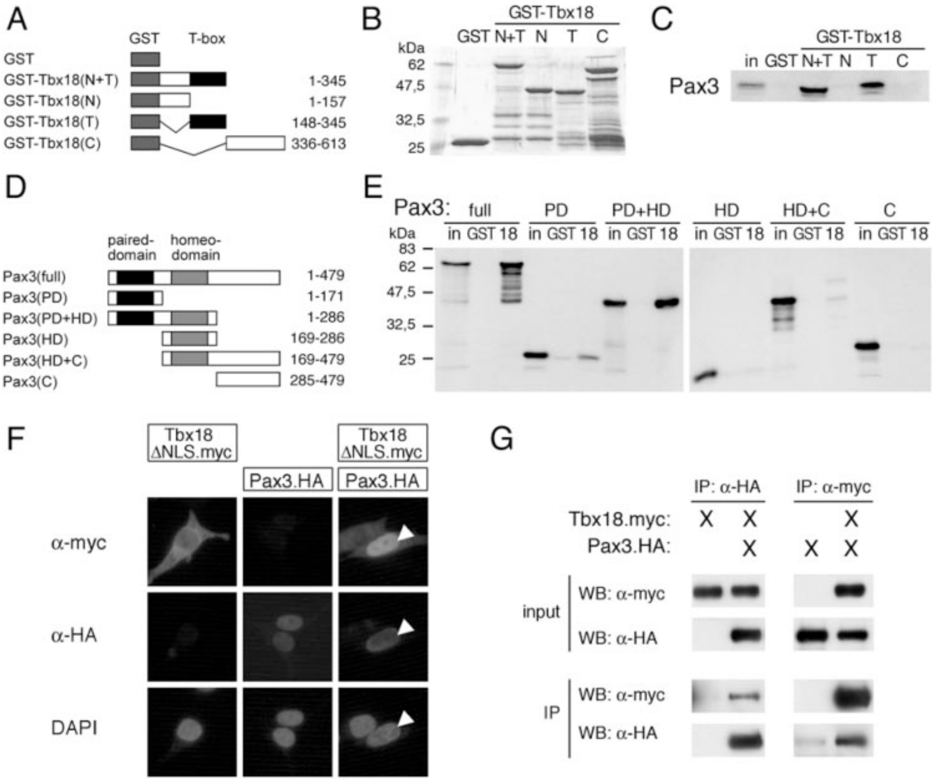

FIGURE 1. **Tbx18 and Pax3 interact *in vitro*.** *A–C*, mapping of the Tbx18 interaction domain with Pax3. *A*, schematic representation of the GST-Tbx18 deletion mutants used in this study; the T-box (*T*) is *shaded* in *black*, and N- and C-terminal domains (*N* and *C*) are shown in *white*. The *numbers* refer to the length of the expressed proteins in aa. *B*, Coomassie Brilliant Blue-stained gel of the purified GST-Tbx18 proteins. *C*, Western blot analysis of HA-tagged Pax3 protein in GST pull-downs. The T-box region of Tbx18 mediates binding to Pax3. *D*, schematic representation of a series of the Pax3 deletion mutants (HA-tagged) with the paired domain (*PD*) marked in *black* and the homeodomain (*HD*) marked in *gray*. *E*, binding analysis of Pax3 peptides to GST alone or GST-Tbx18(N+T) protein (*18*). The paired box region of Pax3 mediates binding to Tbx18. 10% of the input fraction (*in*) was loaded as control. *F*, Pax3 mediates nuclear recruitment of Tbx18ΔNLS in HEK293 cells. HEK293 cells were transfected with expression constructs for Myc-tagged NLS-deficient Tbx18 (Tbx18ΔNLS; *upper row*) in the presence or absence of HA-tagged full-length Pax3 protein (*middle row*). The *white arrowhead* indicates that Tbx18ΔNLS is efficiently relocalized to the nucleus upon co-expression of Pax3 (compare 4′,6-diamidino-2-phenylindole (*DAPI*) nuclear counter staining). *G*, complex formation between Myc-tagged Tbx18 and HA-tagged Pax3 as revealed by co-immunoprecipitation assays in transfected HEK293 cells. Western blot (*WB*) analysis of input fractions and immunoprecipitates (*IP*) using anti-HA or anti-Myc antibodies.

Pax3, additionally contain a homeodomain as a second DNA-binding region. Pax3 peptides containing the paired domain were efficiently bound to GST-Tbx18(N+T), whereas peptides containing the homeodomain only and/or the C terminus of Pax3 were not efficiently retained (Fig. 1*E*). In summary, our *in vitro* binding assays showed that binding of Tbx18 and Pax3 is mediated by the two conserved DNA binding regions, the T-domain and the paired domain.

The interaction between Tbx18 and Pax3 was additionally validated in a mammalian cell system using a nuclear recruitment assay. Transfection of an expression construct for HA-tagged Pax3 revealed constitutive nuclear localization of Pax3. In contrast, Myc-tagged Tbx18 protein lacking the nuclear localization signal (Tbx18ΔNLS) (13) was excluded from the nucleus and localized to the cytoplasm. Upon co-transfection of constructs encoding HA-tagged Pax3 protein and Myc-tagged Tbx18ΔNLS protein, nuclear localization of Tbx18 was regained (Fig. 1*F*), suggesting that Tbx18ΔNLS in complex with Pax3 is shuttled to the nuclear environment.

Furthermore, co-immunoprecipitation assays were performed in HEK293 cells transfected with full-length constructs for Myc-tagged Tbx18 alone or in the presence of HA-tagged Pax3. In immunoprecipitates obtained with the HA antibody, an enrichment of Myc-tagged Tbx18 protein was detected only upon co-transfection of the Pax3 expression construct (Fig. 1*G*, *left*). Conversely, Pax3.HA protein was specifically coimmunoprecipitated with the anti-Myc antibody when Tbx18.Myc protein was present (Fig. 1*G*, *right*), providing further proof for complex formation of Tbx18 and Pax3 in a cellular system.

T-box and Paired Box Interaction Is Promiscuous—We next investigated whether binding of Tbx18 to Pax3 is unique among T-box and Pax proteins or whether Tbx18 and Pax3 interact with additional members of the other family as well. In a GST pull-down assay, we found that, similar to Pax3, the closely related Pax7 and the more divergent proteins Pax1 and Pax9 exhibited binding to the T-domain of Tbx18 (Fig. 2*A*). This interaction was confirmed in the nuclear recruitment assay, where Tbx18ΔNLS was shuttled to the nucleus upon co-expression of HA-tagged Pax1 and Pax9 but not with unrelated nuclear proteins (data not shown).

Conversely, we analyzed if Pax3 is able to bind to other members of the T-box protein family. Therefore, GST fusions of the T-box region of the closely related Tbx15, Tbx18, and Tbx22 proteins and the distant family member Brachyury (Fig. 2*B*) were expressed in bacteria, purified (Fig. 2*C*), and incubated with *in vitro* expressed Pax3 protein. Binding of Pax3 protein was detected to all T-box proteins analyzed; however, binding of Pax3 to Tbx18 was the strongest (Fig. 2*D*).

Together, these findings suggest promiscuity of binding between T-box and paired box regions, but binding affinities between individual family members might differ substantially.

Comparative Expression Analysis of Tbx15, Tbx18, Tbx22, and Pax3—The facts that we only detected Pax3 but not other Pax family member in our yeast two-hybrid screen and the high affinity binding of Tbx18 with Pax3 in the *in vitro* assays prompted us to analyze whether this interaction is functionally relevant *in vivo*. To determine in which tissues such a molecular interaction may occur, we compared the expression patterns of *Pax3* and *Tbx18* and the two closely related *Tbx15* and *Tbx22* genes using *in situ* hybridization analysis of E9.5 wild-type mouse embryos (Fig. 3).

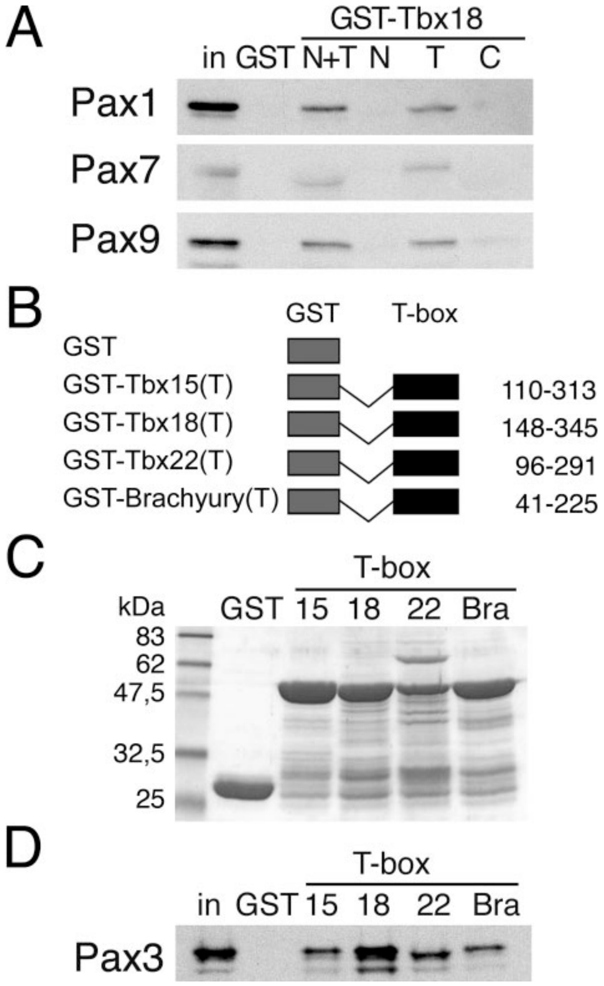

FIGURE 2. **Interaction between T-box and paired box regions is promiscuous.** *A*, Western blot analysis of HA-tagged full-length Pax1, Pax7, and Pax9 proteins in GST pull-downs with GST-Tbx18 fusion protein, as shown in Fig. 1. *B*, schematic representation of GST fusion proteins of the T-box regions of Tbx15, Tbx18, Tbx22, and Brachyury (*Bra*). *C*, visualization of purified GST proteins by Coomassie Brilliant Blue staining. *D*, Western blot analysis of HA-tagged Pax3 protein in GST pull-downs.

At this stage, *Tbx15* expression was confined to the mesenchyme of the forelimb buds (Fig. 3*A*, *arrow*). *Tbx18* was co-expressed with *Tbx15* in this tissue (Fig. 3*B*, *arrow*) but showed additional expression domains in the sinus venosus, the proepicardial organ (Fig. 3*B*, *white arrowhead*), and the head mesenchyme (Fig. 3*B*, *black arrowhead*). In derivatives of the paraxial mesenchyme, *Tbx18* expression was observed in the anterior halves of epithelial somites and additionally in two stripes representing the anterior halves of somites that were about to form (*S0* and *S−1*) (Fig. 3*E*). With differentiation of somites, *Tbx18* expression in anterior somite halves became restricted to the lateral sclerotome (Fig. 3*E*, arrow). *Tbx15* expression was absent during somite development (Fig. 3*A*). However, the closely related *Tbx22* gene was co-expressed with *Tbx18* in anterior halves of somitomeres and early somites (*S−1* to *S1*) (Fig. 3, *C* and *F*). Expression of *Tbx22* in anterior somite halves was then rapidly down-regulated, but expression was reinitiated in forming myotomes (Fig. 3*F*, *arrow*).

Pax3 was strongly expressed in the dorsal neural tube (Fig. 3*D*, *arrow*). Furthermore, *Pax3* expression was found in the anterior PSM and in epithelial somites (Fig. 3, *D* and *G*). Expression was maintained in the dermomyotomal compartment (Fig. 3*G*, *arrow*) and in migrating precursors of the limb musculature (Fig. 3*D*, *arrowhead*) (17).

Hence, *Tbx18*, *Tbx22*, and *Pax3* are co-expressed in the PSM and undifferentiated somites, but expression domains segregate during the differentiation of the sclerotome, myotome, and dermomyotome.

Tbx18 and Pax3 Cooperate in the Development of the Axial Skeleton—The observed physical interaction and the co-expression of *Tbx18* (and *Tbx22*) with *Pax3* during somitogenesis suggested that these factors also interact genetically during this process. We analyzed this possibility by generating embryos compound mutant for null alleles of *Tbx18* ($Tbx18^{GFP}$) and *Pax3* ($Pax3^{lacZ}$). On the outbred background on which we maintained these alleles, $Pax3^{-/-}$ embryos were viable at E14.5. This is in contrast to studies where lethality of $Pax3^{-/-}$ embryos was observed between E13.5 and E14.5 when the mutant allele was kept on an inbred background, such as a mix of C3H/101 and BA/Ca or C57Bl6 (17, 18). $Tbx18^{-/-}$ embryos died shortly after birth as reported before (12).

Mice double heterozygous for $Tbx18^{GFP}$ and $Pax3^{lacZ}$ mutant alleles were viable and fertile and were intercrossed to obtain all possible allelic combinations. We harvested embryos at E14.5 and analyzed the skeletons as a read-out of defects of somite patterning and differentiation. We noted that embryos double homozygous for *Pax3* and *Tbx18* null alleles were severely underrepresented at this stage. Of a total of 123 embryos harvested, we only obtained two double mutants (1.6%) instead of the expected eight (1 of 16; 6.3%). Similarly, the observed number of nine $Tbx18^{-/-}$,$Pax3^{+/-}$ embryos (7.3%) displayed a reduction from the expected value (15 embryos; 1 of 8; 12.5%), suggesting that the removal of one or two copies of one wild-type allele in the mutant background of the other gene dramatically enhanced the severity of the embryonic defects. All other genotypes were found in the expected Mendelian frequencies (data not shown).

In wild-type embryos of E14.5, the cartilagenous preskeleton was invested with a segmental array of orderly spaced ribs and vertebra (Fig. 4*A*). At the thoracic level, ribs were connected to vertebral pedicles (Fig. 4*G*, *black arrowhead*).

Strikingly, in 12 of 30 embryos (40%) double heterozygous for both *Tbx18* and *Pax3* null alleles, we detected isolated expansions of proximal ribs (Fig. 4, *B* and *H*, *white arrowhead*), whereas these malformations were never observed in single heterozygous embryos.

In $Tbx18^{-/-}$ embryos, pedicles and proximal ribs were expanded and formed contiguous cartilagenous bands in the vertebral column at the cervical and thoracic levels and the rib cage, respectively (Fig. 4, *C* (*brackets*) and *I* (*arrowheads*)) (12).

In all $Tbx18^{-/-}$,$Pax3^{+/-}$ embryos analyzed ($n = 9$), expansions of proximal ribs were increased in frequency and extended more caudally (Fig. 4*D*, *brackets*) and medially (Fig. 4*J*, *white arrowheads*) compared with $Tbx18^{-/-}$ embryos. A further expansion of pedicles was not observed (Fig. 4*J*, *black arrowhead*).

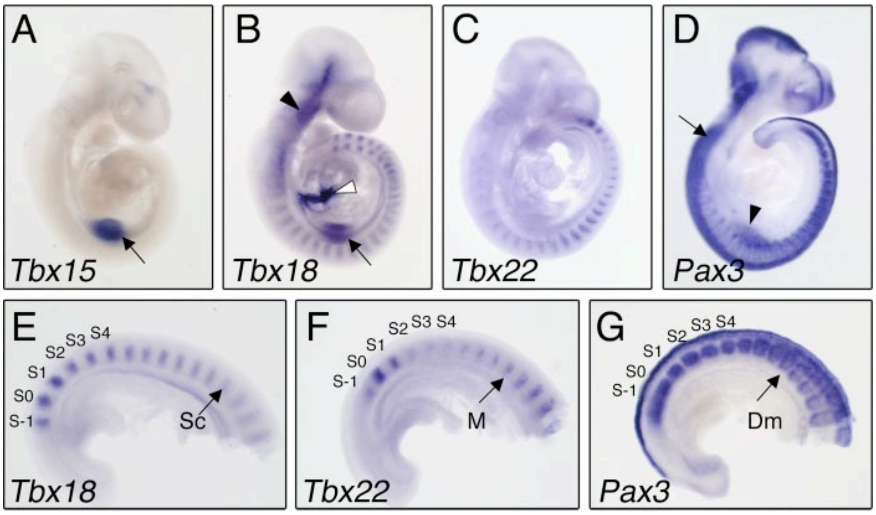

FIGURE 3. **Comparative expression analysis of *Tbx15*, *Tbx18*, *Tbx22*, and *Pax3*.** Whole mount *in situ* hybridization analysis of E9.5 wild-type mouse embryos using RNA probes specific for *Tbx15* (*A*), *Tbx18* (*B* and *E*), *Tbx22* (*C* and *F*), and *Pax3* (*D* and *G*). *A–C*, overview of the expression of *Tbx15* (*A*) in forelimb buds (*arrow*); *Tbx18* (*B*) in the mesenchyme of the forelimb (*arrow*), the proepicardial organ and sinus venosus (*white arrowhead*), and head mesenchyme (*black arrowhead*); and *Tbx22* (*C*). *D*, expression of *Pax3* in the dorsal neural tube (*arrow*) and precursors of limb muscles (*arrowhead*). *E–G*, higher magnification of expression domains in somitogenesis; presumptive (*S−1* and *S0*) and newly formed somites (*S1–S4*) are labeled. *E*, *Tbx18* is expressed in anterior halves of somitomeres (*S0* and *S−1*), epithelial somites, and differentiating sclerotomes (*Sc*). *F*, *Tbx22* in somitomeres and early somites (*S−1* to *S1*) and in the forming myotomes (*M*). *G*, *Pax3* expression can be seen in the anterior PSM (*S−1* to *S0*), the entire epithelial somite, and later in the dermomyotome (*Dm*).

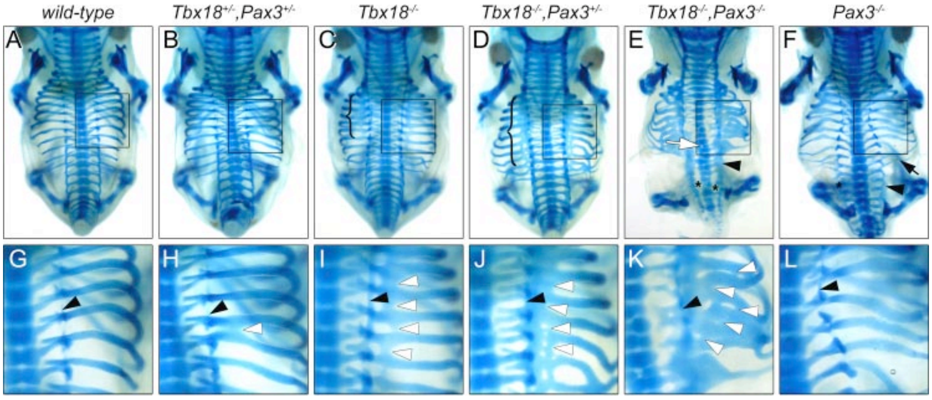

FIGURE 4. **Dose-dependent requirement of *Tbx18* and *Pax3* in the formation of the axial skeleton.** Alcian blue-stained preparations of cartilaginous preskeletons of E14.5 *Tbx18/Pax3* compound mutant embryos with genotypes indicated on the *top*. *A–F*, dorsal views; *G–L*, magnifications of the *boxed regions*. The arrangement of pedicles (*black arrowheads*) and proximal ribs (*white arrowheads*) is highlighted. In contrast to wild-type embryos (*A* and *G*), a fraction of $Tbx18^{+/-}$,$Pax3^{+/-}$-embryos (12 of 30; 40%) displays expansions of proximal ribs (*B* and *H*). $Tbx18^{-/-}$ embryos show contiguous bands of proximal ribs (*C*, *bracket*) and expanded pedicles (*I*, *black arrowhead*). Rib defects are further increased in severity in $Tbx18^{-/-}$,$Pax3^{+/-}$ compound (*D*, *bracket*; *J*, *white arrowheads*) and $Tbx18^{-/-}$,$Pax3^{-/-}$ double homozygous embryos (*K*, *white arrowheads*). In $Tbx18^{-/-}$,$Pax3^{-/-}$ embryos, pedicles and neural arches are contiguous in thoracic and lumbar regions (*E* and *K*, *black arrowheads*) and frequently unconnected to the vertebral bodies (*E*, *asterisks*). The *white arrow* indicates split vertebra. In contrast, fusions of neural arches in *Pax3* single mutants are present mainly in lumbar regions (*F*, *arrowhead*), and rib fusions and bifurcations occur more distally (*F*, *arrow*).

In mutants double homozygous for *Tbx18* and *Pax3* null alleles, the body axis was dramatically shortened (n = 2; Fig. 4*E*). The severity of the skeletal defects in cervical vertebrae was unchanged compared with *Tbx18* mutant embryos. In contrast, the lateral parts of the vertebrae, neural arches and pedicles, were largely expanded at the thoracic and lumbar level (Fig. 4*E*, *black arrowhead*) and frequently misconnected to the vertebral bodies that were often split (Fig. 4*E*, *asterisks* and *white arrow*, respectively). Proximal parts of ribs constituted large contiguous plates of cartilage on both sides of the vertebral column (Fig. 4*K*, *white arrowheads*).

In $Pax3^{-/-}$ embryos, defects of the axial skeleton, including fusions of neural arches of adjacent vertebrae, occurred mainly in the lumbosacral region (Fig. 4*F*, *arrowhead*), and rib fusions and bifurcations were apparent (Fig. 4*F*, *arrow*). However, skeletal defects were generally less severe than the ones described for *Pax3* alleles maintained on inbred genetic backgrounds (17, 18). Notably, and in contrast to *Tbx18* mutants, the proximal ribs were unaffected, and the pedicles were spaced regularly (Fig. 4*L*).

Together, our results demonstrate genetic interaction of *Pax3* and *Tbx18* in the formation of the axial skeleton. Removal of *Pax3* function enhances the phenotypic changes associated with the loss of *Tbx18*, namely the expansion of derivatives of the posterior lateral sclerotome, pedicles, and proximal ribs.

Tbx18 and Pax3 Cooperate in the Maintenance of Anterior Somite Halves—Co-expression of *Tbx18* and *Pax3* in undifferentiated somites suggests that not only the lateral sclerotome but also other somitic compartments could be affected by the combined loss of *Pax3* and *Tbx18* functions. To determine patterning and differentiation of the somitic mesoderm into myotome and sclerotome more carefully, we analyzed expression of molecular markers at E10.5. Within the collected embryos at this stage (n = 221), all genotypes were found in the expected frequencies, indicating that lethality of *Tbx18/Pax3* double mutant embryos occurred between E10.5 and E14.5.

In the E10.5 wild-type embryo, *Myogenin* was expressed in the myotomes in a repeating metameric pattern (Fig. 5*A*) (19). In $Pax3^{-/-}$ embryos, *Myogenin* was segmentally expressed in myotomes, but its hypaxial domain appeared truncated (Fig. 5*C*, *arrowhead*). This is in agreement with the known role of Pax3 as a regulator of migration and survival of myotomal cells (20–23). In *Tbx18* mutant embryos, *Myogenin* expression was unchanged (Fig. 5*B*), and no increase of the $Pax3^{-/-}$ phenotype was observed in double mutants

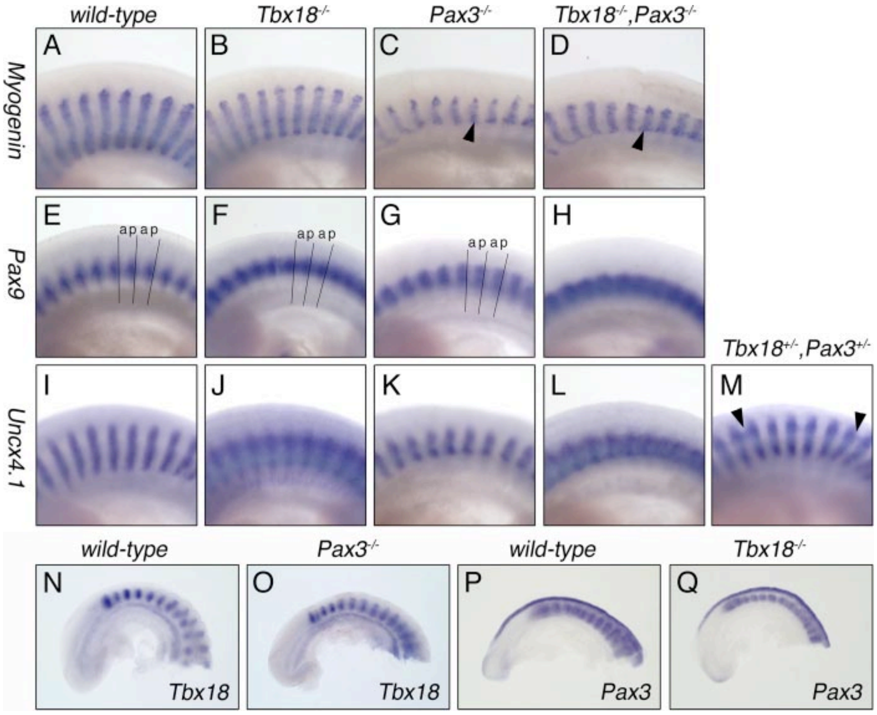

FIGURE 5. ***Tbx18* and *Pax3* cooperate in AP-somite compartmentalization.** *A–M*, expression analysis of somite differentiation markers in E10.5 *Tbx18*/*Pax3* compound mutant embryos. Lateral views of differentiated somites at the interlimb level, with anterior to the *left*. Genotypes are indicated on *top*. *A–D*, *Myogenin* expression reveals that combined loss of *Tbx18* and *Pax3* does not affect formation of the myotome. The hypaxial domain of the dermomyotome is truncated equally in $Pax3^{-/-}$ (*C*) and $Tbx18^{-/-}$,$Pax3^{-/-}$ embryos (*D*, *arrows*). *E–H*, polarized expression of the lateral sclerotome marker *Pax9* is cooperatively regulated by *Tbx18* and *Pax3*. Segment boundaries are highlighted with *black lines*, demonstrating expansion of *Pax9* expression in $Tbx18^{-/-}$ embryos into anterior (*a*) somite halves (*F*). In $Tbx18^{-/-}$ $Pax3^{-/-}$ embryos ($n = 3$), *Pax9* expression appears almost homogenous between anterior and posterior (*p*) somite halves (*H*). Note that in somites of $Pax3^{-/-}$ embryos, polarization of *Pax9* expression is normal (*G*). *I–M*, restriction of *Uncx4.1* expression to the sclerotome of posterior somite halves depends on both *Tbx18* and *Pax3*. Anterior expansion of *Uncx4.1* somite expression in $Tbx18^{-/-}$ embryos (*J*) is further increased by additional loss of *Pax3* ($n = 2$) (*L*). Note that in $Pax3^{-/-}$ embryos, *Uncx4.1* is restricted to the sclerotome of posterior somite halves ($n = 2$) (*K*). Isolated expansions of adjacent *Uncx4.1*-positive segments were observed in 3 of 10 $Tbx18^{+/-}$,$Pax3^{+/-}$ embryos (*M*, *arrowheads*). *N–Q*, comparative *in situ* hybridization analysis of *Tbx18* expression in E9.5 wild-type (*N*) and $Pax3^{-/-}$ embryos (*O*) and of *Pax3* expression in E9.5 wild-type (*P*) and $Tbx18^{-/-}$ embryos (*Q*) shows that somitic expression of *Tbx18* and *Pax3* is independent of each other.

(Fig. 5*D*, *arrowhead*), indicating that both genes do not cooperate in the myogenic program.

Next we analyzed *Pax9* that is expressed in the ventro-lateral sclerotome compartment with a strong up-regulation in the posterior somite halves in wild-type embryos (Fig. 5*E*) (24). In $Pax3^{-/-}$ embryos, polarized expression of *Pax9* was maintained, whereas in $Tbx18^{-/-}$ mutant embryos, *Pax9* expression became progressively homogenous with somite maturation (Fig. 5*F*). In $Tbx18^{-/-}$,$Pax3^{-/-}$ embryos ($n = 3$), *Pax9* expression was homogeneously strong in somites along the entire axial extension (Fig. 5*H*), suggesting that *Pax3* cooperates with *Tbx18* in AP-somite polarization.

To further analyze AP-somite patterning in *Tbx18/Pax3* compound mutant embryos, we used *Uncx4.1* as a marker of the posterior somite half and the caudo-lateral sclerotome (Fig. 5*I*) (9). In *Tbx18* mutant embryos, *Uncx4.1* expression was progressively expanded, demonstrating the gain of posterior and the loss of anterior somite fates (Fig. 5*J*) (12). In *Pax3* mutant embryos ($n = 2$), the domain of *Uncx4.1* was reduced in its dorso-ventral extension. However, AP polarization of expression was largely unaffected (Fig. 5*K*). In $Pax3^{-/-}$,$Tbx18^{-/-}$ embryos ($n = 2$), up-regulation of *Uncx4.1* expression was even enhanced compared with $Tbx18^{-/-}$ embryos, demonstrating a further expansion of posterior somitic identity (Fig. 5*L*). In embryos heterozygous mutant for *Pax3* or *Tbx18*, *Uncx4.1* expression was normal. In contrast, in 3 of 10 double heterozygous embryos, expansions of *Uncx4.1* expression into anterior halves of differentiated somites were detected (Fig. 5*M*, *arrowheads*).

Cooperativity of *Pax3* and *Tbx18* in AP polarization of somites may also derive from mutual regulation of the two genes in early somitogenesis. However, unchanged expression of *Tbx18* in $Pax3^{-/-}$ somites (Fig. 5*O*) and of *Pax3* in $Tbx18^{-/-}$ embryos (Fig. 5*Q*) indicates that genetic cooperativity more likely stems from co-regulation of transcriptional target genes.

Genetic Interactions in the Development of the Scapula Blade—Upon inspection of the skeletal preparations of E14.5 *Tbx18/Pax3* compound mutant embryos (for numbers see above), we detected additional defects in the appendicular skeleton indicative of a genetic interaction of the two genes in scapula development. In 4 of 19 embryos of the $Tbx18^{+/-}$,$Pax3^{-/-}$ genotype (21%), a central hole was present in the scapular blades on both sides (Fig. 6*E*). This phenotype was not observed in $Tbx18^{-/-}$ and $Pax3^{-/-}$ single or in $Tbx18^{-/-}$,$Pax3^{+/-}$ compound mutant embryos (Fig. 6, *A–D*), demonstrating a stronger contribution of *Pax3* in the genesis of this phenotypic trait. Interestingly, the appendicular skeleton of the pelvic girdle was unaffected (data not shown).

Since a similar scapula phenotype has been reported for mice homozygous mutant for *Tbx15* (15, 25), the gene most closely related to *Tbx18*, we decided to test whether *Pax3* shows genetic interaction with *Tbx15* in scapula development as well. All combinations of compound mutants were found in the expected ratio in E14.5 embryos ($n = 63$).

Similar to *Tbx18*, we observed the scapula defect in $Tbx15^{+/-}$,$Pax3^{-/-}$ embryos (Fig. 5*F*), although with a much higher penetrance (5 of 7 embryos; 71%). In addition, we noted that loss of *Pax3* in the *Tbx15* mutant background caused a dose-dependent increase in the phenotypic severity of the scapula defects (Fig. 5, *G–I*). In fact, in *Tbx15*,*Pax3* double mutant embryos, the proximal region of the scapula was almost completely absent (Fig. 5*I*).

Comparative expression analysis of *Pax3* and *Tbx15*, *Tbx18*, and *Tbx22* during limb development revealed co-expression of *Tbx15* and *Tbx18* in mesenchymal precursor cells of the scap-

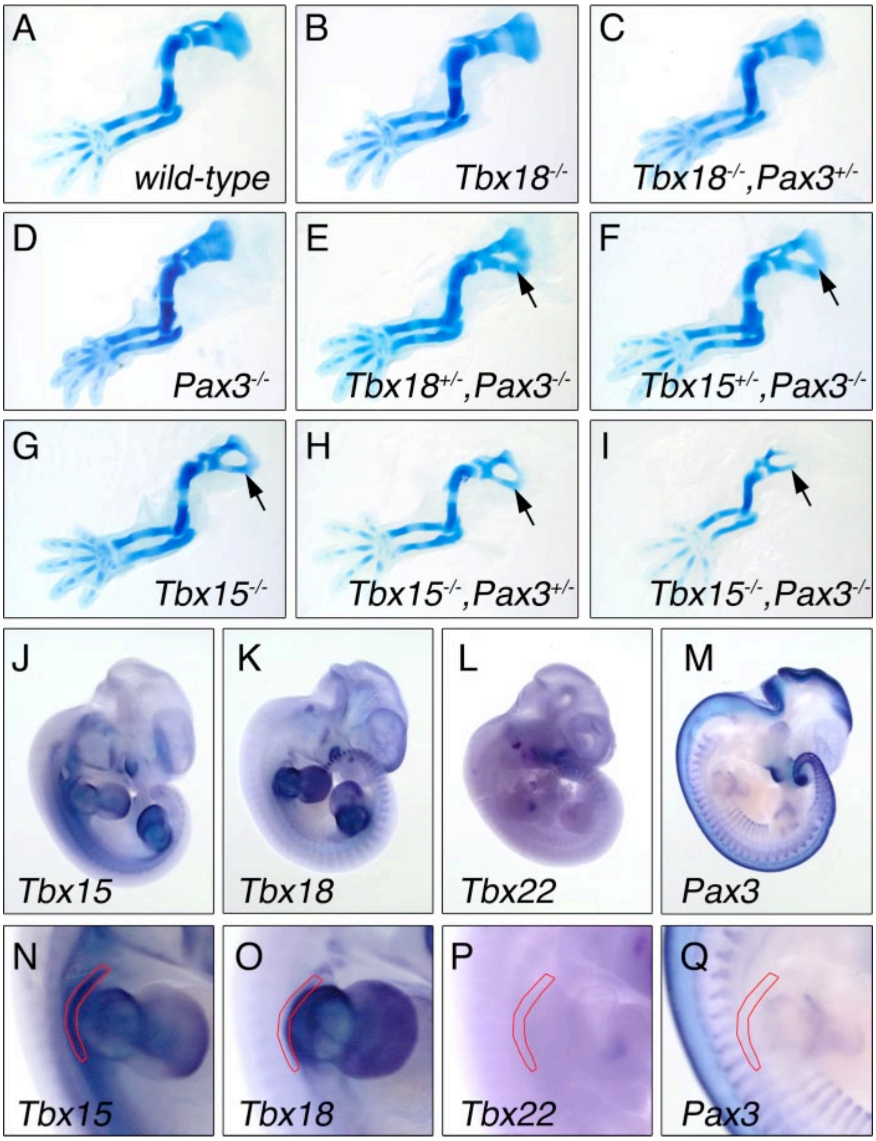

FIGURE 6. **Genetic interaction between *Pax3* and *Tbx18*/*Tbx15* in the development of the scapula blade.** *A–I*, Alcian blue-stained preparations of cartilaginous preskeletons of E14.5 forelimbs of compound mutant embryos. Limbs of *Tbx18*$^{-/-}$ (*B*) and *Pax3*$^{-/-}$ (*D*) single mutants were unaffected. However, in 4 of 19 *Tbx18*$^{+/-}$,*Pax3*$^{-/-}$ embryos (21%), a central hole in the scapula blade is present (*E, arrow*). In an allelic series of *Pax3* and *Tbx15* mutant alleles, we noted a similar defect in *Tbx15*$^{+/-}$,*Pax3*$^{-/-}$ embryos (*F*) although with an increased frequency (5 of 7 embryos; 71%). The scapula defect of *Tbx15*$^{-/-}$ (*G*) embryos increases in severity with the additional loss of one (*H*) or both alleles (*I*) of *Pax3* (*arrows*). *J–Q*, comparative expression analysis of *Tbx15* (*J* and *N*), *Tbx18* (*K* and *O*), *Tbx22* (*L* and *P*), and *Pax3* (*M* and *Q*) in the forelimb region. Shown is an overview of expression patterns in E11.5 wild-type embryos (*A–I*) and a higher magnification of forelimb buds (*N–Q*). *Tbx15* and *Tbx18* are co-expressed in the proximal region of the limb bud, whereas *Tbx22* and *Pax3* are not expressed. In *N–Q*, the scapula-forming region (26) is surrounded with a *red line*.

ula in the proximal region of the E11.5 embryo limb bud (Fig. 6, *J*, *K*, *N*, and *O*) (26). Expression of *Tbx22* was not detected in this region (Fig. 6, *L* and *P*). Surprisingly, *Pax3* was not expressed in these cells (Fig. 6, *M* and *Q*), suggesting that scapular defects might arise from an earlier requirement of *Tbx15*, *Tbx18*, and/or *Pax3* in precursor cells of the somitic mesoderm from which the scapula is derived.

DISCUSSION

Members of the T-box and the paired box families of transcriptional regulators control a diverse array of processes during vertebrate embryonic development. Here, we provide evidence that two individual members of these gene families, *Tbx18* and *Pax3*, cooperatively regulate subprograms in the development of the axial and appendicular skeletons. Direct interaction of Tbx18 and Pax3 proteins *in vitro* and in mammalian cells, co-expression of *Tbx18* and *Pax3* in the anterior PSM and in newly formed somites, and enhancement of phenotypic defects of *Tbx18* mutant embryos upon loss of *Pax3* gene function in the derivatives of the lateral sclerotome and the scapula blade suggest that these proteins cooperatively regulate gene expression programs necessary for the maintenance of the AP-somite compartmentalization and the formation of the scapula blade.

Tbx18 and Pax3 Cooperate in the Maintenance of AP-somite Polarity—Loss-of-function mutations of *Pax3* cause a wide array of developmental defects. In mice, the spontaneous *Pax3* mutation *Splotch* causes the lack of limb muscles, spina bifida and exencephaly, and defects in neural crest derivatives (27). Human patients with impaired *Pax3* function suffer from Waardenburg syndrome (28), a disease complex characterized by varying degrees of deafness, defects in structures arising from the neural crest, and pigmentation anomalies. These defects have been conceptualized by a functional requirement for *Pax3* in survival, migration, and differentiation of the hypaxial dermomyotome and the neural crest (20–23).

In the present study, we report on the genetic interaction of *Pax3* and *Tbx18* that results in phenotypic alterations affecting the development of the axial skeleton, demonstrating that beyond its well established function in the dermoyotome, *Pax3* also affects the development of the sclerotomal lineage.

In *Tbx18* mutant embryos, pedicles, and proximal ribs, derivatives of the posterior lateral sclerotome are expanded. This phenotype was traced back to a failure in maintaining the compartmentalization of somites into distinct anterior and posterior halves (12). The severity of the *Tbx18* mutant phenotype was dose-dependently increased by loss of one or two alleles of *Pax3*, resulting in an even stronger loss of anterior somite identity and expansion of elements derived from the posterior somite halves. Most notably, in double heterozygous embryos, we observed expansions of proximal ribs, which we never detected in single heterozygotes. On the molecular level, these phenotypic changes were paralleled by a further expansion of the expression domain of *Uncx4.1*, demonstrating a requirement of both *Pax3* and *Tbx18* in maintenance of the anterior somite fate.

Tbx18 and *Pax3* are coexpressed in the anterior PSM and epithelial somites, but expression domains subsequently segregate to the anterior lateral sclerotome in the case of *Tbx18* and the dermomyotome for *Pax3*, respectively. This and the finding that Pax3 and Tbx18 interact on the protein level (see below) suggest that Pax3 and Tbx18 cooperativity results from molecular interaction occurring in early somite development.

It is noteworthy that a functional requirement for *Pax3* in early somite development has previously also been suggested by Schubert *et al.* (17), who studied defects of the axial skeleton in the *Pax3* mutant mice maintained on the C57/Bl6 inbred genetic background. There, defects in AP-somite patterning and disturbed somite boundaries were noted and also correlated with *Pax3* expression during early somite formation. The skeletal phenotype of *Tbx18*/*Pax3* double heterozygous embryos exhibited a partial penetrance only, further indicating that the function of *Pax3* is subject to genetic modification. Genetic modifiers might be represented by other members of the T-box and paired box gene families that are co-expressed with *Pax3* and *Tbx18* in early somitogenesis. We have shown that *Tbx22*, a gene closely related to *Tbx18*, is co-expressed with *Tbx18* in anterior somite halves and exhibits similar biochemical properties (13, 29). Similarly, *Pax3* gene function might be partially compensated by *Pax1* and *Pax9*, which are co-expressed with *Pax3* in early somites (24). Since we have shown that Pax3 can bind to other T-box family members, including Tbx22, and that Tbx18 can also interact with Pax1 and Pax9 *in vitro*, a complex network of Pax and T-box proteins may cooperate in early somite development.

The *Tbx18*/*Pax3* double mutants displayed contiguous cartilagenous elements, similar to *Mesp2* mutant embryos, which have completely caudalized somites (30). Moreover, isolated expansions of proximal ribs, as seen in the *Tbx18*/*Pax3* double heterozygotes, have also been reported for a hypomorphic allele of *Mesp2* (31). Although the expression of *Mesp2* is unchanged in *Tbx18*/*Pax3* double mutants (data not shown), the somitic expression of *Tbx18* is absent, and the expression of *Pax3* is strongly reduced in *Mesp2* null embryos (32, 33), arguing that after the establishment of somite AP polarity, *Tbx18* and *Pax3* act downstream of *Mesp2* to maintain AP-somite compartmentalization.

The cellular and genetic programs that are co-regulated by Tbx18 and Pax3 are currently unclear. We have previously hypothesized that Tbx18 controls maintenance of anterior somite fates by direct repression of *Delta-like 1* (*Dll1*) transcription (13) and, thus, suppression of Notch signaling that confers posterior somite fates (7). When testing the same *Dll1* promoter fragment in transactivation assays using HeLa cells, we failed to detect a cooperative effect of Pax3 and Tbx18 on *Dll1* repression (data not shown). However, elements mediating Pax3 binding may reside in promoter regions outside the fragment tested. A role for Pax3 as a transcriptional repressor that synergizes with Tbx18 is compatible with the described interaction of Pax3 with the transcriptional co-repressors HIRA and Daxx (34).

Pax3 and Tbx18 Interaction Is Mediated by Conserved DNA-binding Regions—In this study, we identified Pax3 as a binding partner of Tbx18 in a yeast two-hybrid screen and validated this interaction *in vitro* and in mammalian cells. We mapped the interaction domain to the T-box region of Tbx18 and the paired domain of Pax3, demonstrating that these DNA-binding domains have an additional role as protein-protein interaction motifs. Although we and others have shown that the T-box region mediates binding to the homeobox region in other homeodomain transcription factors, including Nkx2-5 (13, 35), the homeodomain of Pax3 was not efficiently bound by Tbx18, suggesting that interaction of DNA-binding regions is selective.

However, we found that the interaction between paired box and T-box regions is promiscuous among divergent members of both families, suggesting functional co-operativity of other T-box and Pax proteins in tissues of co-expression. One example has previously been presented by the pair of Tbx5 and Pax6 that may cooperate to regulate dorso-ventral patterning of the optic cup (36).

Interaction among different classes of DNA-binding transcription factors is likely to represent a common mechanism to increase specificity of target gene recognition. For T-box proteins, the combinatorial function with other classes of DNA-binding proteins in target promoter regulation is well established. One example is the interaction of Tbx2, Tbx5, Tbx18, and Tbx20 with the transcription factors Gata4 and Nkx2–Nkx5 to regulate cardiac expression of *Nppa* (*natriuretic peptide precursor type a*) (13, 35, 37–41). Likewise, Pax proteins have been shown to interact with a number of different DNA-binding proteins, including Pax3 interacting with Sox10 and Mox2 and Pax6 binding to pRB (34). Future approaches for the identification of target genes of Tbx18 could benefit from a search of the combined presence of conserved T-sites and paired binding sites (42).

Pax3 Cooperates with Tbx15 and Tbx18 in the Development of the Scapula Blade—Our analysis of the phenotypes of *Tbx18*/*Pax3* compound mutants uncovered an additional requirement for both genes in the formation of the scapula blade. In compound mutant embryos, the scapula blade exhibited a central hole. In addition, loss of *Pax3* dose-dependently increased the severity of the scapula defect in the mutants for *Tbx15* (15, 25), the T-box gene most highly related to *Tbx18*.

The formation of the scapula blade, the thin posterior extension of the shoulder girdle is unusual in the respect that it neither derives from the sclerotomal cells of the somite nor from the lateral plate mesoderm like the limb skeleton but from a set of eight dermomyotomes from somites 17 to 24 as revealed by chick-quail chimeric analysis (43). Hence, a common Pax3 positive pool of precursor cells contributes to both limb muscles and the scapula. Under the influence of signaling pathways from the surroundings, including the surface ectoderm, the subpool of scapula precursor cells switches expression from Pax3 to Pax1 and enters chondrogenic differentiation (44). The scapula blade is an extremely thin bone that is exquisitely sensitive to slight alterations in proliferation and thus reduction of the pool of precursor cells. Since we did not detect co-expression of *Pax3* with *Tbx15* and *Tbx18* in the scapula-forming region (26), *Pax3* and *Tbx15/Tbx18* may act subsequently rather than simultaneously. Loss of *Pax3* function my lead to a reduction of the dermomyotomal precursor pool that becomes available for *Tbx15/Tbx18* to act on. Further loss of *Tbx15* and *Tbx18* function may then reduce the number of mesenchymal precursor cells of the scapula under a critical threshold required for the condensation and/or chondrification process. Alternatively, Pax3 protein may persist in the precursor cells of the scapula for some time, given an opportunity for molecular interaction with these T-box transcription factors.

Interestingly, *Tbx15* has been shown to synergize with a number of other transcription factor genes, including *Gli3* and aristaless-type homeobox genes (*Alx4* and *Cart1*) in scapula development (25), arguing for a complex network of developmental regulators involved in patterning/differentiation of this bone.

Acknowledgment—We thank Eric Olsen (Southwestern Medical Center) for the Myogenin probe.

REFERENCES

1. Goldstein, R. S., and Kalcheim, C. (1992) *Development* **116,** 441–445
2. Aoyama, H., and Asamoto, K. (2000) *Mech. Dev.* **99,** 71–82
3. Christ, B., Huang, R., and Scaal, M. (2007) *Dev. Dyn.* **236,** 2382–2396
4. Aulehla, A., and Herrmann, B. G. (2004) *Genes Dev.* **18,** 2060–2067
5. Saga, Y. (2007) *Dev. Dyn.* **236,** 1450–1455
6. Morimoto, M., Takahashi, Y., Endo, M., and Saga Y. (2005) *Nature* **435,** 354–359
7. Barrantes, I. B., Elia, A. J., Wunsch, K., Hrabe de Angelis, M. H., Mak, T. W., Rossant, J., Conlon, R. A., Gossler, A., and de la Pompa, J. L. (1999) *Curr. Biol.* **9,** 470–480
8. Kraus, F., Haenig, B., and Kispert, A. (2001) *Mech. Dev.* **100,** 83–86
9. Neidhardt, L. M., Kispert, A., and Herrmann, B. G. (1997) *Dev. Genes Evol.* **207,** 330–339
10. Leitges, M., Neidhardt, L., Haenig, B., Herrmann, B. G., and Kispert, A. (2000) *Development* **127,** 2259–2267
11. Mansouri, A., Voss, A. K., Thomas, T., Yokota, Y., and Gruss, P. (2000) *Development* **127,** 2251–2258
12. Bussen, M., Petry, M., Schuster-Gossler, K., Leitges, M., Gossler, A., and Kispert, A. (2004) *Genes Dev.* **18,** 1209–1221
13. Farin, H. F., Bussen, M., Schmidt, M. K., Singh, M. K., Schuster-Gossler, K., and Kispert, A. (2007) *J. Biol. Chem.* **282,** 25748–25759
14. Mansouri, A., Pla, P., Larue, L., and Gruss, P. (2001) *Development* **128,** 1995–2000
15. Singh, M. K., Petry, M., Haenig, B., Lescher, B., Leitges, M., and Kispert, A. (2005) *Mech. Dev.* **122,** 131–144
16. Wilkinson, D. G., and Nieto, M. A. (1993) *Methods Enzymol.* **225,** 361–373
17. Schubert, F. R., Tremblay, P., Mansouri, A., Faisst, A. M., Kammandel, B., Lumsden, A., Gruss, P., and Dietrich, S. (2001) *Dev. Dyn.* **222,** 506–521
18. Henderson, D. J., Conway, S. J., and Copp, A. J. (1999) *Dev. Biol.* **209,** 143–158
19. Edmondson, D. G., and Olson, E. N. (1989) *Genes Dev.* **3,** 628–640
20. Williams, B. A., and Ordahl, C. P. (1994) *Development* **120,** 785–796
21. Bober, E., Franz, T., Arnold, H. H., Gruss, P., and Tremblay, P. (1994) *Development* **120,** 603–612
22. Daston, G., Lamar, E., Olivier, M., and Goulding, M. (1996) *Development* **122,** 1017–1027
23. Borycki, A. G., Li, J., Jin, F., Emerson, C. P., and Epstein, J. A. (1999) *Development* **126,** 1665–1674
24. Neubüser, A., Koseki, H., and Balling, R. (1995) *Dev. Biol.* **170,** 701–716
25. Kuijper, S., Beverdam, A., Kroon, C., Brouwer, A., Candille, S., Barsh, G., and Meijlink, F. (2005) *Development* **132,** 1601–1610
26. Pellegrini, M., Pantano, S., Fumi, M. P., Lucchini, F., and Forabosco, A. (2001) *Dev. Biol.* **232,** 149–156
27. Epstein, D. J., Vogan, K. J., Trasler, D. G., and Gros, P. (1993) *Proc. Natl. Acad. Sci. U. S. A.* **90,** 532–536
28. Tassabehji, M., Read, A. P., Newton, V. E., Patton, M., Gruss, P., Harris, R., and Strachan, T. (1993) *Nat. Genet.* **3,** 26–30
29. Andreou, A. M., Pauws, E., Jones, M. C., Singh, M. K., Bussen, M., Doudney, K., Moore, G. E., Kispert, A., Brosens, J. J., and Stanier, P. (2007) *Am. J. Hum. Genet.* **81,** 700–712
30. Saga, Y., Hata, N., Koseki, H., and Taketo, M. M. (1997) *Genes Dev.* **11,** 1827–1839
31. Morimoto, M., Kiso, M., Sasaki, N., and Saga, Y. (2006) *Dev. Biol.* **300,** 687–698
32. Takahashi, Y., Yasuhiko, Y., Kitajima, S., Kanno, J., and Saga, Y. (2007) *Dev. Biol.* **304,** 593–603
33. Takahashi, Y., Takagi, A., Hiraoka, S., Koseki, H., Kanno, J., Rawls, A., and Saga, Y. (2007) *Dev. Dyn.* **236,** 1484–1494
34. Buckingham, M., and Relaix, F. (2007) *Annu. Rev. Cell Dev. Biol.* **23,** 645–673
35. Hiroi, Y., Kudoh, S., Monzen, K., Ikeda, Y., Yazaki, Y., Nagai, R., and Komuro, I. (2001) *Nat. Genet.* **28,** 276–280
36. Leconte, L., Lecoin, L., Martin, P., and Saule, S. (2004) *J. Biol. Chem.* **279,** 47272–47277
37. Bruneau, B. G., Nemer, G., Schmitt, J. P., Charron, F., Robitaille, L., Caron, S., Conner, D. A., Gessler, M., Nemer, M., Seidman, C. E., and Seidman, J. G. (2001) *Cell* **106,** 709–721
38. Garg, V., Kathiriya, I. S., Barnes, R., Schluterman, M. K., King, I. N., Butler, C. A., Rothrock, C. R., Eapen, R. S., Hirayama-Yamada, K., Joo, K., Matsuoka, R., Cohen, J. C., and Srivastava, D. (2003) *Nature* **424,** 443–447
39. Stennard, F. A., Costa, M. W., Elliott, D. A., Rankin, S., Haast, S. J., Lai, D., McDonald, L. P., Niederreither, K., Dolle, P., Bruneau, B. G., Zorn, A. M., and Harvey, R. P. (2003) *Dev. Biol.* **262,** 206–224
40. Habets, P. E., Moorman, A. F., Clout, D. E., van Roon, M. A., Lingbeek, M., van Lohuizen, M., Campione, M., and Christoffels, V. M. (2002) *Genes Dev.* **16,** 1234–1246
41. Plageman, T. F., Jr., and Yutzey, K. E. (2004) *J. Biol. Chem.* **279,** 19026–19034
42. Ovcharenko, I., and Nobrega, M. A. (2005) *Nucleic Acids Res.* **33,** W403–W407
43. Huang, R., Christ, B., and Patel, K. (2006) *Anat. Embryol.* **211,** Suppl. 1, 65–71
44. Huang, R., Zhi, Q., Patel, K., Wilting, J., and Christ, B. (2000) *Development* **127,** 3789–3794

TBX15 Mutations Cause Craniofacial Dysmorphism, Hypoplasia of Scapula and Pelvis, and Short Stature in Cousin Syndrome

Ekkehart Lausch[1], Pia Hermanns[1], Henner F. Farin[2], Yasemin Alanay[3], Sheila Unger[1,4], Sarah Nikkel[1,5], Christoph Steinwender[1], Gerd Scherer[4], Jürgen Spranger[1], Bernhard Zabel[1,4], Andreas Kispert[2], and Andrea Superti-Furga[1]*

[1]Centre for Pediatrics and Adolescent Medicine, Department of Pediatrics, University of Freiburg, 79106 Freiburg, Germany

[2]Institute for Molecular Biology, Medizinische Hochschule Hannover, 30625 Hannover, Germany

[3]Department of Pediatrics, Ihsan Dogramaci Children's Hospital, Hacettepe University, 06100 Sihhiye, Ankara, Turkey

[4]Institute of Human Genetics, University of Freiburg, 79106 Freiburg, Germany

[5]Department of Genetics, Children's Hospital of Eastern Ontario, Ottawa, Ontario K1H 8L1, Canada

*Correspondence: asuperti@uniklinik-freiburg.de

Published in The American Journal of Human Genetics 83, 649–655, November 7, 2008.

Reprinted with permission
(http://download.cell.com/images/EdImages/ajhg/AJHG_Information_for_Authors.pdf).

TBX15 Mutations Cause Craniofacial Dysmorphism, Hypoplasia of Scapula and Pelvis, and Short Stature in Cousin Syndrome

Ekkehart Lausch,[1] Pia Hermanns,[1] Henner F. Farin,[2] Yasemin Alanay,[3] Sheila Unger,[1,4] Sarah Nikkel,[1,5] Christoph Steinwender,[1] Gerd Scherer,[4] Jürgen Spranger,[1] Bernhard Zabel,[1,4] Andreas Kispert,[2] and Andrea Superti-Furga[1,*]

Members of the evolutionarily conserved T-box family of transcription factors are important players in developmental processes that include mesoderm formation and patterning and organogenesis both in vertebrates and invertebrates. The importance of T-box genes for human development is illustrated by the association between mutations in several of the 17 human family members and congenital errors of morphogenesis that include cardiac, craniofacial, and limb malformations. We identified two unrelated individuals with a complex cranial, cervical, auricular, and skeletal malformation syndrome with scapular and pelvic hypoplasia (Cousin syndrome) that recapitulates the dysmorphic phenotype seen in the Tbx15-deficient mice, *droopy ear*. Both affected individuals were homozygous for genomic *TBX15* mutations that resulted in truncation of the protein and addition of a stretch of missense amino acids. Although the mutant proteins had an intact T-box and were able to bind to their target DNA sequence in vitro, the missense amino acid sequence directed them to early degradation, and cellular levels were markedly reduced. We conclude that Cousin syndrome is caused by TBX15 insufficiency and is thus the human counterpart of the *droopy ear* mouse.

We studied two unrelated girls of German (patient 1) and Turkish (patient 2) ancestry. The girls shared an identical phenotype consisting of short stature and macrocephaly. Patient 1 had a birth length of 43 cm (−2.4 standard deviation [SD]) and head circumference of 38 cm (+ 0.83 SD) and an adult height of 115 cm (−8.18 SD) and a head circumference of 61.5 cm (+4.12 SD). Patient 2 at her most recent follow-up at 10 years of age had a height of 105 cm (−4.41 SD) and a head circumference of 53 cm (50th percentile). Their dysmorphic features included frontal bossing, narrow palpebral fissures with deep set globes and hypertelorism, strabismus, low-set ears with posterior rotation and dysplasia of the conchae, narrow auditory canals and hypoacusis, a short neck with redundant skinfolds, and a low hairline (Figure 1). The habitus of both girls was characterized by macrocephaly, fixed flexion at the elbow joints, a short neck, and leg shortening caused by bilateral dislocation of the hips and hip flexion. The main radiographic features were hypoplastic scapulae and iliac bones, short femurs, humeroradial synostosis, and moderate brachydactyly. In addition, the skull base was abnormally shaped, resulting in markedly low attachment of the ears and in caudal displacement of the occipital bone (Figure 2). Both girls had normal intelligence and attended normal school (at age 12 years; patient 2) or college (at age 19 years; patient 1). Both parent couples were consanguineous (second and first cousins, respectively) and showed none of the clinical and radiographic signs seen in their daughters. Patient 1 had been given a diagnosis of campomelic dysplasia (MIM 114290) because of scapular and iliac hypoplasia; patient 2 had been diagnosed with Kosenow scapuloiliac dysostosis (MIM 169550). However, their phenotype did not fit either campomelic dysplasia or Kosenow scapuloiliac dysostosis; sequence analysis of the *SOX9* gene (MIM 608160) was normal. We found that the dysmorphic pattern in these girls corresponded closely to a condition described by Cousin et al. in 1982[1] as "*Dysplasie pelvi-scapulaire familiale avec anomalies épiphisaires, nanisme, et dysmorphies*" (familial pelvis-scapular dysplasia with epiphyseal anomalies, dwarfism, and dysmorphisms; listed in OMIM as Cousin syndrome or pelviscapular dysplasia; MIM 260660). Cousin syndrome has not been reported again since the original description, although some patients reported as having Kosenow syndrome may in fact have had Cousin syndrome.[2]

Guided by the findings of scapular hypoplasia and abnormal cranio-facio-cervical morphology, we identified the *Tbx15*-deficient mouse phenotype as a possible homolog to Cousin syndrome. Murine *Tbx15* deficiency occurs as the result of a deletion involving several exons of *Tbx15* in the spontaneous mouse mutant, *droopy ear* (*de*)[3], and has been reproduced by targeted disruption of the gene.[4,5] First described in 1959, *droopy ear* exhibits a complex craniofacial malformation including small, widely spaced eyes with short palpebral fissures, a broad nasal area, a shortened skull held in an elevated position, misshapen and rotated external ears, and an abnormal coat-color patterning.[3,6] The skeletal phenotype of *Tbx15*-inactivated mice includes

[1] Centre for Pediatrics and Adolescent Medicine, Department of Pediatrics, University of Freiburg, 79106 Freiburg, Germany; [2] Institute of Molecular Biology, Medizinische Hochschule Hannover, 30625 Hannover, Germany; [3] Department of Pediatrics, Ihsan Dogramaci Children's Hospital, Hacettepe University, 06100 Sihhiye, Ankara, Turkey; [4] Institute of Human Genetics, University of Freiburg, 79106 Freiburg, Germany; [5] Department of Genetics, Children's Hospital of Eastern Ontario, Ottawa, Ontario K1H 8L1, Canada
*Correspondence: asuperti@uniklinik-freiburg.de
DOI 10.1016/j.ajhg.2008.10.011. ©2008 by The American Society of Human Genetics. All rights reserved.

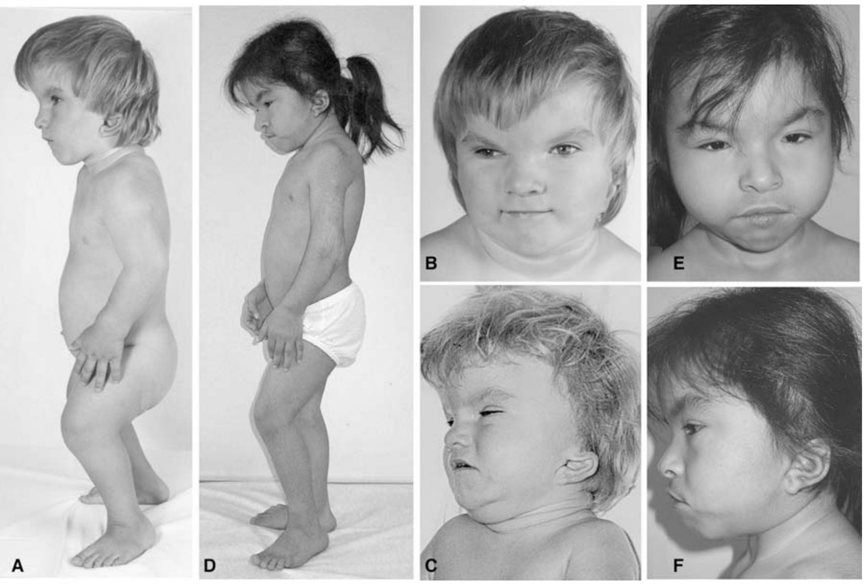

Figure 1. Clinical Features of the Two Girls with Cousin Syndrome and TBX15 Mutations
Patient 1 is age 5 yr in (A) and (B) and age 3 yr in (C); patient 2 is age 10 yr in (D), (E), and (F). The main features are bossing, malar hypoplasia, and a small chin; narrow palpebral fissures; a short neck with redundant skinfolds; low-set, posteriorly rotated, and dysplastic external ears; apparent femoral shortening because of femoral head dislocation; and short stature.

small overall size, hypoplastic scapulae, moderate shortening of several long bones, and a dysmorphogenesis of cranial bones and cervical vertebrae, including vertical displacement of the supraoccipital bone, a small basiooccipital bone, a small foramen magnum, and changes in the shape of the squamosum and of the first and second vertebrae.[4,5] These changes were reminiscent of those observed in the two patients studied.

Peripheral blood DNA was obtained with appropriate fully informed consent from the two individuals with Cousin syndrome and from their parents. Human studies were approved by the ethical review boards of the two hospitals (Freiburg and Ankara). The TBX15 genomic sequences were determined with PCR amplifications of individual exons by standard methods; primer sequences were designed with the TBX15 genomic sequences available at Ensembl (see Web Resources; accession number ENSG00000092607). We studied the consequences of the mutatons by inserting the mutations into TBX15 expression vectors. TBX15 was amplified from normal human fibroblast cDNA, oligonucleotides were based on transcript ENST00000207157 (TBX15S, 496 amino acids), and transcript ENST00000369429 (TBX15L, 602 amino acids). PCR products were inserted into pCRII-TOPO (Invitrogen), the disease-associated mutations TBX15-1042 delA, TBX15-1044 delA, and the deletion mutant TBX15-ΔC (amino acids 1–344, stop codon at base pair 1045) were introduced by site-directed mutagenesis. Wild-type and mutated ORFs were fully sequence verified and subcloned into pBABE-puro,[7] pBABE-EGFP,[8] and pCDNA3 (Invitrogen). N-terminal tags for the FLAG (pBABE), EGFP (pBABE), and the Myc epitope (pCDNA3, pSP64) were fused in frame by PCR or subcloning. For in vitro expression, TBX15 cDNAs were subcloned in the vector pSP64 (Promega) that was modified to contain a 5′ β-globin leader and a 3′ β-globin trailer, suitable for the TNT®SP6 High-Yield Protein Expression System (Promega). We performed the electrophoretic mobility shift assay (EMSA) as described[9] to test the DNA binding ability of

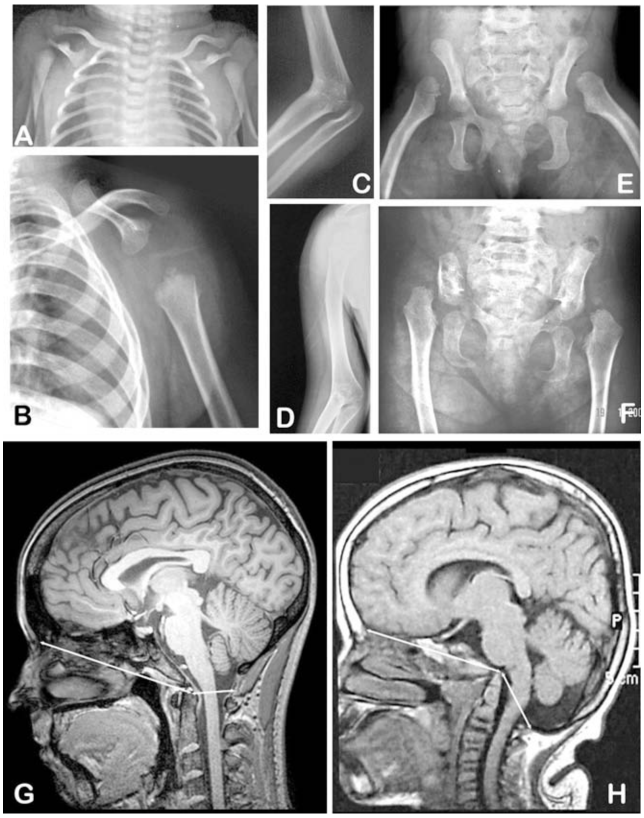

Figure 2. Radiographic Findings in Cousin Syndrome
(A, C, and E) Patient 1. (B, D and F) Patient 2. Skeletal features seen in the two patients include aplasia of the blade of the scapula, humeroradial synostosis, marked hypoplasia of the iliac bones, and dislocation of the femoral heads. (G) A sagittal section of a cranial MRI of a normal woman aged 19 years. (H) A corresponding section from patient 2 at age 12 years. From the tip of the odontoid process in the center of each panel, the arrows extend anteriorly to the frontal bone and posteriorly to the posterior margin of the foramen magnum. Caudal displacement of the occipital bone is evident in the patient; note also the redundant skin fold over the posterior aspect of the neck. The cranial and skeletal features are remarkably similar to those seen in Tbx15-ablated mice.[5]

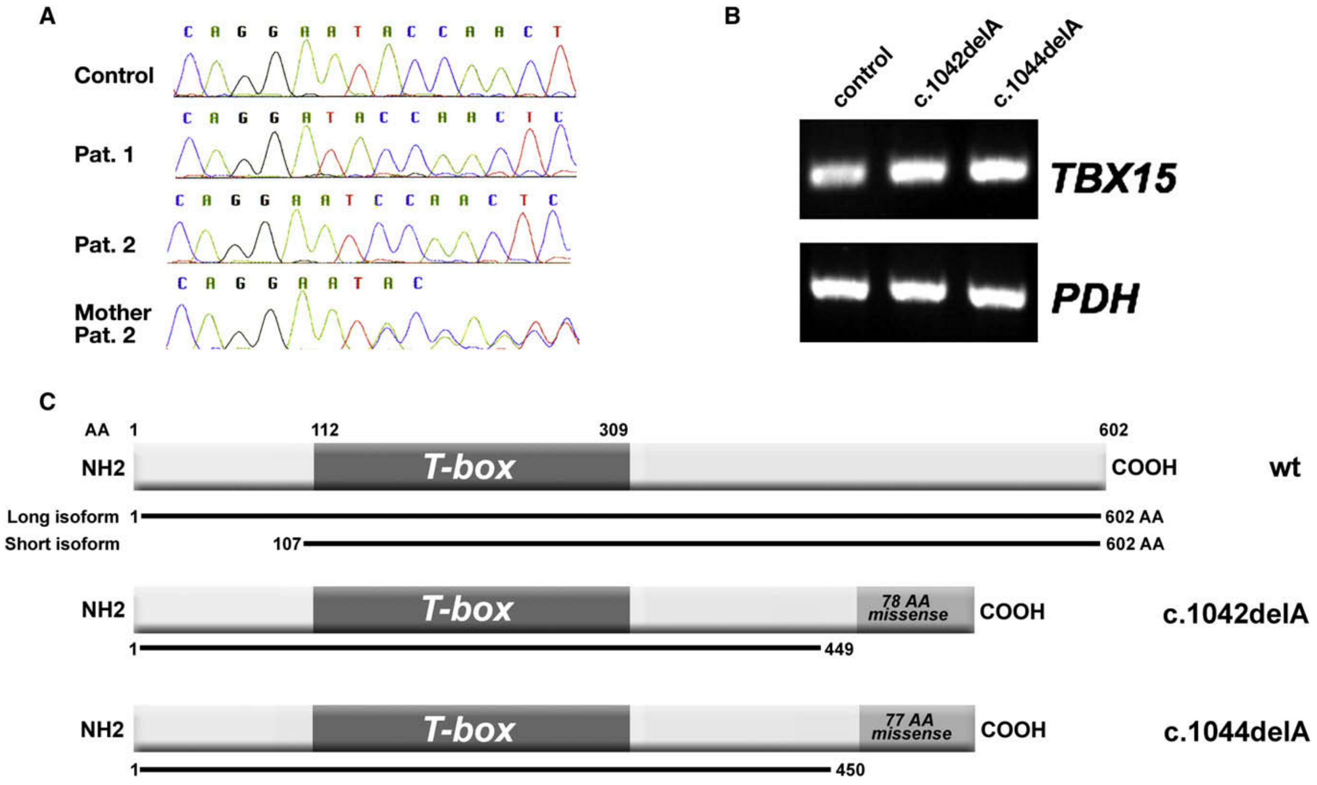

Figure 3. Genomic *TBX15* Mutations

(A) The genomic *TBX15* sequences in patient 1, patient 2, the mother of patient 2, and a control. Patient 1 is homozygous for c.1042 delA, and patient 2 is homozygous for c.1044 delA in the same codon. (B) The *TBX15* mRNA levels in an age-matched control and patients' fibroblasts of the same passage by semiquantitative RT-PCR; expression of the mutant alleles was verified by cDNA sequencing. (C) A schematic representation of the two physiological transcripts of the TBX15 protein (differing in the start codon) as well as of the two predicted mutant ORFs; in the mutant proteins, the normal amino acid sequence is interrupted after amino acid 449 or 450 and is followed by a stretch of 78 or 77 missense amino acids. The DNA-binding T-box is preserved in both mutant variants.

mutant TBX15 protein. Oligonucleotides used to generate binding sites were BS.dirF 5′-GATCCGGAGGTGTGAAG GTGTGAAAGGA-3′ and BS.dirR 5′-GATCTCCTTTCACACC TTCACACCTCCG-3′. Cell culture, gene transfer, and expression analysis were performed as described.[8,9] High-titer retroviral gene transfer via BING packaging cells[10] was used for transduction of human chondrosarcoma (HCS, ATCC) and human fibrosarcoma cells (HT1080, ATCC). Viral supernatants were titered prior to infection to give an MOI (multiplicity of infection) of 10 for each construct. Transduced cell populations were analyzed either 48 hr after infection or after selection with 5 μg/ml puromycin for 72 hr. Whole-cell lysates and subcellular protein fractions were obtained 48 hr after transfection by lysis in 1× SDS sample buffer or by hypotonic lysis,[8] followed by sonification and immunoblot analysis. Patients' fibroblasts derived from skin biopsies were expanded to passage five; RIPA buffer was used for extracting proteins for immunoblot analysis. Antibodies included anti-FLAG M5 (Sigma), anti-GFP (Santa Cruz), anti-β-actin (Sigma), and a polyclonal serum generated by immunization of rabbits with a GST fusion protein containing the amino acids 1–300 of TBX15. For direct fluorescent detection of EGFP fusion proteins, cells were cultured on chamber slides, fixed in 4% paraformaldehyde for 10 min at room temperature, washed thrice with PBS, and counterstained with DAPI antifade (Q Biogene). Images were captured with a Leica (DMRXA) microscope with a cooled CCD (Sensys Photometrics). For proteasome inhibition, MG-132 (Sigma) was added to the culture medium at 25 μM prior to the collection of cell lysates.

To test the possible homology between Cousin syndrome and the mouse *Tbx15* deficiency, we obtained DNA from the two individuals with Cousin syndrome and their parents after having obtained informed consent and then searched directly for *TBX15* genomic sequence variations (primer information and PCR conditions are available upon request). We identified two different single-nucleotide deletions that segregated in each family and were homozygous in the affected girls, heterozygous in their parents, and absent in a panel of over 216 control chromosomes. Both deletions occurred at codon 344; in family 1, deletion of adenosine 1042 (c.1042 delA at the first position within codon 344) led to a frame shift with 78 missense amino acids followed by a stop codon; in family 2, the deletion occurred at the third position of the same codon (c.1044 delA) an led to 77 missense amino acids and the stop codon (Figure 3A); both missense stretches include five cysteine residues. Both mutations

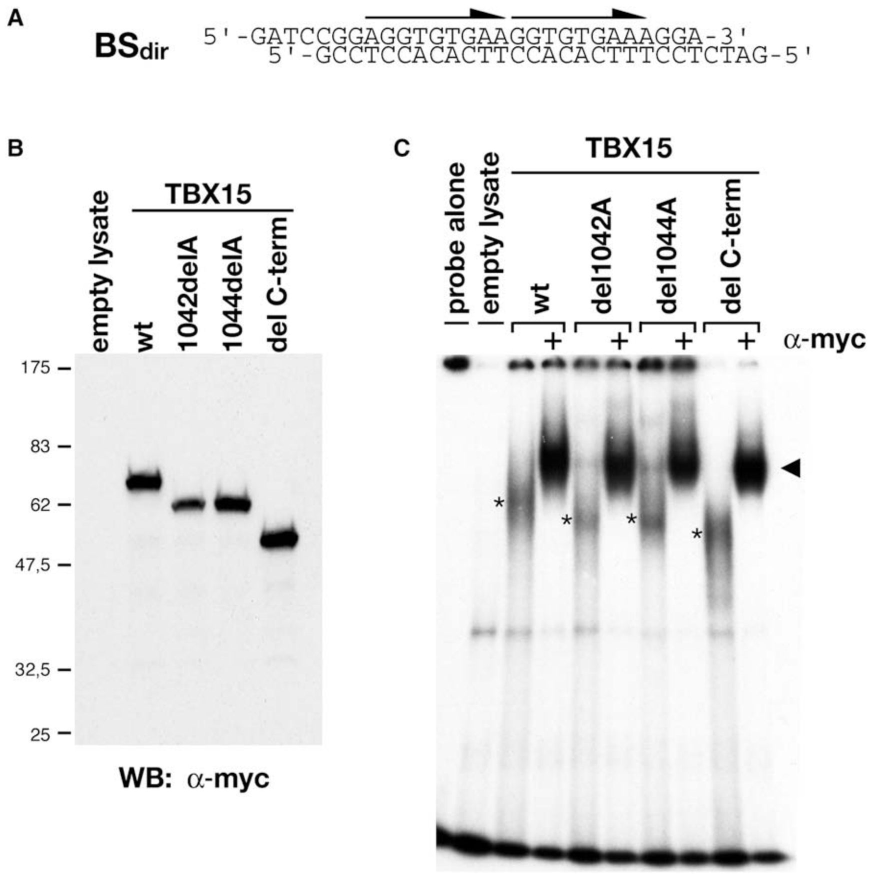

Figure 4. In Vitro DNA Binding Analysis of Mutant TBX15 Proteins

(A) The previously identified[7] binding site of mouse Tbx15 (BS_{dir}) that was tested in EMSAs. Arrows indicate the orientation of T-half sites. (B) Assays were performed with equal amounts of in vitro-synthesized Myc-tagged TBX15 proteins, as determined by anti-Myc immunoblot. All proteins were expressed with the expected molecular weights. (C) No differences in DNA binding to the site BS_{dir} are observed between the C-terminally truncated form TBX15-del C-term protein and the wild-type form of TBX15 or the c.1042 delA and c.1044 delA mutants in a gel-shift assay. Equally strong complexes were detected for all proteins (asterisks). Specificity of binding was confirmed by addition of anti-Myc antibody, which resulted in the formation of a prominent supershifted complex (black arrowhead).

predicted the abolition of the C-terminal 152 amino acids of the principal short and long isoforms of the mature TBX15 protein (Figure 3C; for the reference sequence of TBX15 isoforms, see Web Resources). Semiquantitative PCR and sequencing of cDNA isolated from patients' and controls' fibroblasts showed that the mutant mRNA was expressed at a level that was the same as or higher than that of wild-type mRNA (Figure 3B).

We then investigated whether the mutations affected the ability of mutant TBX15 protein to bind their target DNA sequences in an EMSA after incubation of in vitro-synthesized wild-type and mutant TBX15 proteins (Figure 4B) with oligonucleotides corresponding to the mouse *Tbx15* target DNA sequence that was identified previously[9] (Figure 4A). Target DNA binding of the mutant proteins was similar to that of wild-type protein (Figure 4C), in keeping with the notion that the DNA-binding region of the protein, the T-box, was unaffected by the mutations.

Given that the DNA-binding ability of the mutant proteins was conserved, we then focused on the localization and stability of mutant TBX15 proteins. Immunoblot analysis of cytoplasmic and nuclear extracts of patients' fibroblasts with antiserum raised against the amino terminal part of the long isoform of TBX15 (TBX15L) showed an almost complete loss of the TBX15L signal in the patients, whereas bands of the expected size were detected in the nuclear fraction of both age-matched controls (Figure 5A). For further studies, the wild-type and mutant cDNA sequences were cloned into expression vectors. Figure 5B shows expression of FLAG-tagged TBX15 proteins in human chondrosarcoma (HCS) cells. The wild-type protein was readily detectable and showed the expected predominantly nuclear localization; no TBX15 protein was detected after transduction with either of the two mutants, in spite of adequate mRNA levels (data not shown). When EGFP-tagged TBX15 protein isoforms were analyzed by direct fluorescence microscopy, the wild-type protein gave a strong signal in both the cytoplasm and the nucleus (short isoform, Figure 6B) or exclusively in the nucleus (long isoform, Figure 6A); the mutant constructs gave a barely detectable signal, indicating that protein stability was compromised. Similar results were obtained when Myc-tagged TBX15 proteins and anti-Myc immunofluorescence detection were used in HeLa and HEK293 cells (data not shown).

To elucidate the mechanisms leading to instability of the mutant proteins, we transfected HeLa cells with wild-type human *TBX15*, the two mutants identified in the Cousin syndrome patients, or a synthetic mutant harboring the truncation of the protein after amino acid residue 344. Cellular levels of the C-truncated protein were similar to that of the wild-type, whereas levels of the two human mutants were significantly reduced; these could be partially restored by addition of the proteasome inhibitor, MG-132 (Figure 5D). Thus, simple truncation of 152 amino acids at the C terminus did not affect stability, but the presence of the 78 (versus 77) missense amino acids in the mutants directed the TBX15 protein to proteasomal degradation. To confirm this interpretation, we generated constructs in which EGFP was fused directly onto either the wild-type carboxy-terminal portion of TBX15 or the two stretches of missense amino acids predicted by the human mutations.

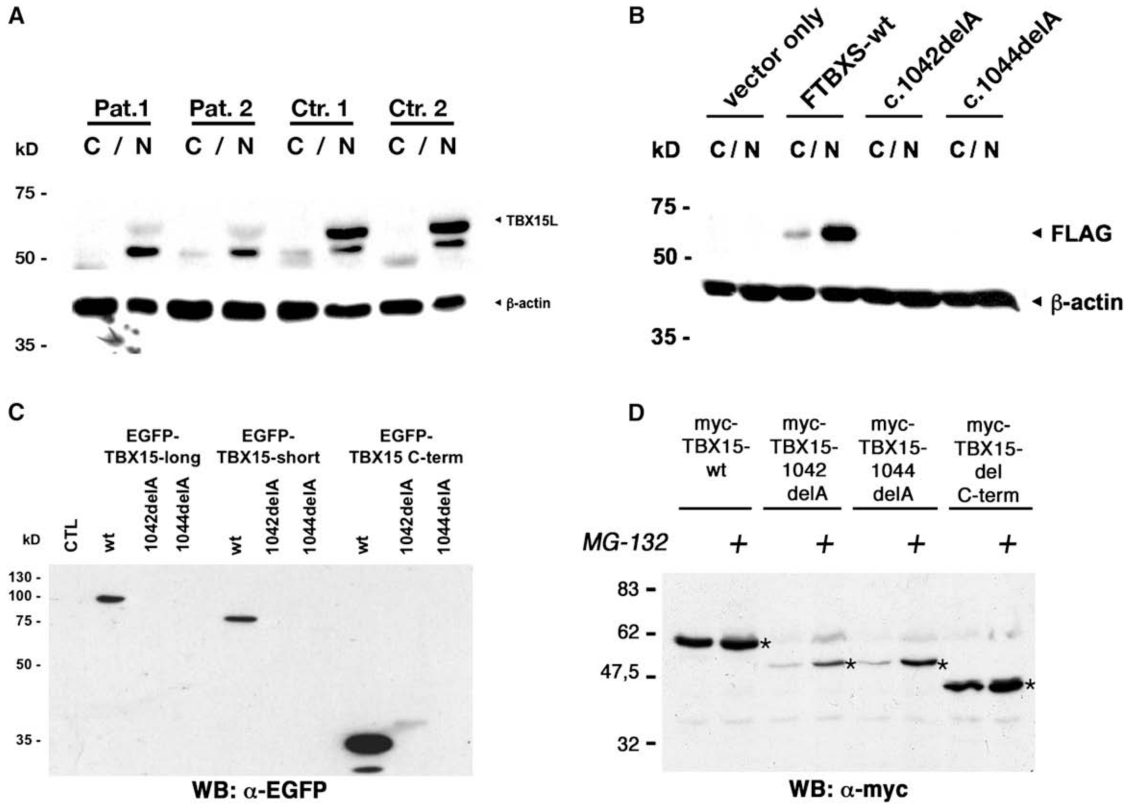

Figure 5. Immunoblot Analysis of TBX15 Protein in Patients' Fibroblasts and in Cell Transfection Experiments

(A) Analysis of TBX15 proteins in subcellular fractions (C = cytoplasmic extract, N = nuclear extract) of patients' and control fibroblasts. A polyclonal antiserum directed against the amino-terminus of the long isoform of TBX15 (TBX15L) was used for the immunoblots, which show a strong reduction of the signal for the long isoform of TBX15 in both patients. The nature of the band that has an apparent molecular weight of approximately 50 kDa and migrates below TBX15L is unclear but may be due to cross-reactivity of the antiserum with the related protein TBX18. Membranes were reprobed with an antibody against β-actin so that equal loading could be ensured.

(B) Disease-associated mutations confer instability to transgenic TBX15. Analysis of TBX15 proteins in subcellular fractions (C = cytoplasmic extract, N = nuclear extract) of human chondrosarcoma (HCS) cells overexpressing either FLAG-tagged wild-type short variant TBX15 or analogous constructs carrying the disease-associated mutations. An anti-FLAG immunoblot shows the presence of the wild-type recombinant protein only.

(C) Disease-associated mutations confer instability to all isoforms of TBX15 and other proteins. Analysis of TBX15 proteins in human chondrosarcoma (HCS) cells overexpressing either EGFP-tagged wild-type TBX15 or constructs carrying the disease-associated mutations is shown. In addition, EGFP was fused directly to either the wild-type C-terminal portion of TBX15 (152 amino acids) or to the two stretches of 78 or 77 missense amino acids predicted by the human mutations. Whole-cell lysates were analyzed by anti-GFP immunoblot. Only lanes loaded with the wild-type fusion constructs gave a signal of the expected size.

(D) The C-terminal sequences resulting from disease-associated TBX15 mutations confer instability by directing proteins to proteosomal degradation. Protein analysis of Myc-tagged wild-type TBX15, c.1042 delA, c.1044 delA, and ΔC proteins in HeLa cells probed in an anti-Myc immunoblot. Expression of TBX15 mutants c.1042 delA and c.1044 delA is strongly reduced in comparison to that of the TBX15-wt and Tbx15ΔC proteins (asterisks), indicating that the missense amino acids, and not the truncation, affect protein stability. Incubation with the proteasome inhibitor MG-132 (25 μM) leads to a marked stabilization of TBX15-c.1042 delA, and c.1044 delA proteins. No more slowly migrating bands that could represent poly-ubiquitinylated proteins were observed.

Immunoblot analysis showed a strong signal for the wild-type C terminus, but the two mutant C termini were not detectable (Figure 5C). Upon direct fluorescence microscopy, a signal was detected with the constructs containing the wild-type but not the mutant isoforms of TBX15 (Figures 6A and 6B). When the constructs consisting of EGFP and the C-terminal portions only were analyzed, fluorescence was detected with the constructs containing the wild-type C terminus but not with the constructs containing the mutant C termini, confirming that the stretches of missense amino acids produced by the frameshift mutation conferred instability to the EGFP protein (Figure 6C).

In summary, genomic sequencing indicated that two similar mutations segregated in the two families; these mutations predicted the synthesis of TBX15 protein that had an intact T-box but lacked a significant portion of the C-terminal region and had instead a stretch of 78 (or 77) missense amino acids that included five cysteine residues. The subsequent set of experiments indicated that although TBX15 protein synthesized from the two mutant

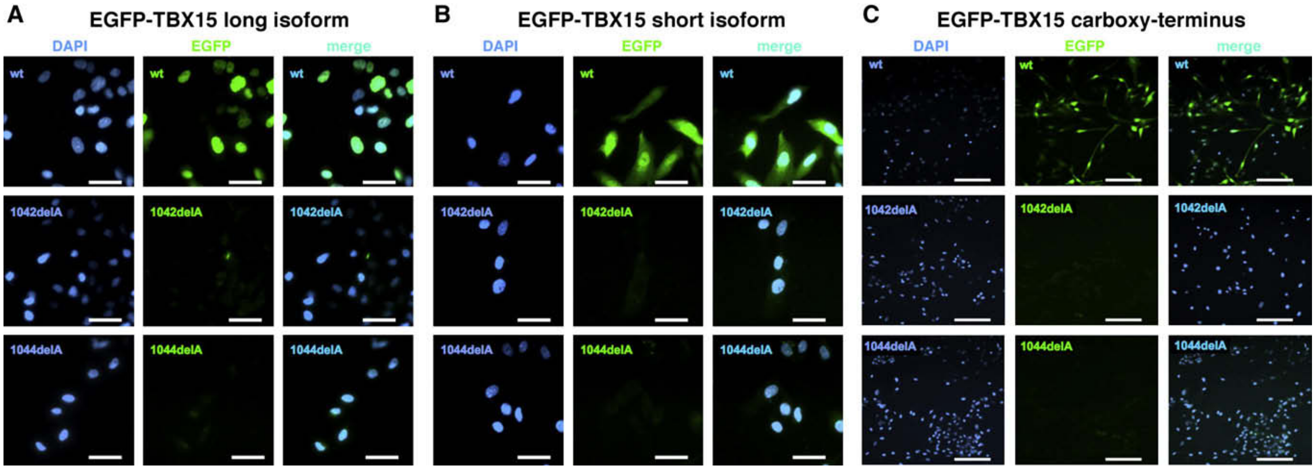

Figure 6. Fluorescence Studies of EGFP-Tagged TBX15 Constructs
Intracellular localization of EGFP-tagged TBX15 proteins in HCS cells as detected by direct EGFP fluorescence microscopy. The TBX15 protein localizes exclusively (long variant [A]) or predominantly to the nucleus (short variant [B]; compare nuclear staining with DAPI), whereas TBX15-c.1042 delA and c.1044 delA are barely detectable, both in the context of the long and of the short variant. A similar loss of fluorescent signal was observed when the C terminus of the disease-associated protein variants was fused to EGFP (C). HCS cells were transduced with titered recombinant virus at the same MOI for all constructs. Scale bars represent 15 (A and B) or 25 (C) µm.

alleles retained the ability to bind their DNA targets in vitro, cellular levels of TBX15 were drastically reduced or abolished because of proteasome-associated degradation directed by the C-terminal missense stretch. A similar mutation in the *TNSALP* gene (MIM 171760), causing the addition of a stretch of 80 missense amino acids including four cysteine residues, has been shown to cause proteasomal degradation of the mutant alkaline phosphatase protein and to result in severe hypophosphatasia (MIM 241500)[11]. Thus, the two affected subjects were homozygous for mutations that resulted in functional TBX15 deficiency, confirming the initial hypothesis of a shared molecular basis for the changes seen in the craniocervical bones, the scapula, and the pelvis in the subjects with Cousin syndrome and in *Tbx15*-deficient mice.

T-box genes encode a family of transcription factors that regulate a variety of developmental processes in metazoa ranging from hydra to humans. Mammalian genomes are known to harbor 17 family members involved in patterning and differentiation processes during gastrulation and organogenesis. Notably, mutations in human *TBX* genes, *TBX1*, *TBX3*, *TBX4*, *TBX5*, *TBX19(TPIT)*, *TBX20*, and *TBX22*, are known to cause congenital disorders with craniofacial, endocrine, limb, and cardiac malformation.[12–19] The identification of Cousin syndrome as a *TBX15*-related disorder in humans further underscores the importance of the T-box gene family for human development and disease and adds an important piece to the mosaic of our understanding of human genetic anomalies of the skeleton.[20] It also allows for molecular diagnosis and genetic counseling; in fact, prior to our studies, the two families reported here had been given other diagnoses and had been counseled for dominant inheritance.

Tbx15 is known to be required for the condensation of mesenchymal precursor cells in early development of the skeleton.[4,5,21] In the mouse embryo, *Tbx15* is expressed first in mesenchyme of the limb buds and subsequently in the developing zeugopodal elements. In the cranium, expression begins in the mesenchyme near the surface ectoderm and then can be detected in various craniofacial elements that include the mandibular process of the first mandibular arch and the dorsal edge of the hyomandibular cleft, which will eventually become the external auditory meatus; the surface of the second branchial arch as well as the maxillary and the mandibular portions of the first branchial arch surrounding the developing mouth; and the area that is dorsal to each optic prominence and that later extends to surround most of the eye.[4,5,21] No expression is seen in internal organs between embryonic days 8.5 and 12.5, whereas data from EST libraries suggest an expression in adult tissues of bone, brain, intestine, liver, muscle, testis, and thymus. Although no expression data in the human are available, the mouse expression pattern fits reasonably well with the phenotype observed in Cousin syndrome.

The target genes of TBX15 and of its closely related family member TBX18 (MIM 604613) have remained elusive so far. Scapular and pelvic hypoplasia are features of campomelic dysplasia (MIM 114290) caused by *SOX9* (MIM 608160) mutations; scapular hypoplasia with humeroradial synostosis is a feature of Antley-Bixler syndrome (MIM 207410, 201750) associated with mutations in either *FGFR2* or *POR*; the phenotypic relationship suggests that TBX15 may act within this contextual frame and/or share target genes with *SOX9*, *FGFR2* (MIM 176943), and *POR* (MIM 124015). Kosenow syndrome (scapuloiliac dysostosis, MIM 169550) is a dominantly inherited condition with hypoplasia of the scapula and pelvis but no craniocervical malformation; its molecular basis is unknown. If Cousin syndrome is caused by homozygosity for recessive *TBX15* null mutations, there may be a phenotype associated with dominant mutations within the T-box region, and Kosenow syndrome would be a possible candidate.

Acknowledgments

We thank the families for their gracious participation in this study. We are particularly grateful to subject 1, a language student whose strive for independence and ability to comment on her condition with philosophy and humor make her a leading figure in the German Association for Little People and their Families (BKMF, www.bkmf.de). Work in the Freiburg Skeletal Dysplasia Centre and laboratory (www.skeldys.org) was supported by the SKELNET project of the German Bundesministerium für Bildung und Forschung (BMBF), by the European Community EuroGrow consortium, and by individual grants of the Deutsche Forschungsgemeinschaft (DFG). Work in the laboratory of A.K. in Hannover was supported by individual grants of the DFG and the DFG-funded Cluster of Excellence REBIRTH (From Regenerative Biology to Reconstructive Therapy).

Received: September 1, 2008
Revised: October 8, 2008
Accepted: October 15, 2008
Published online: November 6, 2008

Web Resources

The URLs for data presented herein are as follows:

Online Mendelian Inheritance in Man (OMIM), http://www.ncbi.nlm.nih.gov/Omim/

Ensembl Human Gene View, www.ensembl.org; for human TBX15, see www.ensembl.org/Homo_sapiens/geneview?gene = ENSG00000092607; the short isoform (TBX15S; 496 amino acids) corresponds to transcript ENST00000207157, and the long isoform (TBX15L; 602 amino acids) corresponds to transcript ENST00000369429.

References

1. Cousin, J., Walbaum, R., Cegarra, P., Huguet, J., Louis, J., Pauli, A., Fournier, A., and Fontaine, G. (1982). Dysplasie pelvis-scapulaire familiale avec anomalies epiphysaires, nanisme et dysmorphies: Un nouveau syndrome? Arch. Fr. Pediatr. *39*, 173–175.
2. Elliott, A.M., Roeder, E.R., Witt, D.R., Rimoin, D.L., and Lachman, R.S. (2000). Scapuloiliac dysostosis (Kosenow syndrome, pelvis-shoulder dysplasia) spectrum: Three additional cases. Am. J. Med. Genet. *95*, 496–506.
3. Candille, S.I., Van Raamsdonk, C.D., Chen, C., Kuijper, S., Chen-Tsai, Y., Russ, A., Meijlink, F., and Barsh, G.S. (2004). Dorsoventral patterning of the mouse coat by *Tbx15*. PLoS Biol. *2*, e3.
4. Kuijper, S., Beverdam, A., Kroon, C., Brouwer, A., Candille, S., Barsh, G., and Meijlink, F. (2005). Genetics of shoulder girdle formation: Roles of Tbx15 and aristaless-like genes. Development *132*, 1601–1610.
5. Singh, M.K., Petry, M., Haenig, B., Lescher, B., Leitges, M., and Kispert, A. (2005). The T-box transcription factor Tbx15 is required for skeletal development. Mech. Dev. *122*, 131–144.
6. Curry, G.A. (1959). Genetical and development studies on droopy-eared mice. J. Embryol. Exp. Morphol. *7*, 39–65.
7. Morgenstern, J.P., and Land, H. (1990). Advanced mammalian gene transfer: High titre retroviral vectors with multiple drug selection markers and a complementary helper-free packaging cell line. Nucleic Acids Res. *18*, 3587–3596.
8. Trost, T.M., Lausch, E.U., Fees, S.A., Schmitt, S., Enklaar, T., Reutzel, D., Brixel, L.R., Schmidtke, P., Maringer, M., Schiffer, I.B., et al. (2005). Premature senescence is a primary fail-safe mechanism of ERB2-driven tumorigenesis in breast carcinoma cells. Cancer Res. *65*, 840–849.
9. Farin, H.F., Bussen, M., Schmidt, M.K., Singh, M.K., Schuster-Gossler, K., and Kispert, A. (2007). Transcriptional repression by the T-box proteins Tbx18 and Tbx15 depends on Groucho corepressors. J. Biol. Chem. *282*, 25748–25759.
10. Pear, W.S., Nolan, G.P., Scott, M.L., and Baltimore, D. (1993). Production of high-titer helper-free retroviruses by transient transfection. Proc. Natl. Acad. Sci. USA *90*, 8392–8396.
11. Komaru, K., Ishida, Y., Amaya, Y., Goseki-Sone, M., Orimo, H., and Oda, K. (2005). Novel aggregate formation of a frame-shift mutant protein of tissue-nonspecific alkaline phosphatase is ascribed to three cysteine residues in the C-terminal extension. Retarded secretion and proteasomal degradation. FEBS J. *272*, 1704–1717.
12. Bamshad, M., Lin, R.C., Law, D.J., Watkins, W.C., Krakowiak, P.A., Moore, M.E., Franceschini, P., Lala, R., Holmes, L.B., Gebuhr, T.C., et al. (1997). Mutations in human TBX3 alter limb, apocrine and genital development in ulnar-mammary syndrome. Nat. Genet. *16*, 311–315.
13. Basson, C.T., Bachinsky, D.R., Lin, R.C., Levi, T., Elkins, J.A., Soults, J., Grayzel, D., Kroumpouzou, E., Traill, T.A., Leblanc-Straceski, J., et al. (1997). Mutations in human TBX5 cause limb and cardiac malformation in Holt-Oram syndrome. Nat. Genet. *15*, 30–35.
14. Merscher, S., Funke, B., Epstein, J.A., Heyer, J., Puech, A., Lu, M.M., Xavier, R.J., Demay, M.B., Russell, R.G., Factor, S., et al. (2001). TBX1 is responsible for cardiovascular defects in velo-cardio-facial/DiGeorge syndrome. Cell *104*, 619–629.
15. Yagi, H., Furutani, Y., Hamada, H., Sasaki, T., Asakawa, S., Minoshima, S., Ichida, F., Joo, K., Kimura, M., Imamura, S., et al. (2003). Role of TBX1 in human del22q11.2 syndrome. Lancet *362*, 1342–1343.
16. Wilson, V., and Conlon, F.L. (2002). The T-box family. Genome Biol. *3*, 3008.1–3008.7.
17. Naiche, L.A., Harrelson, Z., Kelly, R.G., and Papaioannou, V.E. (2005). T-box genes in vertebrate development. Annu. Rev. Genet. *39*, 219–239.
18. Vallette-Kasic, S., Brue, T., Pulichino, A.M., Gueydan, M., Barlier, A., David, M., Nicolino, M., Malpuech, G., Déchelotte, P., Deal, C., et al. (2005). Congenital isolated adrenocorticotropin deficiency: An underestimated cause of neonatal death, explained by TPIT gene mutations. J. Clin. Endocrinol. Metab. *90*, 1323–1331.
19. Kirk, E.P., Sunde, M., Costa, M.W., Rankin, S.A., Wolstein, O., Castro, M.L., Butler, T.L., Hyun, C., Guo, G., Otway, R., et al. (2007). Mutations in cardiac T-box factor gene TBX20 are associated with diverse cardiac pathologies, including defects of septation and valvulogenesis and cardiomyopathy. Am. J. Hum. Genet. *81*, 280–291.
20. Superti-Furga, A., and Unger, S. (2007). Nosology and classification of genetic skeletal disorders: 2006 revision. Am. J. Med. Genet. A. *143*, 1–18.
21. Agulnik, S.I., Papaioannou, V.E., and Silver, L.M. (1998). Cloning, mapping, and expression analysis of TBX15, a new member of the T-Box gene family. Genomics *51*, 68–75.

Proximal-Distal Compartmentalization of the Developing Limb Bud by T-Box Transcription Factors Tbx15 and Tbx18 is Prerequisite for Formation of Stylopod and Zeugopod

Henner F. Farin, Manvendra K. Singh[1], Karin Schuster-Gossler and Andreas Kispert[2]

From the Institute for Molecular Biology, Medizinische Hochschule Hannover, 30625 Hannover, Germany

[1]Current address: Cardiovascular Research Center, University of Pennsylvania, 1154 BRB II/III, 421 Curie Blvd, Philadelphia, PA 19104, USA

[2]Address correspondence to: Andreas Kispert, Medizinische Hochschule Hannover, Institute for Molecular Biology, OE5250, Carl-Neuberg-Str. 1, D-30625 Hannover, Germany. Tel. +49 511 532 4017; Fax: +49 511 5324283; E-mail: kispert.andreas@mh-hannover.de

Manuscript in preparation.

ABSTRACT

The vertebrate limb bud is patterned by proximal and distal signaling centers, however it is currently unknown how cells interpret these signals to elaborate specific skeletal elements along this axis. *Tbx18* and *Tbx15* encode a closely related pair of vertebrate specific T-box transcription factors that are co-expressed in the proximal limb bud mesenchyme. Here, we show that proximal confinement is achieved by a combination of locally activating and repressing signals from adjacent tissues including the AER. Both genes are redundantly required for the formation of limb skeletal structures derived from this region, since the skeletal elements of the stylopod and zeugopod are absent in mouse embryos double mutant for *Tbx15* and *Tbx18*. Our molecular and cellular analysis revealed a reduction of chondrogenic precursors, as well as reduced proliferation and increased apoptosis in the proximal limb bud mesenchyme, whereas the global pattering of the proximal-distal limb axis is unaffected in double mutant embryos. Mislocalization of Tbx18-positive cells to distal limb regions, accompanied by de-regulated expression of Eph/Ephrin molecules, suggests that cell adhesion/repulsion properties are changed in the proximal mesenchyme of double mutant limb buds. This hypothesis is supported by misexpression experiments *in vivo* that demonstrate that Tbx18-positive cells are recruited to whereas Tbx18-negative cells are excluded from the proximal limb bud mesenchyme. Together our results provide evidence for a Tbx15/18-regulated compartmentalization of the proximal limb domain as a prerequisite for specification of proximal limb skeletal elements.

INTRODUCTION

The vertebrate limb is characterized by an array of three distinct skeletal elements along its proximal-distal axis: the proximal stylopod (humerus/femur), the intermediate zeugopod (radius/tibia and ulna/fibula), and the distal autopod (carpals/tarsals and digits). Generation of this stereotyped array of elements follows a complex developmental program that is generally thought to involve the establishment of opposing signal centers in an initially homogenous developmental field of the early limb bud and the subsequent translation of positional information generated by these centers into distinct cellular programs that specify the individual elements. However, the molecular and cellular mechanisms that underlie specification of these different proximal-distal (PD) cell fates are poorly understood.

The early limb bud consists of a core of lateral plate derived mesenchymal cells that are covered by surface ectoderm. At the distal dorso-ventral boundary of the limb bud the ectoderm thickens and forms a specialized structure, the apical ectodermal ridge (AER). The AER is source of Fibroblast growth factors (Fgf) signaling that induces proliferation in the underlying mesenchyme, directs proximal-distal outgrowth and distalizes cell fates (for a recent review refer Towers and Tickle, 2009). The AER interacts with another signaling center, the zone of polarizing activity (ZPA), which is established in the mesenchyme of the posterior limb bud margin. The ZPA secretes Sonic hedgehog (Shh) that induces posterior cell fates in the limb bud and is also required for late phase PD-outgrowth by mediating AER maintenance. At the proximal end the limb bud mesenchyme remains under the influence of signals from the trunk mesoderm, mainly retinoic acid (RA) whose distal diffusion generates a stable gradient that is thought to mediate positional information for the specification of the proximal most elements (Mercader et al., 2000).

The limb skeleton is generated in a process known as endochondral bone formation. Initiated by a mesenchymal condensation, cells undergo chondrogenic differentiation, which is followed by the longitudinal expansion of the cartilages and the subsequent replacement of this pre-skeleton by osteocytes that secrete the definitive bone matrix. Embryological studies have shown, that the skeletal elements of the limbs are generated in a proximal to distal sequence. Manipulation of chick embryos led to the formulation of the classical ‘Progress zone model’ for the specification of skeletal elements along the PD-limb axis, that is based on the observation that AER removal leads to progressively more distal limb skeletal truncations depending on the time of removal. In this model PD positional values are thought to be specified by the length of time that undifferentiated mesenchymal cells spend proliferating at the tip of the limb bud, the so called the progress zone. However there is currently no convincing evidence for a cell-autonomous clock capable of affecting limb patterning, which is at the heart of the Progress zone model. In contrast the more recently postulated ‘Early specification model’, proposes that the PD limb pattern is established at very early stages, followed by an expansion of the individual elements. This concept is supported by several genetic models that display a selective failure in the generation of proximal structures while distal elements are still formed (Levandoski et al., 2000; Barna et al., 2005; Mariani et al. 2008). However, as a major caveat of this model, neither fate mapping studies in the early limb bud, nor gene expression patterns reflect the early specification of three distinct compartments along the PD axis of the limb.

T-box genes encode a family of DNA binding transcription factors that regulate a variety of patterning and differentiation processes during vertebrate organogenesis (Naiche et al., 2005). During limb development the closely related genes *Tbx4* and *Tbx5* have a conserved role as transcriptional activators in initiating outgrowth of hind- and forelimb buds, respectively (Naiche and Papaioannou, 2003; Agarwal et al., 2003). *Tbx2* and *Tbx3* encode a related pair of transcriptional repressors that are co-expressed in the anterior and posterior flanks of the limb bud and the interdigital mesenchyme. Inactivating mutations of either gene were reported to cause limb defects and a role in specifying digit identity was proposed (Davenport et al., 2003; Harrelson et al., 2004; Suzuki et al., 2004). Mutations in *TBX3*, *TBX4* and *TBX5* genes cause Ulnar-Mammary, Small-Patella and Holt-Oram syndromes, respectively, diseases that also manifest themselves with limb malformations (for a review refer Packham and Brook, 2003).

Tbx18 and *Tbx15* encode another phylogenetically closely related pair of vertebrate specific T-box proteins. Our biochemical analyses have revealed that Tbx15 and Tbx18 share identical DNA binding properties and protein interaction partners (Farin et al., 2007; Farin et al., 2008) suggesting functional redundancy in regions of co-expression. Mice carrying a null allele of *Tbx18* die shortly after birth due to severe malformations of the axial skeleton, a phenotype that was traced back to the function of *Tbx18* in maintaining the anterior somite compartment (Bussen et al., 2004). Additionally, *Tbx18* regulates the condensation of mesenchymal cells around the distal ureter stalk, the formation and myocardialization of the sinus horns from the mesenchyme of the pericardial wall, and the differentiation of otic fibrocytes in the inner ear (Airik et al., 2006; Christoffels et al., 2006; Trowe et al., 2008). Mice homozygous for a targeted null allele of *Tbx15*, or for the spontaneous mutation *droopy ear*, in which *Tbx15* is deleted, exhibit defects in skin pigmentation, and in the axial and appendicular skeletons, phenotypic changes pointing to a role for *Tbx15* in dorso-ventral patterning of the mouse coat and in mesenchymal aggregation that precedes endrochondral bone formation (Candille et al., 2004; Singh et al., 2005). Based on phenotypic similarity with the murine phenotype, mutations in the human orthologue *TBX15* have recently been identified to underlie Cousin syndrome in man (Lausch et al., 2008).

Despite this impressive accumulation of data on the phenotypic requirements of this transcription factor pair during development, the molecular insight into Tbx15/18 function is scarce since neither the cellular programs nor the transcriptional targets for either factor have been identified. Here, we analyze the role of the *Tbx15* and *Tbx18* in mouse limb development. We show that both genes are co-expressed in the proximal limb bud mesenchyme, and that *ex vivo* their expression domains are subject to regulation by proximal and distal signals. The inspection of *Tbx15, Tbx18* double mutants showed that both factors are redundantly required for the formation of the proximal limb skeleton, the stylopod and zeugopod. We define the onset of the phenotypic changes and demonstrate that Tbx15/18 mediate a cellular migration/adhesion program that is both necessary and sufficient to recruit cells into a previously uncharacterized proximal mesenchymal compartment. Our data therefore shows how specific aspects of proximal-distal limb patterning can be achieved by the modulation of sizes of precursor populations and their cellular attributes to locally allow the formation of specific skeletal elements.

EXPERIMENTAL PROCEDURES

Limb explant culture – Limb buds from E10.5 *wild type* NMRI embryos were dissected in PBS and placed on Nucleopore filters (Whatman, pore size 1.0 µm) on top of a stainless steel mesh at the air-liquid interface in 3.5 cm cell culture dishes. The culture was performed at 37°C and 5% CO_2 in organ culture medium (DMEM, supplemented with 10% FCS and 1X solutions (Gibco) of Penicillin/Streptomycin, Glutamax, sodium pyruvate, and non-essential amino acids). For ablation experiments the AER or ZPA was cut-off using 26-gauge needles. The surgical removal of the ectoderm was performed with forceps in DMEM 10% FCS, after incubation of limb buds in 2% Trypsin/PBS (w/v) for 20 minutes at 4°C.

For bead implantation experiments, Affi-Gel blue beads (100-200 µm diameter, Bio-Rad) were rinsed in PBS and incubated at room temperature for 1 h in either recombinant mouse Fgf-8b (500 µg/ml, R&D Systems) human Bmp4 (100 µg/ml, AbD Serotech) or in 1 mg/ml BSA (control). AG1-X2 ion exchange resin beads (100-200 µm diameter, Bio-Rad) were rinsed in DMSO and incubated under light exclusion for 1 h at room temperature, in either all trans retinoic acid (RA, 0.5 mg/ml or 1.66 mM in DMSO, Sigma) or vehicle alone. Beads were rinsed in PBS before implantation into the limb mesenchyme. Wnt3a and ß-Galactosidase (control) expressing NIH3T3 cells (Kispert et al., 1998) were maintained in DMEM, 10% FCS, 1x Penicillin/Streptomycin, 1x Glutamax and 0.6 mg/ml G418. To induce the formation of cell pellets, cells from one confluent 10 cm cell culture dish were seeded on a 10 cm bacterial plate. After 2 days of culture the cell pellets were tapped off the surface and implanted.

Micromass cultures were established by dissociation of E10.5 fore- and hindlimb buds in

DMEM, 10% FCS, after incubation in 2% Trypsin/PBS (w/v) for 5 min at 37°C. A single cell suspension was obtained by gentle pipetting and clumps of ectoderm were removed after sedimentation. Cells were adjusted to 1.5 X 10^7 cells/ml in organ culture medium (as above), before 10 μl spots were placed on 24 well plates. Cells were incubated for 1 h at 37°C to allow adherence, before the wells were filled with medium. RA, recombinant Bmp4 (both as above) or Dorsomorphin (10 mM stock solution in DMSO, Sigma) were added to the medium at time points and concentrations as indicated in the text.

RT-PCR analysis – Total RNA was extracted from single micromass cultures with PeqGOLD reagent (Peqlab). RNA (500 ng) was reverse transcribed using oligodT primer and RevertAid M-MuLV Reverse Transcriptase (Fermentas) following the manufacturer's recommendations. For semi-quantitative PCR the number of cycles was adjusted to the mid-logarithmic phase. Quantification was performed with Quantity One software (Bio-Rad) and expression levels were normalized to the endogenous *Hprt*-expression. The error bars represent the variation between duplicate PCR reactions and all experiments were repeated at least twice. Primer sequences and PCR conditions are available on request.

In situ hybridization analysis – was performed with Digoxigenin-labeled antisense riboprobes following standard procedures on whole embryos (Wilkinson and Nieto, 1993) or on 10 μm sections of embryonic limb buds (Moorman et al., 2001). Details of probes used are available upon request.

Targeting constructs, ES cell culture, transgenic mice – For the production of conditional misexpression alleles we designed a 'knock-in' strategy into the X-chromosomal *Hypoxanthine guanine phosphoribosyl transferase* (*Hprt*) gene locus. The targeting vectors for homologous recombination were generated to replace mayor parts of the *Hprt* exon 1 (including the ATG) by a cassette suited for cre-mediated (mis-) expression of genes as described previously by Luche et al. (2007). Homologous recombination of this targeting vector results in a functional *Hprt* null allele, allowing direct selection of successfully targeted ES cells by 6-Thioguanine (refer PhD thesis of Aravind Sekar). The targeting vectors contained a 2.2 kb 5'-homology region, followed by the ubiquitously expressed CMV early enhancer/chicken β actin (CAG) promoter, the conditional expression cassette (Luche et al., 2007), and a 5.1 kb 3'-homology region (Fig. S1, A). To generate the $Hprt^{CAG::Tbx18}$ and $Hprt^{CAG::Tbx18\text{-}VP16}$ targeting constructs, the open reading frames (ORFs) of mouse *Tbx18* (cDNA AF306666) and

Tbx18-VP16 activator fusion construct (Farin et al., 2007) were first subcloned in the vector pSL1180 (GE-healthcare), 5' of an *IRES-EGFP* sequence, and then shuttled as 5' NheI-ORF-*IRES-EGFP*-MluI-3' fragments into the MluI and NheI-sites of the targeting vector. This results in a reverse orientation of the ORF, relative to the CAG promoter, avoiding 'leaky' expression. After cre-mediated 'flipping'- and excision events between pairs of loxP and loxM sequences, the ORF locates in sense direction, directly downstream of the CAG promoter (Fig. S1, A). Induction of Tbx18 protein expression was assessed after transient transfection of the circular targeting constructs in HeLa cells either alone (control), or together with a cre expression plasmid (pCAG::turbo-cre, kind gift from Achim Gossler), using the calcium phosphate method. Four days after transfection cell lysates were harvested and subjected to Western blot analysis (Fig. S1, B) using a rabbit polyclonal serum raised against the C-terminus of the murine Tbx18-protein (unpublished). Targeting vectors were additionally verified by sequencing before electroporation of the linearized vector in *Hprt*-positive SV129 ES cells (maintained beforehand in HAT medium). A two-step selection protocol was employed, starting 24 h after electroporation with the addition of 100 μg/ml G418, followed by the addition of 1.67 μg/ml 6-Thioguanine (Sigma) after additional 5 days. Surviving colonies were expanded and genotyped by PCR (conditions are available upon request). To test the functionality of the expression cassette in candidate ES clones, the GFP-epifluorescence was analyzed (Fig. S1, C) 6 days after electroporation with a cre-expression plasmid (see above). Verified ES clones were microinjected into CD1 mouse blastocysts. Chimeric males were obtained and mated to NMRI females, to produce heterozygous F1 females.

Mice and Genotyping – Transgenic mouse lines used in this study were maintained on an outbred (NMRI) background. Generation of null alleles for *Tbx18* ($Tbx18^{tm2Akis}$, synonym: $Tbx18^{GFP}$) and *Tbx15* ($Tbx15^{tm1Akis}$, abbreviated: $Tbx15^{-}$), of the *Pax3::cre* transgenic line (synonymes: *Pax3-Pro-Cre, Tg(Pax3-cre)1Joe*,) and the reporter line *R26R* (synonymes: $R26^{lacZ}$) were described before (Singh et al., 2005; Li et al., 2000; Soriano et al., 1999). For the generation of compound mutants, double heterozygous mice were intercrossed. For conditional misexpression experiments, females heterozygous for the $Hprt^{CAG::Tbx18}$ or the $Hprt^{CAG::Tbx18\text{-}VP16}$ alleles were crossed with males heterozygous for the *Pax3::cre* transgene. Genomic DNA prepared from yolk sacs or tail biopsies was used for genotyping by PCR (details on PCR strategies are available upon request). For timed pregnancies, vaginal plugs were checked in the morning after mating, noon was taken as embryonic day (E) 0.5.

Skeletal Preparations – Skeletal preparations of embryos were prepared essentially as previously described (Bussen et al., 2004). E14.5 embryos were fixed in 95% ethanol overnight, cartilaginous elements were then stained for 2 d in Alcian blue solution (150 mg/L Alcian blue 8GX in 80% ethanol/20% acetic acid). Embryos were transferred in methanol and cleared in benzylbenzoate/benzylalcohol (2:1) for documentation. E18.5 embryos were incubated for 2 min in water heated to 65°C to facilitate the removal of skin before Alcian blue staining was performed as above. Bony elements were stained in 100 mg/L Alizarin Red in 0.5% KOH (w/v) for 2 h, followed by several washes in ddH_20 before soft tissues were removed by digestion in 0.5% KOH and later 0.1% KOH. Skeletons were cleared in a 30% Glycerol/ 70% H_2O solution for documentation.

Histological analysis and immunohistochemistry – For Alcian blue staining on 10 μm limb sections, slides were deparaffinized and incubated for 30 minutes in a solution of 1% (w/v) Alcian blue 8GX in 3% (v/v) acetic acid for 30 minutes at RT, followed by washes and counterstaining with Nuclear Fast Red solution (Sigma), dehydration and mounting in Permount.
ß-galactosidase staining on sections and whole embryos was done as described (Echelard et al., 1994).
Recombinant fusion proteins of the extracellular domain of Eph/Ephrin molecules linked to the constant chain of human IgG (Eph/Efn-Fcs, R&D systems) were used to determine the binding patterns of different Eph receptors and Ephrin ligands on 10 μm forelimb cryosections as described previously (Gale et al., 1996). Working concentrations were 2.5 μg/ml Efna4-Fc (human), 5 μg/ml Epha4-Fc (mouse), 10 μg/ml Efnb1-Fc (mouse) and 5 μg/ml Ephb2-Fc (mouse). As secondary antibody anti-human IgG (H+L), AP-conjugate (Promega) was used at a dilution of 1:1000 and the detection was performed using INT/BCIP substrate (Roche) following the manufacturer's instructions.

Proliferation and apoptosis assays – Cell proliferation in tissues of E10.5 embryos was investigated by detection of incorporated BrdU similar to published protocols (Bussen et al., 2004). A total of nine sections from three individual embryos per genotype was used for quantification. The relative number of proliferating cells (the labeling index) was defined as the number of BrdU-positive nuclei to the number of total nuclei, as detected by DAPI counterstaining. Statistical analysis was performed using Student's t-test. Data were expressed as mean ± SEM.

Detection of apoptotic cells in 5 μm paraffin sections of E10.5 and E11.5 embryos was based on modification of genomic DNA utilizing terminal deoxynucleotidyl transferase (TUNEL assay) and indirect detection of positive cells by fluorescein-conjugated anti-digoxigenin antibody. The procedure followed exactly the recommendation of the manufacturer (Serologicals Corp.) of the ApopTag kit used.

Documentation – Whole-mount specimens were photographed on Leica M420 with Fujix digital camera HC-300Z. Whole-mount GFP-epifluorescence was documented on a Leica MZFLIII macroscope equipped with a Leica DFC300 camera. Sections of *in situ* hybridizations and immunostainings were photographed using a Leica DM5000 microscope with a Leica DFC300FX digital camera. All images were processed in Adobe Photoshop CS.

RESULTS

Co-expression of Tbx15 and Tbx18 during mouse limb development.

We compared the spatial and temporal dynamics of *Tbx15* and *Tbx18* expression during limb development to characterize the processes that might be regulated by the genes in a redundant fashion. *In situ* hybridization of E9.5 and E10.5 forelimbs showed expression of *Tbx15* along the proximal-distal extent of the limb bud including a very proximal crescent shaped domain containing the precursors of the future scapula at E10.5 (Fig. 1, A, B). Expression was confined to the mesenchyme and absent from the ectoderm as revealed by expression analysis on sections (Fig. 1, I, J, asterisks). Anterior and posterior flanks of the limb bud mesenchyme were negative for *Tbx15* expression (Fig. 1, A, B, black arrowheads). At these stages, *Tbx18* expression was found in a spatially more restricted manner in the proximal and central limb bud mesenchyme with a clear border to very proximal, and exclusion from the distal limb mesenchyme (white arrows) and anterior and posterior flank regions (black arrowheads) (Fig. 1, E, F, M, N). Similar expression patterns were recapitulated in the developing hindlimb with a temporal delay (data not shown). In fore- and hindlimbs (not shown) of E11.5 and E12.5 embryos a broad mesenchymal expression of *Tbx15* and *Tbx18* was found. *Tbx15* expression remained absent from the anterior and posterior flanks of the hand/foot plate (Fig. 1, C, D, black arrowheads), whereas an additional expression of *Tbx18* was now found at the very distal end of the limb (Fig. 1, G, O, grey arrows). Concomitantly with chondrogenic aggregation, expression of both *Tbx15* and *Tbx18* was down regulated in developing cartilages (Fig.

1, G, H, K, L, O, P, black arrows) but maintained in the perichondrium at later stages (data not shown).

Taken together, *Tbx15* and *Tbx18* co-expression occurs in two spatio-temporal phases: in a proximal-central region of the limb bud mesenchyme at early bud stages, and after initiation of mesenchymal condensations in the perichondrium of developing cartilages. Hence, Tbx15 and Tbx18 could be redundantly involved in early proximal-distal patterning of the limb, or in endochondral bone formation.

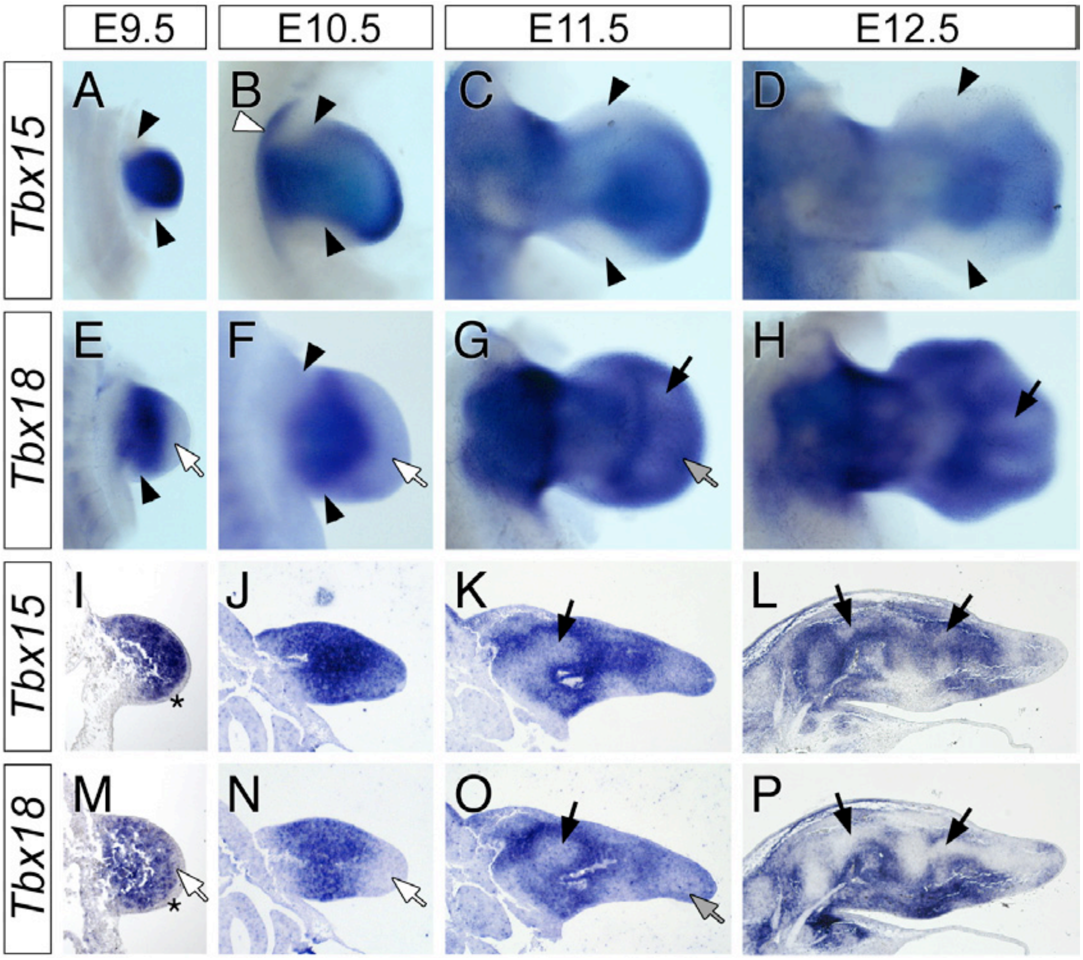

Fig. 1. **Comparative study of *Tbx15* and *Tbx18* expression during mouse limb development.**

Whole forelimbs (A-H) and transverse forelimb sections (I-P) of E9.5, E10.5, E11.5, and E12.5 *wild type* embryos were used for the analysis of *Tbx15* (A-D, I-L) and *Tbx18* mRNA expression (E-H, N-P). Co-expression of *Tbx15* and *Tbx18* is observed in the central mesenchyme of the limb bud (A, B, E, F), no expression is detected in the limb ectoderm (I and M, asterisks). Expression of *Tbx15* in precursor cells of the scapula (B, white arrowhead). The expression of both genes is excluded from the anterior and posterior flanks of the limb bud (A, B, E, F, black arrowheads), in case of *Tbx15* this exclusion is maintained in the developing hand plate (C, D). In E9.5 and E10.5 limb buds, *Tbx18* expression is absent from the distal limb bud mesenchyme (E, F, white arrows). At later stages the mesenchymal expression of *Tbx15* and *Tbx18* is maintained, and *Tbx18* expression is induced in the distal region of limb bud (G, O, grey arrows). The expression of both genes is down-regulated in chondrogenic aggregates and developing cartilages (G, H, K, L, O, P, black arrows).

Regulation of Tbx18 and Tbx15 expression during limb development.

We next wanted to explore the cellular and molecular mechanisms that restrict *Tbx15* and particularly *Tbx18* expression to the proximal limb bud mesenchyme. For that we scored expression of both genes after manipulating E10.5 fore limb buds and subsequent culturing of the rudiments for 18 h. In a series of ablation experiments we first studied the effect of known signaling centers on the expression of *Tbx18* (Fig. 2, A-D) and *Tbx15* (data not shown). As an anatomical landmark we visualized the AER by *Fgf8* expression. In non-manipulated control cultures the *Tbx18* and *Tbx15* expression recapitulated the expression *in vivo* (Fig. 2, A, compare Fig. 1, F) demonstrating the suitability of the culture system used. Removal of the distal tip of the limb bud including the AER resulted in an expansion of *Tbx18* expression into the distal mesenchyme (Fig. 2, B, black arrows), suggesting the existence of repressing signals secreted by the AER. The removal of the ZPA caused a weaker but similar distal expansion of *Tbx18* expression (Fig. 2, C, black arrow) but this may actually reflect the local removal of the AER rather than an effect of an endogenous ZPA derived signal (i.e. Shh). In case of *Tbx15*, which normally is expressed in the distal limb mesenchyme (compare Fig. 1, B), ablation of AER and ZPA had no effect (data not shown). Removal of the limb bud ectoderm caused a robust expansion of *Tbx18* expression into distal limb and the anterior flank mesenchyme (Fig. 2, D, black arrows and asterisk, respectively). A similarly broad expression pattern was also observed for *Tbx15* expression after ectoderm removal (data not shown). Together, these results demonstrate that at E10.5 expression of *Tbx15* and *Tbx18* is intrinsic to the limb bud mesenchyme, but that ectodermal and/or AER derived signals mediate local repression of *Tbx18* distally and in the flank region.

In subsequent experiments we analyzed which factors mediate the local repression of *Tbx18* by implantation of beads soaked with candidate signaling molecules. Beads were implanted into the *Tbx18*-positive central domain of the limb bud in presence and absence of ectoderm. Bone morphogenetic proteins (Bmp) 2, 4, 5 and 7 are secreted from the AER and the marginal/distal limb bud mesenchyme, i.e. exactly in those regions devoid of *Tbx18* expression (Capdevilla et al., 1999). In close proximity of beads soaked with Bmp4, but not with BSA (control), *Tbx18* expression was lost (Fig. 2, E-H, white arrows), demonstrating that Bmp4 causes repression of *Tbx18* at high concentrations. Interestingly, *Tbx2*, a known target of BMP-signaling (Ma et al., 2005; Yang et al., 2006), was induced in this domain (Fig. 2, I-L, black arrows). We next tested the effect of Wnt3a, which is secreted from the ectoderm (Barrow et al., 2003) by implantation of Wnt3a-expressing NIH3T3 cells (Kispert et al., 1998). *Axin2*, a target of the canonical Wnt-signaling pathway (ten Berge et al., 2008) was

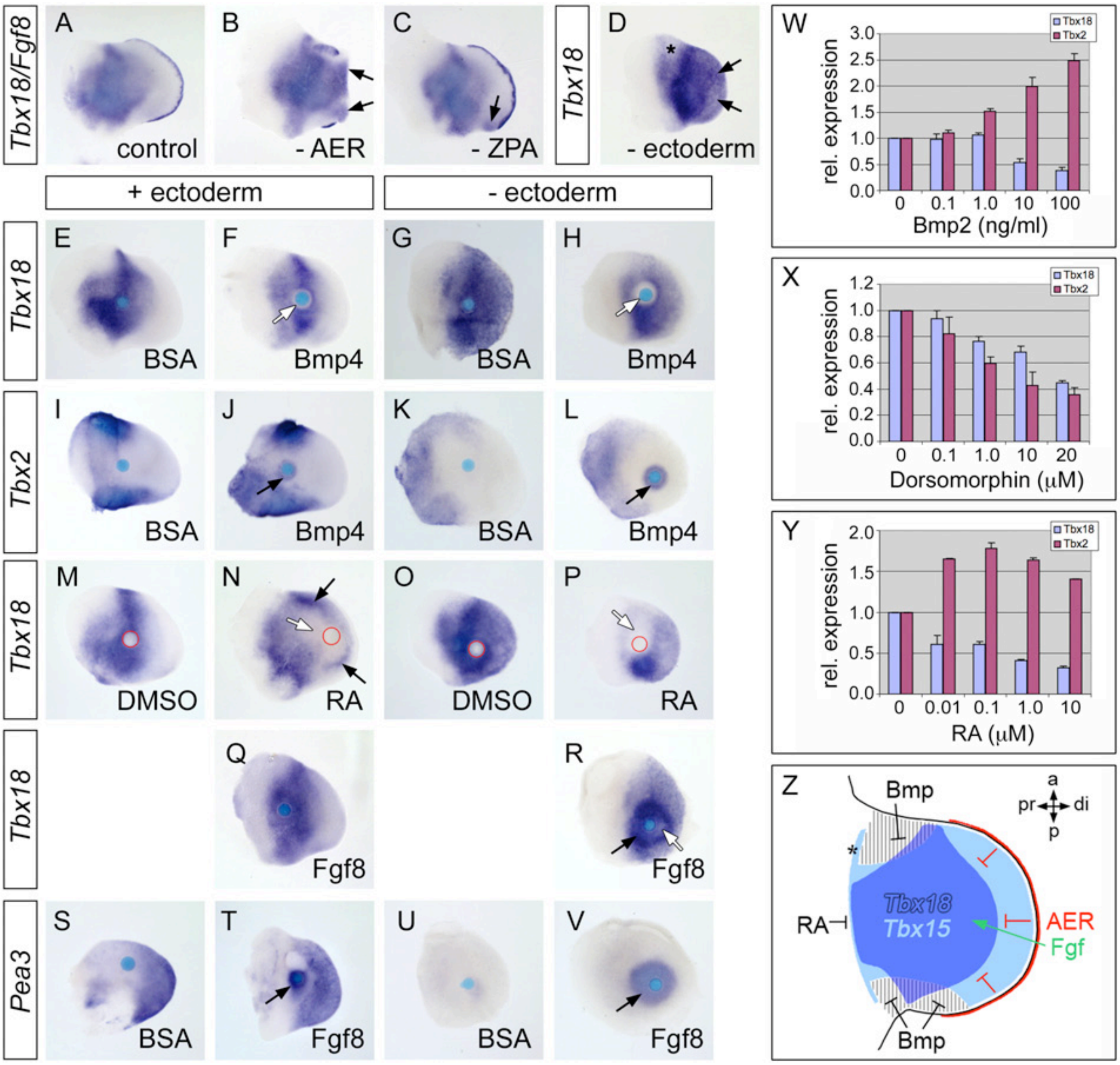
Tbx18/Fgf8
A
control
B
- AER
C
- ZPA
Tbx18
D
*
- ectoderm
+ ectoderm
- ectoderm
Tbx18
E
BSA
F
Bmp4
G
BSA
H
Bmp4
Tbx2
I
BSA
J
Bmp4
K
BSA
L
Bmp4
Tbx18
M
DMSO
N
RA
O
DMSO
P
RA
Tbx18
Q
Fgf8
R
Fgf8
Pea3
S
BSA
T
Fgf8
U
BSA
V
Fgf8
W
rel. expression
3.0
2.5
2.0
1.5
1.0
0.5
0.0
Tbx18
Tbx2
0
0.1
1.0
10
100
Bmp2 (ng/ml)
X
rel. expression
1.2
1.0
0.8
0.6
0.4
0.2
0.0
Tbx18
Tbx2
0
0.1
1.0
10
20
Dorsomorphin (μM)
Y
rel. expression
2.0
1.5
1.0
0.5
0.0
Tbx18
Tbx2
0
0.01
0.1
1.0
10
RA (μM)
Z
Bmp
a
pr
di
p
*
Tbx18
Tbx15
RA
AER
Fgf
Bmp

Fig. 2. **Culture experiments to study the regulation of *Tbx18* expression.**

A-V, whole mount *in situ* hybridization analysis of gene expression in E10.5 *wild type* forelimbs after 18 hours of explant culture. A-D, effects of surrounding tissues on the *Tbx18* expression domain. Representative examples of cultures of non-manipulated limb buds (A), and after removal of the AER (B), the ZPA (C), or ectoderm (D). Black arrows indicate an expansion of *Tbx18* expression domain. The AER was visualized by addition of a riboprobe specific for *Fgf8* (A-C). Asterisk (D) highlights the ectopic expression in the mesenchyme of the anterior flank. E-R, effect of local application of signaling molecules on *Tbx18* (E-H, M-R) and *Tbx2* (I-L) expression. Representative examples of cultured limb buds after bead implantation. Headings indicate presence (+) and absence (-) of ectoderm. Arrows mark induction (black) or repression (white) of gene expression. Compared to BSA controls, the implantation of Bmp4-soaked beads caused repression of *Tbx18* expression (compare E and F, G and H) and induction of *Tbx2* expression (compare I and J, K and L). Retinoic acid (RA) but not vehicle alone (DMSO) caused a massive repression of *Tbx18* expression (compare M and N, O and P) in close proximity while ectopic expression of *Tbx18* was observed at a further distance from the bead (N). Intermediate doses of Fgf8 caused induction of *Tbx18* expression in limb bud mesenchyme weakly in presence, but more strongly in absence of ectoderm (compare Q and R). *Pea3,* a known Fgf target, was analyzed as positive control (S-V).

W-Y, dose-dependant regulation of *Tbx18* expression by Bmp-signaling and RA. Micromass cultures of E10.5 *wild type* limb mesenchymes were cultered for 18 h. During the last 2 hours of culture recombinant Bmp4 (W), the Bmp-inhibitor Dorsomorphin (X), or RA (Y) were added at the concentrations indicated. Relative expression levels of *Tbx18* (blue bars) and *Tbx2* as a control (red bars) were determined by RT-PCR. For further details see experimental procedures.

consistently induced. Expression of *Tbx18* was unchanged (data not shown) arguing against a role of canonical Wnt-signaling in the regulation of *Tbx18* expression. Implantation of RA-soaked beads caused a strong repression of *Tbx18* in limb bud mesenchyme with and without ectoderm, whereas vehicle alone (DMSO) had no effect (Fig. 2, M-P, white arrows). However, regions of increased *Tbx18* expression were observed at some distance from the bead (Fig. 2, N, black arrows). Members of the Fibroblast growth factor family (Fgf) are secreted from the AER and the distal mesenchyme and regulate outgrowth and proximal-distal patterning of the limb bud (Mariani et al., 2008). The implantation of beads loaded with Fgf8 caused an induction of the known Fgf-target gene *Pea3* in limb buds with intact ectoderm (Roehl and Nüsslein-Volhard, 2001, Fig. 2, T, black arrow) but had little effect on the expression of *Tbx18* (Fig. 2, Q). However, after the removal of the limb ectoderm, Fgf8 caused a strong induction of both *Pea3* and *Tbx18* (Fig. 2, R, V, black arrows). Compared to the induction of *Pea3*, which was homogenous, strong induction of *Tbx18* was observed at some distance from the Fgf8 bead, only (Fig. 2, R, white arrow).

To quantify the effects of Bmp-signaling and RA, *Tbx18* expression in limb micromass cultures was studied by RT-PCR (see experimental procedures). Growth factors or inhibitors were added to the culture medium at increasing concentrations during the last two hours of a total culture period of 18 hours (Fig. 2, W-Y). Bmp4 caused a dose-dependant repression of *Tbx18* expression, whereas *Tbx2* expression that was analyzed in parallel was consistently induced (Fig. 2, W), confirming our bead implantation experiments. The application of the BMP-signaling inhibitor Dorsomorphin (Yu et al., 2008) resulted in a reduction of both, *Tbx2* and *Tbx18* expression (Fig. 2, X), suggesting that moderate endogenous levels of Bmp-signaling might also be required for activation of *Tbx18* expression. RA caused the induction *Tbx2* at low concentrations, but inhibited *Tbx18* expression in a dose-dependent manner (Fig. 2, Y). In summary, our results suggest a model in which moderate/low concentrations of Fgf induce *Tbx18* expression, whereas high concentrations of RA (secreted from the trunk) and Bmp (from the anterior/posterior margins of the limb bud) mediate local repression of *Tbx18* in the limb bud mesenchyme (Fig. 2, Z).

Z, model for the regulation of *Tbx15* and *Tbx18* expression in the developing limb bud. Expression domains of *Tbx18* and *Tbx15* in E10.5 forelimb buds are represented by dark and light blue regions, respectively (compare Figure 1, B and F). We propose that RA, synthesized in the trunk region, defines the proximal limit of *Tbx15/18* expression by a repression mechanism. Notably, *Tbx15* expression extends further proximally and also labels precursors of the developing scapula blade (*). At the anterior and posterior margins of the limb bud Bmp molecules could mediate repression of *Tbx15/18* expression, either directly or by induction of *Tbx2/3* expression (their expression is marked by grey hatched regions). In the distal limb bud *Tbx18* expression is repressed in a currently unknown mechanism by signals from the AER (red line). Fgf8 that is secreted from the AER could be implicated in activation of *Tbx15/18* expression in more proximal regions (green arrow). For further details see discussion.

Requirement of Tbx18 and Tbx15 in the development of the proximal limb skeleton.

In order to investigate a redundant role of Tbx15 and Tbx18 during limb development, we generated embryos double mutant for *Tbx15* and *Tbx18* and analyzed the phenotypic consequences. Since *Tbx18*-deficient embryos die shortly after birth (Bussen et al., 2004), we collected offspring at E18.5. At this time point embryonic lethality was not observed and all allelic combinations were found at the expected Mendelian ratio (data not shown). Morphological inspection of $Tbx15^{-/-}$, $Tbx18^{GFP/GFP}$ double mutants (subsequently abbreviated as '*DM*') revealed a dramatic reduction of the length of upper and lower limbs (Fig. 3, A, B). Skeletal preparations revealed that stylopod and zeugopod were rudimentarily formed and fused

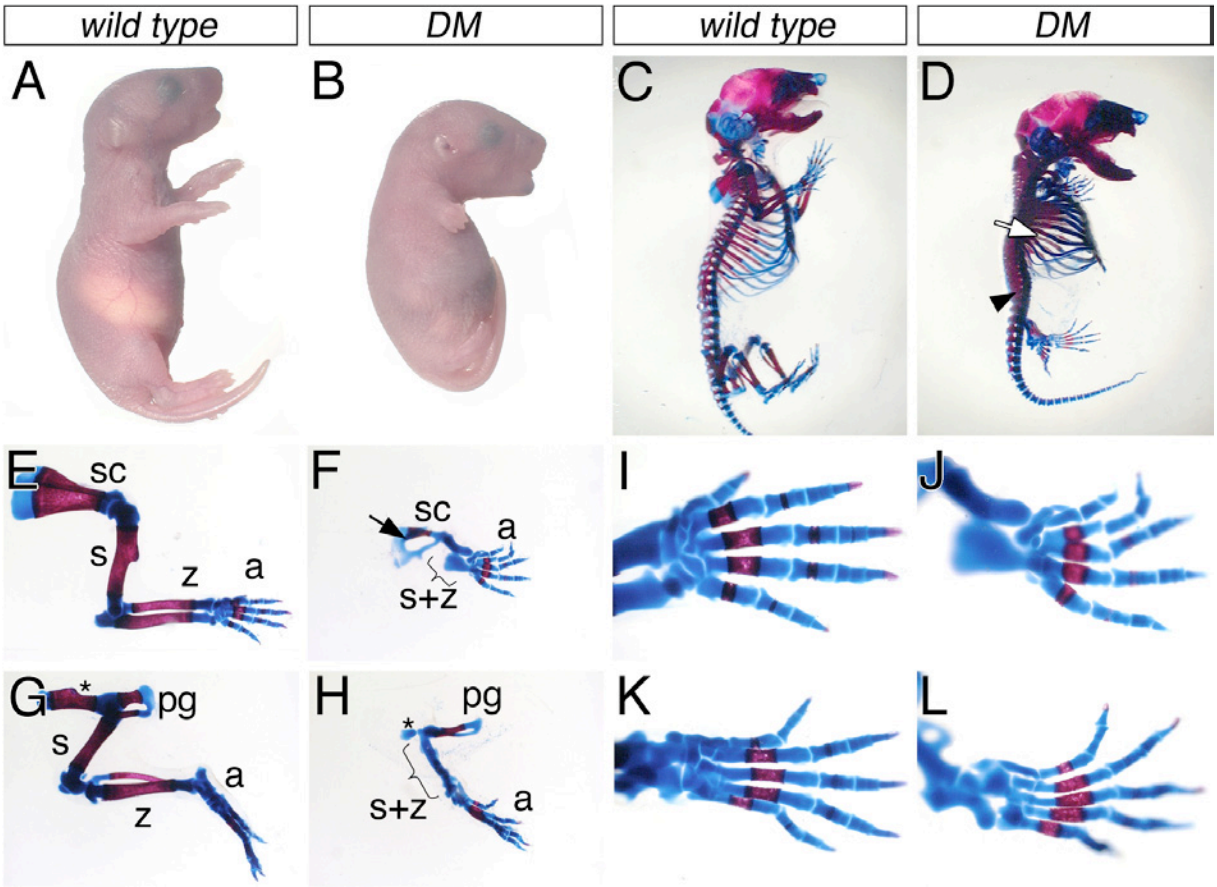

Fig. 3. **Requirement of Tbx15 and Tbx18 in the development of the proximal limb skeleton.**

Morphology (A and B) and skeletal preparations (C-L) of E18.5 *wild type* and *Tbx15*,*Tbx18* double mutant (*DM*) embryos (C-D) and limbs (E-L). Whole mount images reveal a dramatic shortening of upper and lower limbs. The axial skeleton of *DM* embryos displays defects caused by the loss of *Tbx18* alone (D, fusions of proximal ribs, and vertebral pedicles, white arrow and black arrowhead, respectively, Bussen et al., 2004). Higher magnification of the forelimb (E, F) and hindlimb skeleton (G, H) reveals a selective reduction and fusion (brackets) of stylopod and zeugopod elements in *DM* embryos. The scapula blade is reduced in size and shows a central hole (black arrow). Asterisks in G and H highlight the ilium of the pelvic bone, which is reduced in hindlimbs of *DMs*. I-L, dorsal views of the upper (I, J) and lower (K, L) autopod, which are only weakly affected *DM* embryos. Abbreviations are a, autopod; pg, pelvic girdle; s, stylopod; sc, scapula; z, zeugopod.

together both in fore- and hindlimbs (Fig. 3, E-H). The pectoral and the pelvic girdle were strongly reduced, showing an increase in phenotypic severity in comparison with scapula defects of *Tbx15* single mutants (Singh et al., 2005 and Supplemental Fig. 2). Remarkably, however, the distal autopod (phalanges and metacarpals/-tarsals) was essentially normal in *DM* embryos (Fig. 3, I-L) with only mild changes of the tarsal and carpal bones, demonstrating that the observed phenotype is not caused by a general outgrowth defect of the limb. Analysis of compound mutants embryos showed that reduction of the *Tbx18* gene dosage on a *Tbx15* mutant background, or vice versa, produced no major defects of stylopod and zeugopod elements (Supplemental Fig. 2). A mild reduction in the relative length of the humerus and a thickening of radius and ulna were observed in $Tbx15^{+/-}$, $Tbx18^{GFP/GFP}$ forelimbs (Supplemental Fig. 2, E). These data indicate that Tbx15 and Tbx18 have a redundant function in the development of the proximal and intermediate limb skeleton. A single *wild type* allele of either *Tbx15* or *Tbx18* is sufficient to allow normal limb development.

Early defects in chondrogenic aggregation of Tbx18/Tbx15 double mutant limbs.

To determine the temporal requirement of *Tbx15/Tbx18* function, we analyzed phenotypic changes of the limb skeleton at earlier developmental time points. At E14.5, the cartilagenous pre-skeleton of *DM* limbs prefigured the defects observed at E18.5 (Supplemental Fig. 3), excluding defective osteogenesis as a cause of the phenotype. At E12.5, the length of the extremities was strongly decreased, selectively affecting the proximal parts (Fig. 4, A, B, brackets). Cartilagenous anlagen of stylo- and zeugopod elements were absent and the scapula appeared severely reduced (Fig. 4, B, black arrow). The autopod, in contrast, was completely unaffected. Analysis of forelimb sections for the deposition of chondrocyte extracellular matrix (Alcian blue staining) as well as the distribution of chondrogenic precursors and developing joints (by *in situ* hybridization for *Sox9* and *Gdf5*, respectively; Lefebvre et al., 1996; Storm and Kingsley, 1999) revealed a single roundish element most probably representing the remnants of both stylo- and zeugopod anlagen in the *DM* (Fig. 4, F-H, black arrows). The developing humerus of *wild type* embryos exhibited growth plates at the proximal and distal ends, flanked by developing joints as marked expression of *Gdf5* (Fig. 4, C-E). The corresponding cartilage rudiment of *DM* embryos did not proceed to long bone development, and was additionally positive for *Gdf5* expression (Fig. 4, F-H, black arrows). This missegregation of cartilage and joints may explain the observed fusion of stylo- and zeugopodial elements at later stages. Absence of Alcian blue staining and *Sox9* expression in E11.5 DM fore limb sections indicated that mesenchymal condensations of stylopod and zeugopod failed to form (Fig. 4, I-L, circles). At E10.5, the expression of *Sox9* was unaffected as determined by whole mount *in situ* hybridization (Fig. 4, M, N), suggesting that *Tbx15* and *Tbx18* act downstream or in a parallel pathway to *Sox9* to regulate cartilage formation. Together, our results indicate that *Tbx15* and *Tbx18* are required for mesenchymal precursors to condense to the anlagen of stylo- and zeugopod.

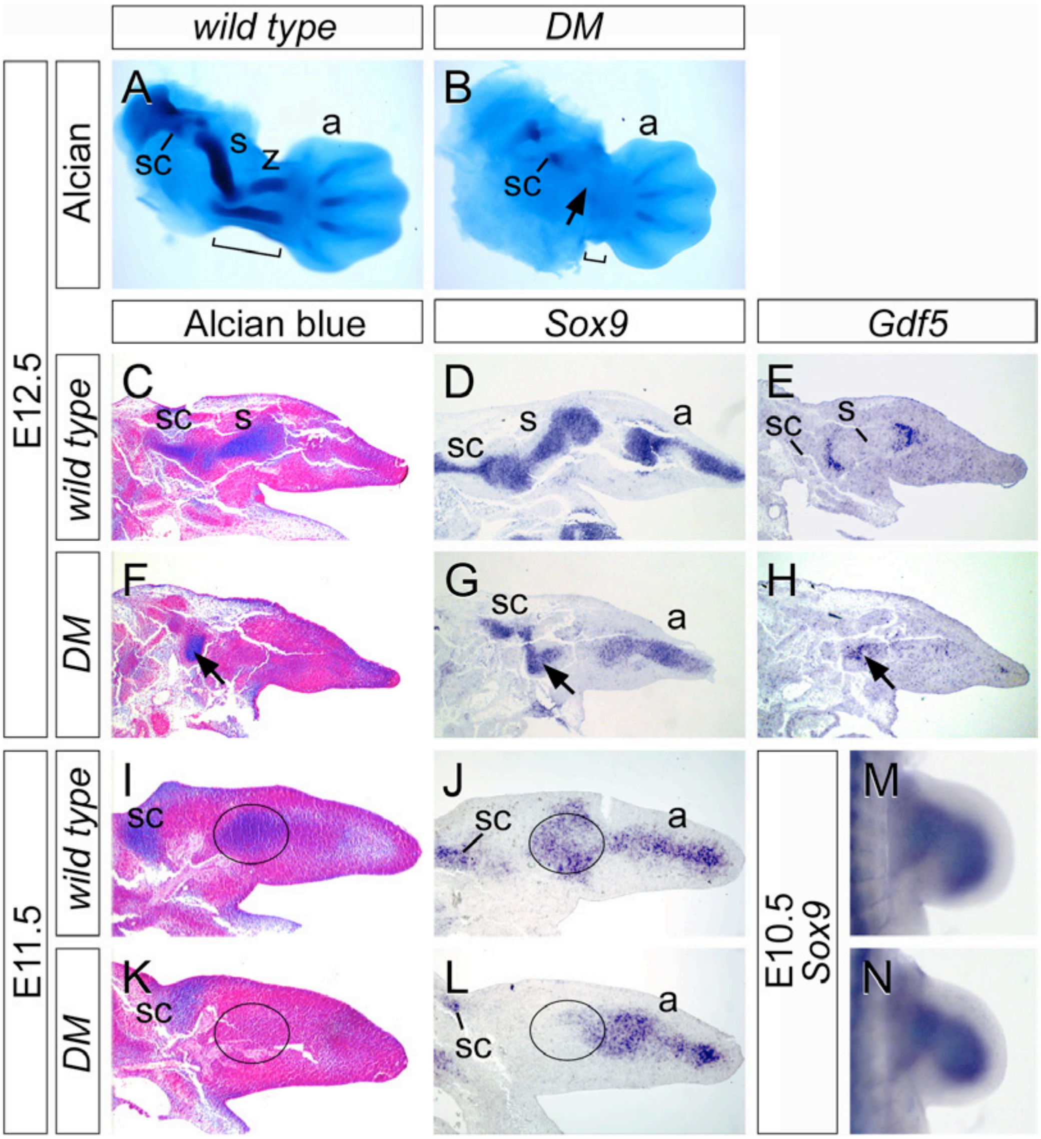

Fig. 4. **Early defect in chondrogenic aggregation of *Tbx18/Tbx15* double mutants.**

A-B, whole mount Alcian blue staining of E12.5 *wild type* and *DM* forelimbs, black arrow marks the reduction of stylo- and zeugopod elements. The reduction in length of *DM* limbs mainly affects the proximal part (brackets). C-H, analysis of chondrogenesis and joint formation on transverse sections of E12.5 *wild type* and *DM* forelimbs. Alcian blue-positive precartilagenous mesenchymal condensations of stylo- and zeugopod (C, F), and *Sox9*-positive chondrogenic precursors (D, G) are reduced (black arrows). In *DM*s the remaining cartilage is additionally positive for the joint marker *Gdf5* (H, black arrow). I-L, Alcian blue staining and *Sox9 in situ* hybridization on E11.5 *wild type* and *DM* transverse limb sections. Black circles indicate the loss of the central chondrogenic aggregate (K), and a reduction of *Sox9*-positive precursors cells in this region (L). M-N, whole mount *in situ* hybridization shows normal *Sox9* expression in E10.5 *DM* forelimb buds. Abbreviations as in Figure 3.

Proximal-distal patterning of the limb bud is not affected in Tbx15/Tbx18 DM embryos

The selective failure of mesenchymal cells to condense to the anlagen of stylopod and zeugopod in *DM* limb buds prompted us to analyze whether defects in proximal-distal patterning may underlie this phenotype (Supplemental Fig. 4). Markers for the proximal domain (*Meis1*, *Meis2*, Mercader et al., 1999, *Rarb*, Mendelsohn et al., 1991, and *Ror1*, Matsuda et al., 2001) were normally expressed in *DM* limb buds, as were markers of the distal region (*Fgf8* and the Fgf8-target genes *Fgf10*, Ohuchi et al., 1997, *Pea3*, Roehl and Nüsslein-Volhard, 2001 and *Cyp26b1*, Yashiro et al., 2004; Supplemental Fig. 4, E-L). Likewise the expression of *Hoxd*-family members (*Hoxd11*, *Hoxd12* and *Hoxd13*, Dollé et al., 1989; Supplemental Fig. 4, M-O) was unchanged, reflecting that the PD-positional identities are correctly established in *DM* limb buds. During the specification of the anterior-posterior axis of the limb, the expression of transcription factor Hand2 at the posterior limb margin is required to induce the expression of Shh, which itself is the mediator of ZPA activity (Charité et al., 2000). In *DM* limbs the expression of *Hand2* and *Shh* was unchanged, as was the Shh target gene *Ptch1* (Marigo et al., 1996; Supplemental Fig. 4, A-C). Likewise, the dorsally restricted expression of *Wnt7a* was unaltered (Parr et al., 1993; Supplemental Fig. 4, D), demonstrating that the anterior-posterior and dorsal-ventral axes are as expected unaffected in *DM* limb buds. We therefore conclude *Tbx15/Tbx18* act downstream of the proximal-distal patterning system to regulate the local aggregation of mesenchymal precursor cells.

Cellular defects caused by the loss of Tbx15 and Tbx18.

The absence of major patterning defects prompted us to analyze the cellular consequences of the combined loss of *Tbx15* and *Tbx18*. We first tested if decreased proliferation precedes the reduction of chondrogenic precursors by using BrdU incorporation assay at E10.5. We determined the BrdU labeling index in the proximal region and as a control in the distal mesenchyme (Fig. 5, A, B, blue boxes). The quantification of S-phase nuclei on transverse forelimb sections (Fig. 5, C) showed a weak, but significant reduction of proliferation in the proximal (20.2 ± 1.1% in the *wild type* and 16.6 ± 0.7% in the *DM*; $p = 2.6 \times 10^{-8}$) but not in the distal region of *DM* limb buds (52.9 ± 5.7% in the *wild type* and 50.3 ± 2.9% in the *DM*; $p = 0.22$). To judge the contribution of programmed cell death to the phenotypic changes, we analyzed the distribution of apoptotic cells on limb sections by the TUNEL assay. A strong increase of cell death was detected in the proximal region of the limb bud at E10.5 (Fig. 5, D, E) and E11.5 (Fig. 5, F, G, white circles). Hence, both reduced proliferation as well as augmented cell death may contribute to the reduction of proximal skeletal structures.

To characterize the fate of Tbx18-expressing cells in the *DM* limbs, we took advantage of the GFP reporter in the *Tbx18*-mutant allele. GFP-epifluorescence of freshly isolated E10.5 forelimbs of *Tbx15*$^{+/+}$, *Tbx18*$^{GFP/GFP}$ embryos recapitulated the endogenous expression of *Tbx18* and was therefore considered as '*wild type*' control (Fig. 5, H-J, compare Fig. 1, F). GFP-positive cells were confined to the proximal/central regions of the limb bud, showing an exclusion from the distal mesenchyme (Fig. 5, J, white dotted line). In contrast, a massive

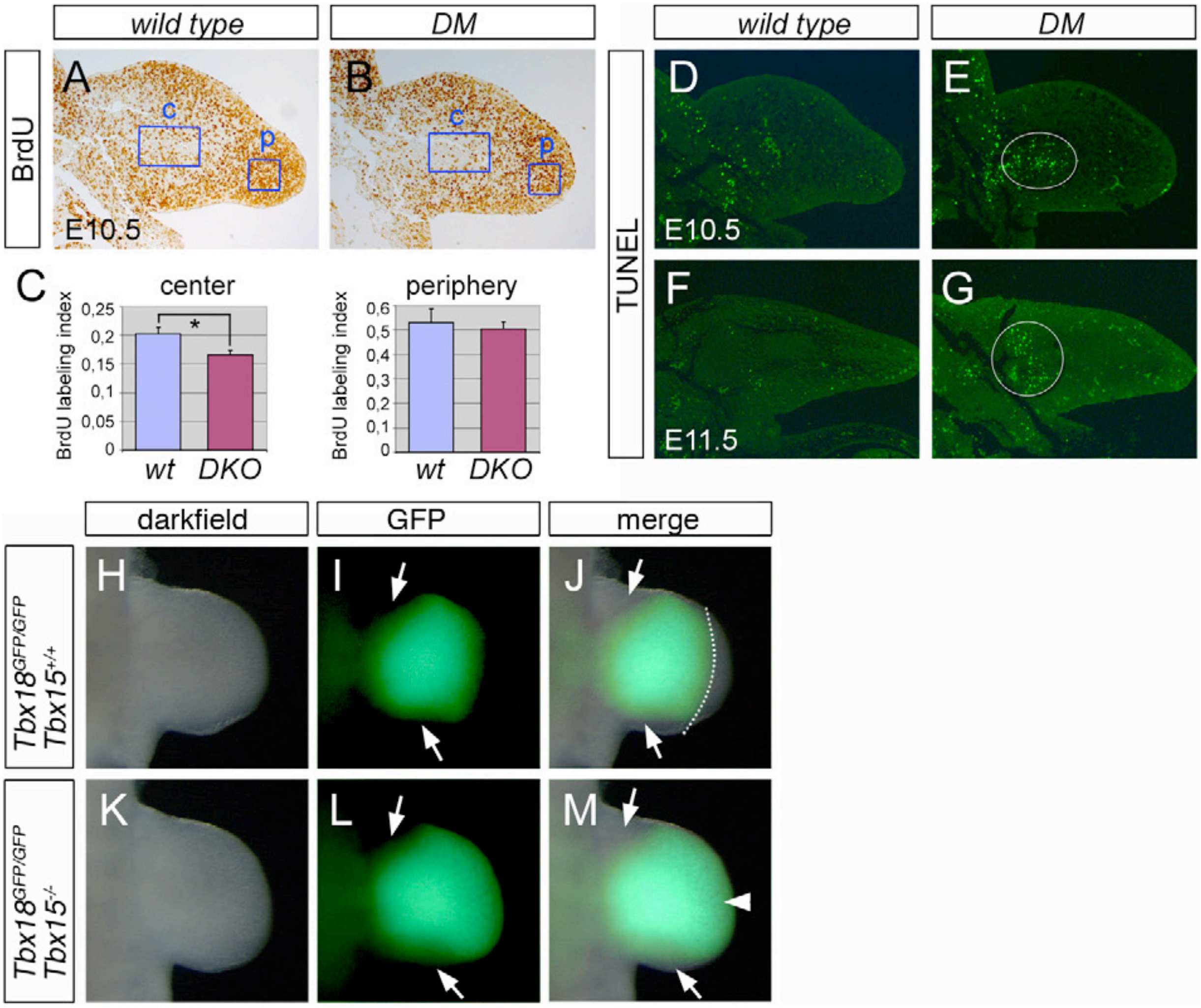
wild type
DM
wild type
DM
BrdU
A
c
p
E10.5
B
c
p
C
center
BrdU labeling index
0,25
0,2
0,15
0,1
0,05
0
*
wt
DKO
periphery
BrdU labeling index
0,6
0,5
0,4
0,3
0,2
0,1
0
wt
DKO
TUNEL
D
E10.5
E
F
E11.5
G
darkfield
GFP
merge
Tbx18GFP/GFP
Tbx15+/+
H
I
J
Tbx18GFP/GFP
Tbx15-/-
K
L
M

Fig. 5. **Cellular defects accompanied with the loss of *Tbx18* and *Tbx15*.**

A-B, anti-BrdU immunohistochemistry on E10.5 *wild type* and *DM* transverse forelimb sections; the BrdU labeling index was determined in central (c) and peripheral (p) regions as indicated by blue boxes. C, quantification of S-phase nuclei. The BrdU labeling index (refer experimental procedures) was reduced in the center of *DM* forelimbs (*: $p = 2.6 \times 10^{-8}$), but not in the periphery. D-G, detection of apoptotic cells on E10.5 (D, E) and E11.5 (F, G) *wild type* and *DM* transverse forelimb sections by TUNEL staining. White circles highlight an increased number of apoptotic cells in the proximal region of mutant forelimbs. H-M, Detection of GFP-positive cells in E10.5 *Tbx18*$^{GFP/GFP}$,*Tbx15*$^{+/+}$ ('*wild type*') and *Tbx18*$^{GFP/GFP}$,*Tbx15*$^{-/-}$ (*DM*) forelimbs. Shown are darkfield (H, K), GFP-epifluorescence (I, L) and merged images (J, M). In control limb buds GFP-positive cells are excluded from the distal mesenchyme (white dotted line), in contrast GFP-positive cells extend to the distal tip of the limb bud in the *DM* (white arrowhead). Exclusion of GFP-positive cells from anterior and posterior flanks is similar in *wild type* and *DM* limb buds (white arrows).

expansion of GFP-positive cells was observed into the distal mesenchyme of *DM* limbs (*Tbx15*$^{-/-}$, *Tbx18*$^{GFP/GFP}$) (Fig. 5, M, white arrowhead), while exclusion of fluorescent signal from the flank mesenchyme was maintained (Fig. 5, J, M, white arrows). Section *in situ* hybridization using a riboprobe specific for *GFP* confirmed the distal expansion of Tbx18-expressing cells in *DM* forelimbs. Notably, we did not observe an expansion of *Tbx18* expression in *Tbx15*$^{-/-}$ single mutants, arguing against a role for Tbx15 as a transcriptional repressor of *Tbx18* in the distal mesenchyme (data not shown). We therefore favor the possibility that the expansion of Tbx18^{GFP}-positive cells results from aberrant migration of proximal mesenchymal cells into the distal region.

Deregulated expression of Eph/Ephrin molecules prefigures the skeletal defects of Tbx15/Tbx18 mutant limbs.

Eph receptor tyrosine kinases and their membrane-bound Ephrin (Efn) ligands mediate cellular adhesion and repulsion by bidirectional signaling in various developmental contexts (for a review refer Klein, 2004). Notably, *in vitro* studies have shown that Eph/Ephrin molecules regulate differential cell adhesion properties of cells isolated from the proximal or distal limb bud mesenchyme (Wada et al., 1998). Eph receptors and ligands can be divided in two subclasses, class A and B. In general, class A receptors (Epha) bind to GPI-anchored Ephrin ligands (Efna), while class B receptors (Ephb) bind to Ephrin ligands containing a transmembrane domain (Efnb) (Gale et al., 1996).

To analyze if changes in Eph/Ephrin distribution underlie the loss of lineage restriction in the *DM* limb bud, we performed *in situ* binding assays using recombinant Eph/Ephrin-Fc fusion proteins, which consist of the extracellular domain of Eph/Ephrin molecules fused to the Fc-region of human IgG. We studied the binding pattern of one representative of each subclass of receptors and ligands to cover the entity of receptors and ligands present in the limb bud. As shown previously, class A receptors and ligands are present in complementary proximal and distal regions of the limb mesenchyme (Gale et al., 1996). Using Efna4-Fc and Epha4-Fc we found that at E10.5 this boundary is correctly established in *wild type* and *DM* limbs (Fig. 6, A, B and E, F). However, at E11.5 the region positive for Efna4-Fc and negative for Epha4-Fc was clearly expanded into more proximal regions of the *DM* limb bud (Fig. 6, C, D, black arrow and G, H, white arrow). Efnb1-Fc displayed a broad binding pattern (data not shown), suggesting that Ephb-receptors are not limiting factors to generate differential adhesion. In contrast, the binding patterns of Ephb2-Fc exhibited a stronger signal in distal than in central regions of *wild type* limb buds at E10.5, compatible with the idea that EfnB ligands are differentially expressed along the proximal-distal axis (Fig. 6, I). In *DM* limbs, staining in proximal regions was augmented (Fig. 6, J, black arrow). The Ephb2-Fc-negative domain covered the central region of *wild type* E11.5 limb buds, whereas a broad staining was observed in the corresponding region of *DM* embryos (Fig. 6, K, L, red circles). Similar changes were also

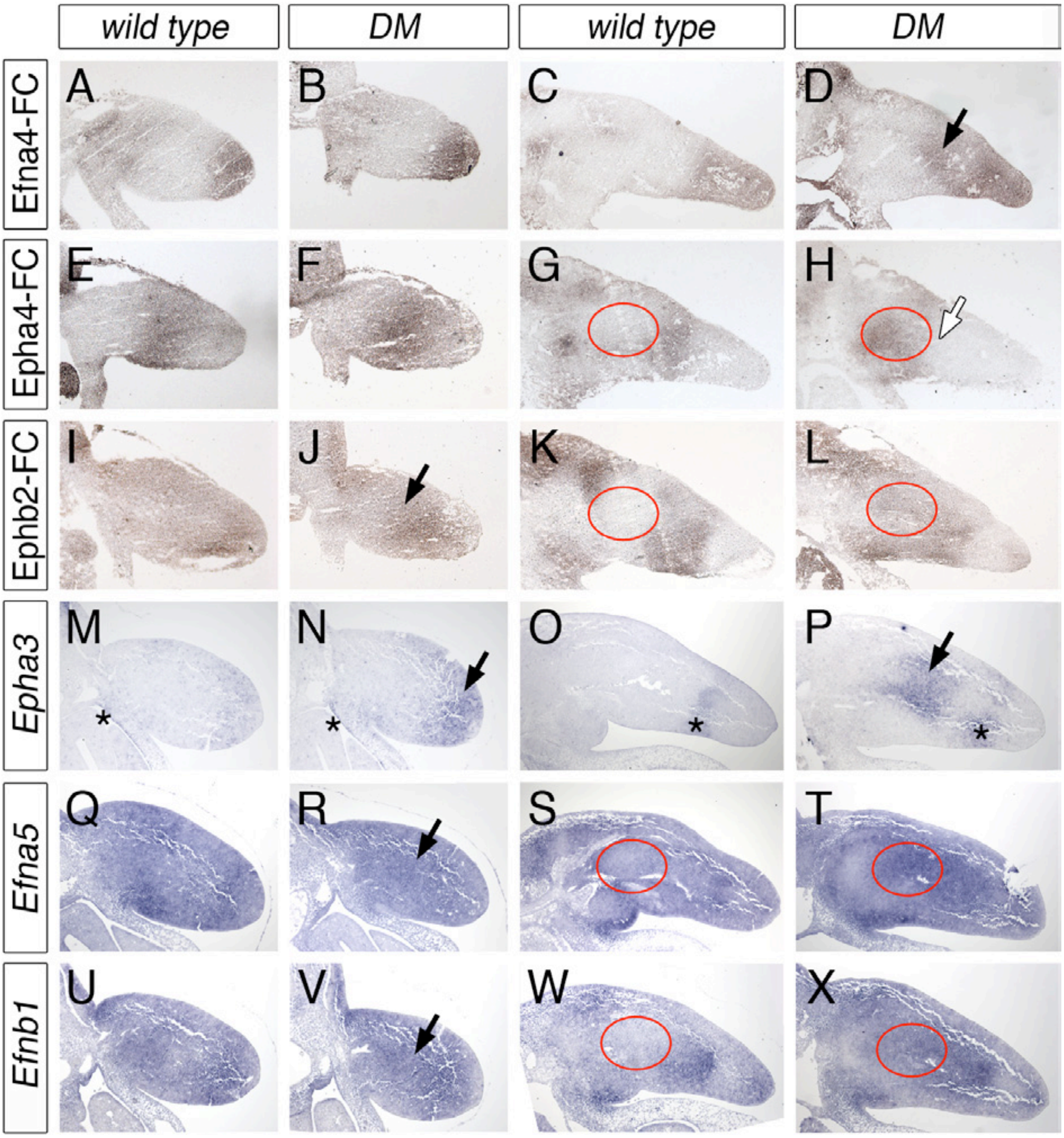

Fig. 6. **Deregulated expression of Eph/Ephrin cell surface molecules in *Tbx18/Tbx15* double mutants.**

A-L, Eph/Ephrin-Fc stainings to detect the distribution of Eph/Ephrin molecules. Shown are the binding patterns of Efna4-Fc (A-D), Epha4-Fc (E-H) and Ephb2-Fc (I-L) on E10.5 and E11.5 *wild type* and *DM* transverse forelimb sections. White and black arrows show reduced and increased signals, respectively. Red circles illustrate up-regulation of ligands detected by Epha4-Fc and Ephb2-Fc in the proximal region of E11.5 *DM* limb buds. The changes are reflected by the mRNA expression patterns of *Epha3* (M-P), *Efna5* (Q-T), *Efnb1* (U-X), as determined by *in situ* hybridization. The asterisks in M-P indicate that the expression of *Epha3* is unchanged in adjacent reverence domains.

observed using Epha4-Fc (Fig. 6, G and H) demonstrating a collective failure to down-regulate Ephrin A and B class ligands in the central region of the limb bud. To explore which members of the Eph/Ephrin gene families are responsible for the observed changes, we analyzed the expression of the majority of the family members by *in situ* expression analysis on *wild type* and *DM* forelimb sections (Fig. 6, M-X and Supplemental Fig. 5). Up-regulation of *Epha3* was observed in the distal mesenchyme of *DM* limb buds at E10.5 and at E11.5, ectopic expression was found in more proximal regions (Fig. 6, N and P, black arrows), in agreement with the expanded binding patterns of Efna4-Fc at this stage (compare Fig. 6, D). *In situ* hybridization analysis failed to detect expression of a class A ligand that reflected the binding patterns of Epha4-Fc at E10.5. This could indicate a posttranscriptional regulation, or alternatively, binding of Epha4-Fc to Ephrin B class members. Interestingly, we detected increased expression of *Efna5* and *EfnB1* – possible ligands for Ephb2-Fc – in the proximal region *DM* limb buds at E10.5 (compare Fig. 6, Q, R and U, V, black arrows). Likewise, expression of both genes was up-regulated in the central domain of E11.5 *DM* limb buds recapitulating the ectopic binding patterns of Epha4 and Ephb2-Fc (Fig. 6, S, T and W, X, red circles). Collectively, our results show that the proximal domain of *DM* limb buds becomes distalized with respect to the expression profile of Eph/Ephrin molecules. This may result in mis-segregation of mesenchymal cells along the proximo-distal axis.

Tbx18 expression mediates homing of mesenchymal cells to the Tbx18-positive proximal limb compartment.

Since combined loss of *Tbx15* and *Tbx18* leads to changed cellular parameters of mesenchymal cells of the proximal limb region including proliferation, apoptosis and lineage restriction, we wished to explore the primary function of Tbx18 in misexpression experiments *in vivo*. We used a transgenic approach based on an inactive bicistronic expression cassette containing the *Tbx18* ORF followed by *IRES-GFP* that was integrated in the ubiquitously expressed *Hypoxanthine guanine phosphoribosyl transferase* (*Hprt*) locus (see experimental procedures and Supplemental Fig. 1, A). Upon cre-mediated recombination the expression cassette is rearranged to localize *Tbx18-IRES-EGFP* downstream of the strong CAG promoter allowing robust activation of Tbx18 in cells and simultaneous expression of EGFP (Supplemental Fig. 1, A-C). Importantly, expression from the X-chromosomal *Hprt*-locus results in a chimeric transgene expression in heterozygous females due to random X-chromosome inactivation at early stages of embryogenesis. Thus, this genetic system provides the opportunity to analyze the behaviour of transgene expressing cells in a *wild type* environment similar to

Drosophila-type mosaic experiments, while in hemizygous males the transgene is homogenously expressed in all cre-positive cells.

To activate transgene expression, we employed the *Pax3::cre* mouse line, which drives expression of cre-recombinase under the control of the 1.6 kb upstream promoter of *Pax3* broadly in the posterior trunk region including the hindlimbs (Li et al., 2000). Using the *Rosa26* lacZ-reporter line (*R26R*) we confirmed the recombination in the hindlimbs by β-galactosidase staining in whole mount embryos and on sections of E10.5 and E12.0 embryos (Supplemental Fig. 6, A-L). At both stages, we detected broad albeit partly variable mesenchymal cre activity. β-galactosidase staining appeared weaker in anterior and ventral regions of the limb bud (Supplemental Fig. 6, F, G, black arrows). Functionality of the system was proven in *Pax3::cre/+*, *Sox9*$^{fl/fl}$ mice that showed a nearly complete reduction of the skeleton of the vertebral column and the hindlimbs compatible with the role of Sox9 as a regulator of chondrogenesis (Supplemental Fig. 6, M-P, Bi et al., 1999).

Mosaic misexpression of Tbx18 in E18.5 female embryos (*Pax3::cre/+*, *Hprt*$^{CAG::Tbx18/+}$ abbreviated as *P3::cre*, *Tbx18*^{GOF}/+) resulted in no obvious morphological or skeletal limb defects (Fig. 7, E-H). In hemizyous male embryos (*Pax3::cre/+*, *Hprt*$^{CAG::Tbx18/Y}$, abbreviated as

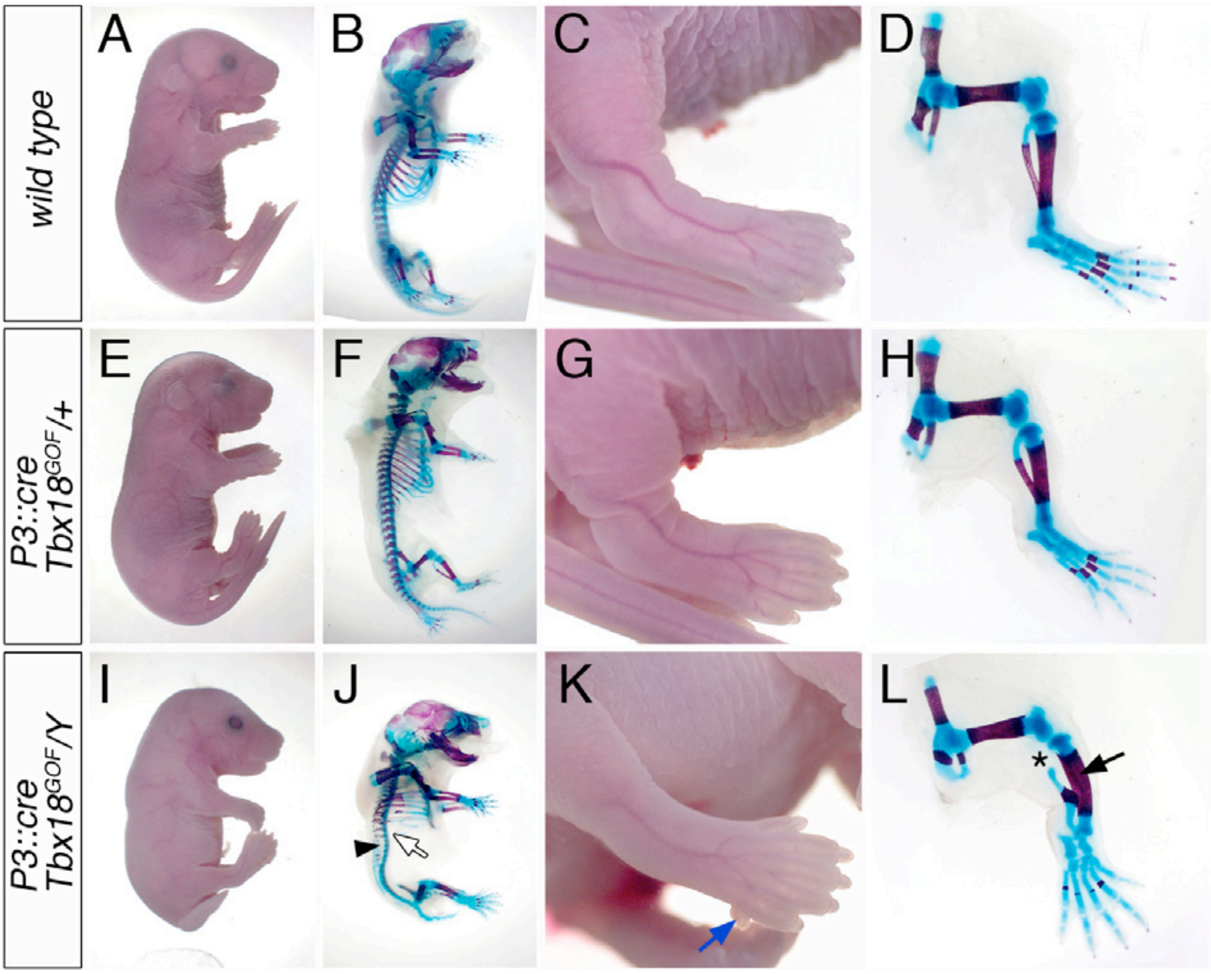

Fig. 7. **Misexpression of Tbx18 in the limb mesenchyme causes only mild skeletal defects.** Morphology and skeletal preparations of *wild type* embryos (A-D), and Tbx18 misexpressing embryos at E18.5. The hindlimb skeleton of *Pax3::cre*, *Hprt*$^{CAG::Tbx18/+}$ females (abbreviated as *P3::cre*, *Tbx18*^{GOF}/+, E-H) appears unchanged. *Pax3::cre*, *Hprt*$^{CAG::Tbx18}$/*Y* males (abbreviated as *P3::cre*, *Tbx18*$^{GOF/}$*Y*, I-L) show axial defects in the posterior part of the body including a strong reduction of pedicles and proximal ribs (J, black arrowhead and white arrow, respectively). The hindlimbs of *P3::cre*, *Tbx18*$^{GOF/}$*Y* embryos are weakly affected, displaying a small ectopic finger (blue arrow), reduced fibula (asterisk) and the thickend tibia (black arrow). During preparation of the hindlimb skeleton the ectopic finger was removed.

P3::cre, *Tbx18*^{GOF}*/Y*) a reduction of the fibula, and an increased thickness of the tibia was observed (Fig. 7, L). The majority of embryos additionally showed a small ectopic finger postaxially (Fig. 7, K). However, surprisingly, patterning of limb skeletal elements of stylopod, zeugo- and autopod was normal. These results demonstrate that broad misexpression of *Tbx18* is compatible with limb development, and furthermore that the down-regulation of the endogenous *Tbx18* expression in prechondrogenic aggregates (compare Fig. 1, G, H, O, P) is not a prerequisite for subsequent cartilage differentiation. In contrast to the situation in the limb, the axial skeleton of *P3::cre*, *Tbx18*^{GOF}*/Y* embryos showed a strong reduction of pedicles and proximal ribs, whereas *P3::cre*, *Tbx18*^{GOF}/+ females were normal (Fig. 7, B, F, J). Since *Pax3::cre* mediates recombination in the presomitic mesoderm (Li et al., 2000), we conclude that these defects recapitulate the known phenotype resulting from misexpression of *Tbx18* in the somitic mesoderm (Bussen et al., 2004), thus, confirming that the *Hprt*$^{CAG::Tbx18}$-allele allows misexpression of functional Tbx18 protein.

The absence of strong limb defects prompted us to analyze the distribution of transgene expressing cells at earlier stages by GFP-epifluorescence. Notably, we found that the mosaic expression in heterozygous females was not random but that GFP-positive cells were exclusively present in the proximal part of E10.5 limb buds (Fig. 8, J). In a similar manner transgene expesing cells were largely excluded from the distal mesenchyme in hindlimbs of *Tbx18*^{GOF}*/Y* male embryos (Fig. 8, P). Most obviously, the autopod domain was GFP-negative except a variable staining in the developing cartilages of the digits at E12.5 (Fig. 8, L, R). The selective localization of Tbx18-expressing cells to the domain of endogenous *Tbx18* expression (the proximal limb bud) can therefore explain the mild limb defects in these embryos. More importantly however, these data reveal a previously unrecognized compartment boundary between cells of the presumptive stylopod/zeugopod and autopod in the E10.5 limb bud.

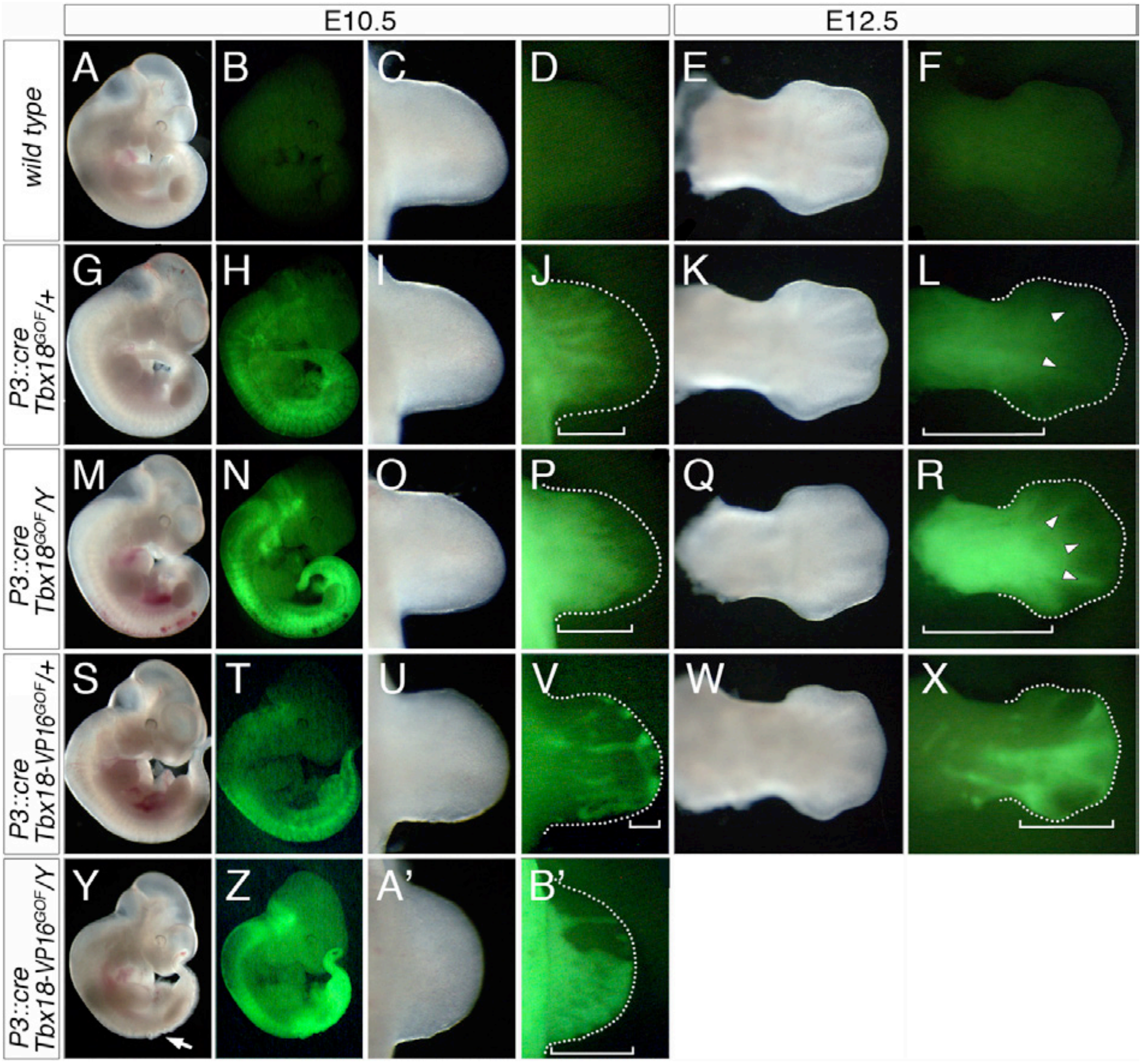

Fig. 8. **Misexpression of Tbx18- and Tbx18-VP16 results in differential localization of transgene expressing cells.**

Darkfield images and GFP-epifluorescence of *wild type* (A-F), Tbx18 (G-R) and Tbx18-VP16 (S-B') misexpressing embryos. Shown are whole mount images of E10.5 embryos, and hindlimbs at E10.5 and E12.5. Adjacent images represent darkfield illumination (left) or GFP-epifluorescence (right) of the same specimen. Dotted lines in J, L, P, R, V, X, B' highlight the outlines the limb bud. In *P3::cre*, *Tbx18*^{GOF}/+ and *Tbx18*^{GOF}/*Y* hindlimbs, GFP-positive cells preferentially locate to the proximal limb mesenchyme, as indicated by white brackets. White arrowheads in L and R mark an additional GFP-signal in the developing digit cartilages at E12.5. In *P3::cre*, *Tbx18-VP16*^{GOF}/+ hindlimbs, GFP-positive cells preferentially locate to the distal mesenchyme (V, X, white brackets). At E10.5 *P3::cre*, *Tbx18-VP16*^{GOF}/*Y* male embryos show a severe segmentation defect and spina bifida in the posterior part of the body (Y, white arrow), and GFP-positive cells are distributed along the entire PD-axis of the hindlimb (B', white bracket). At E12.5 no viable *P3::cre*, *Tbx18-VP16*^{GOF}/*Y* embryos were found.

Since both Tbx15 and Tbx18 protein function as transcriptional repressors *in vitro* (Farin et al., 2007), we hypothesized that a Tbx18-VP16 activator construct would generate a dominant negative protein. To analyze the consequences of Tbx18-VP16 expression on cellular behavior *in vivo*, we generated a $Hprt^{CAG::Tbx18\text{-}VP16}$ allele analogous to the $Hprt^{CAG::Tbx18}$ allele described above (Supplemental Fig. 1, A). *Pax3::cre*-mediated misexpression of Tbx18-VP16 led to severe neural tube closure defects, a lack of segmentation in the posterior body and embryonic lethality before E12.5 in male embryos (abbreviated as *P3::cre*, $Tbx18^{GOF\text{-}VP16}/Y$, Fig. 8, Y and data not shown). At E10.5 the hindlimbs of these *P3::cre*, $Tbx18^{GOF\text{-}VP16}/Y$ embryos were reduced in size (Fig. 8, A'). Mosaic expression in female embryos (*P3::cre*, $Tbx18^{GOF\text{-}VP16}/+$) resulted in normal development of the limb skeleton but caused defects in the axial skeleton (Supplemental Fig. 7, G, H). Strikingly, the pattern of GFP-expression in E10.5 and E12.5 *P3::cre*, $Tbx18^{GOF\text{-}VP16}/+$ females showed a preferential localization of Tbx18-VP16-expressing cells to the distal regions of the limb bud mesenchyme (Fig. 8, V, X), i.e. in a complimentary pattern compared to the misexpression of *wild type* Tbx18 protein (compare Fig. 8, J, L, P ,R). In *P3::cre*, $Tbx18^{GOF\text{-}VP16}/Y$ male embryos the GFP-signal was broader, but again extended to the very distal tip of the limb bud (Fig. 8, B'). GFP-negative regions were present in the anterior half of the limb bud, most likely reflecting the reduced cre-activity in these regions (compare Supplemental Fig. 6, F). Since this situation mimics the distal expansion of $Tbx18^{GFP}$-positive cells in *DM* limbs buds (compare Fig. 5, M), we conclude that the Tbx18-VP16 protein indeed acts as in a dominant negative fashion in this developmental context.

To further explore the causes of the disparate cellular behavior mediated by Tbx18 and Tbx18-VP16 misexpression in the limb, we performed culture experiments to follow the fate of transgene expressing cells over time. Hindlimb cultures of E10.5 *P3::cre*, $Tbx18^{GOF}/+$ and $Tbx18^{GOF\text{-}VP16}/+$ embryos were established and brightfield- and GFP-images were taken at different time points during a total culture period 72 hours (Fig. 9). In *P3::cre*, $Tbx18^{GOF}/+$ cultures the GFP-expressing cells showed an exclusively proximal distribution at all time points studied (Fig. 9, A-E). The border towards the GFP-negative domain of distal mesenchyme was initially diffuse but refined progressively during subsequent culture. At 48 and 72 hours, Tbx18-expressing cells were sharply excluded from the footplate (Fig. 9, D, E, black arrows). In contrast, Tbx18-VP16-expressing cells gradually disappeared form the proximal and accumulated in the distal region of the limb bud (Fig. 9, F-J, white arrows). Given the progressive nature of these differential distributions we conclude that Tbx18 regulates cellular migration and/or adhesion properties to establish a proximal compartment in the limb bud mesenchyme, most likely by a transcriptional repression program.

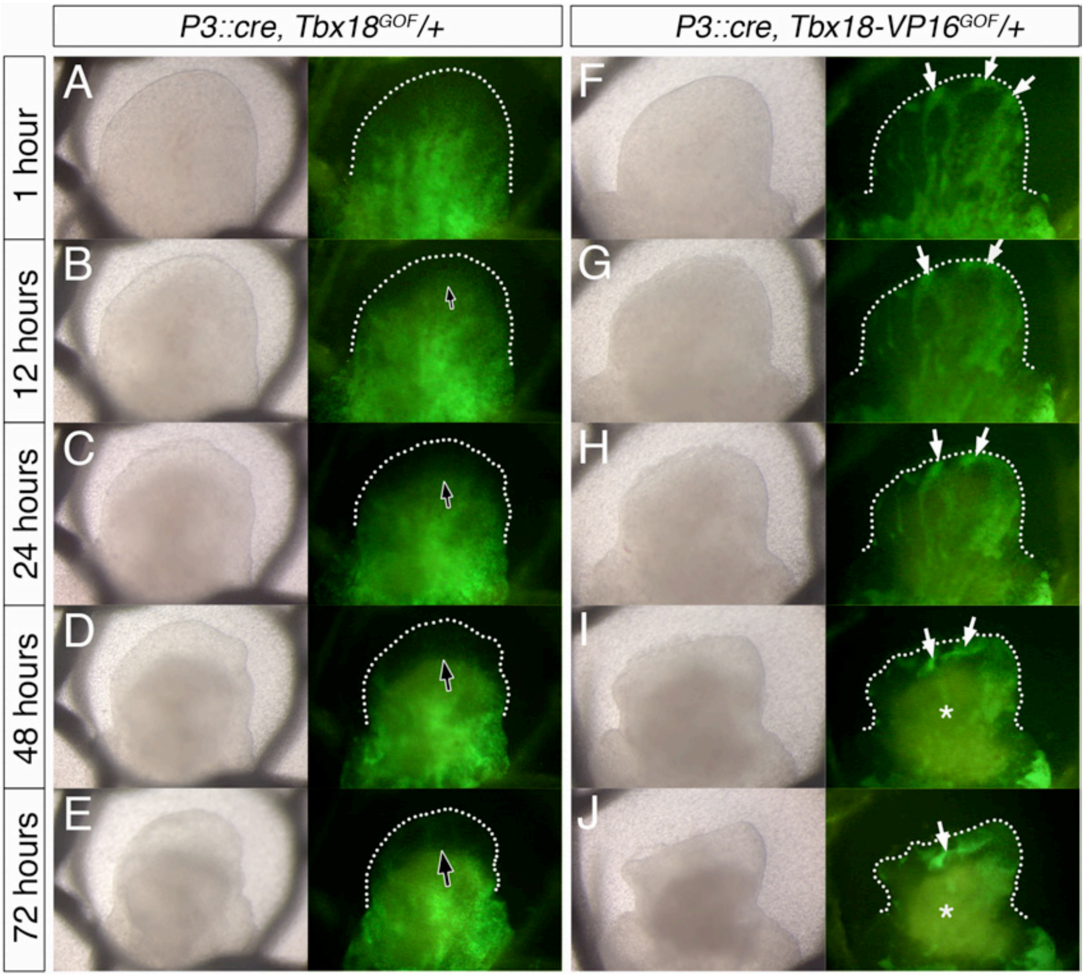

Fig. 9. **Organ culture experiments visualize opposite cellular behaviors of cells expressing Tbx18 and Tbx18-VP16.**

Time course experiment to follow the distribution of GFP-expressing cells in chimeric *P3::cre*, *Tbx18*^{GOF}/+ (A-E) and *Tbx18-VP16*^{GOF}/+ (F-J) limb buds. Hindlimbs of E10.5 embryos were isolated and cultured for a total period of 72 hours. Brightfield images (left) and GFP-epifluorescence (right) were documented at different time points after the establishment of the cultures, as indicated on the left side. White dotted lines highlight the outlines of the limb bud. In *P3::cre*, *Tbx18*^{GOF}/+ limb buds the distal mesenchyme is negative for GFP-expressing cells; the increasing size of the black arrows indicates a progressive elaboration of a sharp boundary between proximal (GFP-positive) and distal (GFP-negative) cells. In contrast, in *P3::cre*, *Tbx18-VP16*^{GOF}/+ hindlimbs, GFP-expressing cells gradually accumulate in the distal limb bud (white arrows). Increase in fluorescence observed in proximal limb bud at later stages (asterisks) is likely to represent background auto-fluorescence possibly caused by local cell death in this thickened tissue.

DISCUSSION

In the developing limb bud the generation of region specific cell identity is required to allow the stereotypic formation the PD array of cartilagous elements. Here, we have shown that the loss *Tbx15* and *Tbx18* causes the dispersal of proximal cells, followed by a reduction of cartilage precursors and subsequently a failure to establish proximal condensations, whereas misexpression of Tbx18 resulted in proximalization of limb cell affinity. We demonstrate that Tbx15/18 function involves a cellular migration/adhesion program, possibly by regulation of Eph/Ephrin molecules, to specify a stylopod/zeugopod domain. Thus, our results provide evidence for the existence a previously unknown proximal mesenchymal compartment, a finding that sheds new light on classical and more recent models for PD patterning. Furthermore, results on the regulation of *Tbx15/18* expression in the limb mesenchyme allows integration of their function in the context of proximal and distal signals. The function of Tbx15/18 in establishing compartment boundaries may have evolved to achieve tissue complexity in a variety of embryological contexts.

The expression of Tbx15 and Tbx18 regulates cellular attributes of the proximal limb mesenchyme.

Region specific cell affinities cause cell sorting in mixed cultures derived from proximal and distal regions of the limb mesenchyme and it has been proposed that this differential adhesion is required for the patterning of cartilaginous elements along the PD limb axis. (Wada and Ide, 1994; Barna et al., 2007). Our present study provides genetic evidence for this interrelation, as we show that Tbx15/18 mediate proximal restriction within the limb mesenchyme that is subsequently required for the formation of stylopod and zeugopod elements. As potential downstream mediators we have identified cell surface molecules of the Eph/Ephrin families that are involved in both, cellular adhesion and repulsion processes (for a review, Klein, 2004). We have found that Tbx15/18 are required for a proximal expression profile of Eph/Ephrin molecules as members that are normally expressed distally were expanded in *DM* limbs both at the mRNA and the protein level. The failure to down-regulate the expression of *Efna5* and *Efnb1* in the central/proximal domain of E10.5 *DM* limb buds coincides with the region of initial condensation of stylo- and zeugopod elements in the *wild type*, and later at E11.5 this domain demarcates the proximal pool of *Sox9*-positive chondrogenic precursors (compare Fig. 4, J and Fig. 6, G, K). Therefore, down-regulation of Efna- and Efnb-ligands could be a prerequisite for subsequent recruitment of cells into developing cartilages. In this scenario the dispersal of *DM* proximal cells would reflect a reduced affinity between mesenchymal cells. Another explanation for the expansion of Tbx18^{GFP}-expressing cells is a defective repulsion-mechanism between the prospective zeugopod and autopod regions. At E10.5 the distal limit of *Tbx18* expression could constitute such a compartment boundary, as it overlaps with the mutually exclusive expression domains of Epha-receptors and Efna-ligands (compare Fig. 1, N and Fig. 6 A, E). Regarding the Eph/Ephrin expression patterns in *DM* embryos, the initial establishment of this boundary seems unaffected. However, the progressive expansion of the *Epha3* expression into the proximal regions of *DM* limb buds suggests that Tbx15/18 may function in maintaining a repulsive boundary of bidirectional Eph/Ephrin-signaling. At present, it remains unresolved whether Tbx15/18 primarily mediate cellular adhesion or repulsion, but cell-aggregation experiments of labeled *wild type* or *Tbx15/18 DM* proximal cells with unlabeled proximal or distal cells from *wild type* limb buds may provide an answer to this problem.

Although cell culture experiments have suggested that Efna-ligands and Epha4 are implicated in PD-specific cell sorting (Wada et al., 1998), loss-of-function studies in the mouse have not yet shown a requirement in this process *in vivo*, suggesting that extensive co-expression results in functional redundancy (Supplemental Fig. 5). In contrast, gain-of-function studies have provided evidence that Eph/Ephrin molecules can influence limb patterning, as Efna2-overexpression in chick embryos induces digit malformations, likely by alterations in cell adhesion properties (Wada et al., 2003). A very similar phenotype was observed in mouse embryos, heterozygous for a null allele of the X-chromosomal *Efnb1* gene (Compagni et al., 2003). In this study the complete loss of *Efnb1* in male embryos caused no phenotype but chimeric expression in female embryos resulted in cell sorting between Efnb1-positive and negative cells. Defects in digit formation were explained by the presence of ectopic Eph/Ephrin-signaling interfaces between *wild type* and *mutant* clones. To clarify the role of individual and combinations of Eph/Ephrin-members in position specific cell adhesion, further loss-of-function studies are required. Also the question if Tbx15/18 mediate direct or indirect transcriptional regulation of *Eph/Ephrin*-genes should be addressed.

The function of Tbx15/18 is upstream of the genetic hierarchy that regulates limb skeletal development.

Our results argue against a direct role of Tbx15/18 during chondrogenic differentiation, as the expression of *Sox9*, which is an obligate factor for mesenchyme-to-cartilage transition (Bi et al., 1999, Barna et al., 2007), is unchanged in E10.5 *DM* limb buds. We conclude that Tbx15/18 regulate initial steps in the mesenchyme that precede a requirement for *Sox9*. Possibly, Tbx15/18 are involved in mesenchymal aggregation or in the subsequent establishment of tight mesenchymal cell associations, a process termed as ‘compaction’, Interestingly a recent study has shown that *in vitro* both processes are Sox9-independent (Barna et al., 2007). The observed loss of *Sox9* expression after E11.5, in contrast, argues that mesenchymal condensations are required for maintenance of *Sox9* expression, which is possibly regulated by para/autocrine signaling within the condensates. Another finding that argues against a role of Tbx15/18 in chondrogenic differentiation is that sustained expression of Tbx18 did not perturb this stepwise and highly regulated differentiation program. Contrarily, the persistent expression of Sox9 causes defective cartilage differentiation and results in shortened bones (Aikima et al., 2004; Aikima et al., 2007).

Tbx15/18 clearly act downstream of signals that establish proximal and distal identities in a cellular program not yet described. Expression of *Shox2*, *Hoxd11* and *Ror1*, known regulators of stylopod and/or zeugopod formation (Cobb et al., 2006; Yu et al., 2007; Boulet et al., 2003; Nomi et al., 2001), was unchanged in E10.5 *DM* limb buds (Supplemental Fig. 4, H, M, R). Yet, a role of *Tbx15/18* downstream of these molecules is unlikely because the phenotypic onset of limb defects in *Tbx15/18 DM*s precedes the defects of *Hoxa11*/*Hoxd11*, *Shox2* or *Ror1/2* mutants, which were collectively shown to result from a relatively late failure of chondrocyte maturation. *Gli3/Plzf* double mutant embryos display reduced stylopod and zeugopod elements, with an early reduction of chondrogenic precursors, a mis-segregation of cartilage and joints and increased apoptosis in the proximal limb bud (Barna et al., 2005), phenotypic changes similar to the ones found in *Tbx15/18 DM* limbs. However, the expression of both, *Gli3* and *Plzf* was unchanged in *Tbx15/18 DM* embryos (Supplemental Fig. 4, P, Q). And as characteristic features that distinguish both phenotypes *Gli3/Plzf* mutants display a loss of *Sox9* expression already at E10.5 and an unaffected length of the limb bud at E12.5, compared to the dramatic reduction in the limb length that was found in *Tbx15/18 DM*s (Fig. 4, B), collectively arguing that Gli3/Plzf are more directly involved in the initiation of the chondrogenic program.

A recent study has shown that the mesenchymal loss of Bmp2 and Bmp4 expression causes a strong reduction of stylo- and zeugopod elements, while the autopod skeleton is less severely affected (Bandyopadhyay et al., 2006). As in case of Tbx15/18, the function of Bmp2/4 is not required for initial *Sox9* expression. Furthermore, the BMP antagonist Noggin was found to inhibit the early ‘compaction’ process in mesenchymal cultures before the onset of chondrogenic differentiation (Barna et al., 2007), indicating a common genetic pathway. The analysis of Bmp-signaling in *Tbx15/18 DM* limbs and expression of *Tbx15* and *Tbx18* in *Bmp2/4* mutants should clarify the epistatic relationships.

Function of Tbx15 and Tbx18 in the context of models for proximal distal limb patterning.

Our loss- and gain-of-function experiments suggest that Tbx15/18-mediated formation of a proximal mesenchymal compartment is prerequisite to formation of stylopod and zeugopod elements. Distal expansion of Tbx18^{GFP}-expressing cells in *DM* limb buds indicates a failure to maintain a lineage boundary towards another more distal compartment that is likely to represent the prospective autopod. Our results are thus consistent with the ‘Early specification model’ that relies on the presence of distinct PD-compartments within the limb bud mesenchyme. Notably, the *Tbx18* expression domain is already restricted to the proximal region in limb buds of E9.5 embryos (Fig. 1, E). The manifestation of differential PD cell adhesion in chick limb buds of a corresponding age (stage 19) (Barna et al., 2007) is compatible with an early function of Tbx15/18 in the regulation of this process. However, previous fate-mapping experiments at this early stage of limb development have not confirmed a definite compartmentalization along the PD-axis (Pearse et al., 2007; Sato et al., 2007, Arques et al. 2007). Rather it has been proposed that the mesenchyme comprises a temporal and spatial gradient of cell fate specification, as cell movements become progressively restricted to more distal areas of the limb bud (Sato et al., 2007). Future lineage tracing experiments of *Tbx18*-expressing cells are required to determine if *Tbx18* expression indeed marks an early autopod-zeugopod boundary. Further insights into the temporal requirement of Tbx15/18 during this specification process could substantially improve our understanding about PD-patterning of the limb.

Our observations argue against the classical ‘Progress zone model’, which predicts that positional information is acquired autonomously depending on the time that cells in the ‘progress zone’ remain undifferentiated under the influence of permissive AER signals. In *Tbx15/18 DM*s the expansion of Tbx18^{GFP}-expressing cells into the ‘progress zone’ is followed by normal development of the autopod, which shows that proximal cells can adapt to the local signals and subsequently participate in autopod formation. Likewise, the expression of proximal markers was not expanded distally in *Tbx15/18 DM* limbs, demonstrating a re-specification of cells in their new environment. In contrast to the ‘Progress zone model’ these findings argue that the AER signals play an instructive, distalizing role, a conclusion that was also drawn in a recent study by the analysis of phenotypic consequences following the genetic removal of AER derived Fgf signals (Mariani et al., 2008). Interestingly, Tbx18 misexpression in distal cells causes insensitivity to these instructive signals as GFP-positive cells were progressively recruited into the proximal compartment, which shows that Tbx18 can antagonize the distal specification cues in a dominant manner. It would therefore be interesting to study if Tbx18 misexpression in the complete mesenchyme causes stronger autopod defects. At E12.5 our mosaic misexpression experiments have shown that the autopod consisted mainly of GFP-negative *wild type* cells, demonstrating that normal limb development tolerates a large amount of cell movements. Together, this considerable plasticity can hardly be explained by either of the two classical models for PD-specification.

As a model that integrates both, the early regionalization, but also the progressivity of PD-specification our results favor the recently postulated 'Two-signal model' of dynamic specification (Mariani et al., 2008; Tabin and Wolpert 2007). It suggests that after the initiation of bud outgrowth the limb mesenchyme is exposed to a proximal signal, most likely retinoic acid (RA) from flank mesoderm and to an opposing distal signal from the AER (Fgfs), which establish proximal and distal domains, the stylopod and autopod, respectively. Intermediate positional values (the zeugopod) would then be intercalated as a result of further outgrowth and interactions between proximal and distal domains. The molecular evidence for this model is based on the finding that RA can antagonize distal Fgf-signaling, and induces the expression of the TALE homeobox transcription factors Meis1/2 initially in the proximal half and later in the stylopod domain of the limb bud (Mercader et al., 2000). Although genetic evidence in the mouse is lacking, over-expression of Meis1 in chick limb buds abolishes distal limb structures and produces a proximal shift of limb identities (Mercader et al., 1999). In contrast, FGF signals are required to restrict *Meis1/2* expression from the distal region and to specify distal identity (Mercader et al., 2000; Yashiro et al., 2004; Mariani et al., 2008).

Our data show that Tbx15/18 are required for the formation of both stylopod and zeugopod elements, and they could thus act in a common pathway with Meis1/2 during stylopod development. Interestingly, both Meis1/2 and Tbx15/18 seem to specify proximal identity in a similar manner by regulating proximal specific cell adhesion, as Meis1-expressing cells that are placed beneath the AER relocate to more proximal compartments (Mercader et al., 2000; Mercader et al., 2005). However, our data provides evidence how the intermediate zeugopod domain is specified during subsequent limb outgrowth. As AER signals repress *Tbx18* expression (see below), cells that leave the distal 'undifferentiated zone' may acquire *Tbx18* expression. This *de novo* induction of *Tbx18* expression could specify a domain distally to the *Meis1/2*-positive stylopod region and the subsequent restriction of cell movements could then define a boundary between prospective zeugopod and autopod regions. As mentioned above, the cell fate mapping of Tbx18-expressing cells will be crucial for the understanding at which stage this boundary is fixed. The observation of Sato et al. (2007) that in chick forelimbs the cell mixing of prospective autopod and zeugopod regions ceases between stage 19 and stage 23 (corresponding to E9.5 and E10.5 in the mouse), indicates that this time frame is critical for the function of Tbx15 and Tbx18.

The expression of Tbx15/Tbx18 in the limb bud is controlled by proximal and distal signals.

Our culture experiments have shown that the expression of *Tbx15/18* in the early limb bud (E10.5) is intrinsic to the mesenchyme, indicating that activating signals are either present in the mesenchyme and/or must operate at earlier stages. Notably, *Tbx15* expression extends distally, whereas *Tbx18* expression is excluded from the sub-AER mesenchyme. We have argued that this proximal restriction is involved in the formation of an autopod-zeugopod boundary, which would imply at least some functional divergence between the Tbx15 and Tbx18 proteins (discussed below). Repressive AER signals mediate this proximal restriction, as the *Tbx18* expression extends distally following AER ablation. With regard to the classical AER removal experiments (Saunders 1948), we suggest that the resulting distal skeletal truncations could at least be caused to some extent by ectopic *Tbx18* expression, which subsequently proximalizes the limb bud mesenchyme.

It is unlikely that AER derived Fgf signals are involved in distal *Tbx18* repression, since Fgf8-loaded beads did not cause a repression but activated *Tbx18* expression at moderate concentrations in E10.5 forelimb buds. However, repression by Fgfs could be restricted to earlier stages. Interestingly, the hindlimbs of *Fgf8* mutants display a selective reduction of the femur accompanied with apoptosis in the proximal mesenchyme (Lewandoski et al., 2000; Sun et al., 2002). These phenotypic similarities argue that Fgf8 is an upstream activator of *Tbx15/18* mediating long-range effects. It therefore would be interesting to analyze if the proximal limit of the *Tbx15/Tbx18* expression domain is shifted distally in *Fgf8* mutant hindlimbs.

As another class of signaling molecules, Bmps are secreted from the AER as well as the limb mesenchyme (Capdevilla et al., 1999). However, distal Bmp-signaling is subject to antagonism by Gremlin1 (Khokha et al., 2003), which confines Bmp-activity to the mesenchyme of the anterior and posterior margins of the limb bud. We therefore conclude that the observed repression of *Tbx15*/*18* in close proximity of Bmp4-soaked beads rather reflects the exclusion of endogenous expression from the AP flank mesenchyme. Consistent with this hypothesis *Tbx2* and *Tbx3*, which are known Bmp-targets (Tümpel et al., 2002; Selever et al., 2004; supplemental information in Karaulanov et al., 2004; Ma et al., 2005; Yang et al., 2006), show an endogenous expression in flank mesenchymes and were induced by high doses of Bmp4 (Fig. 2, I-L, W). The reciprocal expression patterns of *Tbx2/3* and *Tbx15/18* along the AP axis could thus represent a differential response to high levels of Bmp/Smad-signaling. Alternatively, Tbx2/3 may directly repress *Tbx15* and *Tbx18* (Habets et al., 2002; Lingbeek et al., 2002; Vance et al., 2005). We exclude a role of Tbx15/18 in the regulation of *Tbx2/3*, as both genes as well as the T-box activators *Tbx4* and *Tbx5*, were unchanged in *DM* limb buds (Supplemental Fig. 4, S-V). The strong similarity between the phenotypes caused by mesenchymal loss of *Bmp2/4* (Bandyopadhyay et al., 2006; see above) and *Tbx15/18*, suggests that Bmps, probably at moderate doses, could also be involved in activation of *Tbx15/18* expression. This is in agreement with the experimental finding that Dorsomorphin, a small molecule inhibitor of Bmp/Smad-signaling (Yu et al., 2008), caused a down-regulation of *Tbx18* in micromass cultures of limb mesenchymal cells (Fig. 2, X).

With respect to the regulation by proximal signals, we found that RA, unlike its requirement for the induction of *Meis1/2* expression (Mercader et al., 2000), caused a strong down-regulation of *Tbx15/18* expression. In fact, we observed a clear reduction of *Tbx15/18* expression in micromass cultures of E10.5 limb mesenchymal cells already 2 hours after application of 0.01 μM RA (Fig. 2, Y). We deem it unlikely that a RA gradient specifies different PD-positional values by setting different distal limits of *Meis1/2* and *Tbx18* expression, but rather favor the possibility that RA is required to establish the sharp proximal boundaries of the *Tbx15/18* expression domains.

Together, our data show that the expression of *Tbx15* and in particular *Tbx18* underlies a complex and concentration dependent regulation by activating Fgf, and repressing Bmp and RA signals (see model in Fig. 2, Z). However, further experiments are required to elucidate which pathway(s) restrict *Tbx18* expression from the distal mesenchyme. Non-canonical Wnt-signaling could be another candidate as *Wnt5a* is expressed in AER and the underling mesenchyme (Parr et al., 1993). A final goal would be to identify the genomic regulatory regions and trans-acting factors that mediate limb expression of *Tbx15/18*. Although limb expression of the closely related *Tbx15* and *Tbx18* genes is conserved in the zebrafish embryo (Begemann et al., 2002), an alignment of proximal genomic regions did not reveal any sequence conservation (data not shown), indicating that a shared ancestral limb enhancer may have diverged and is conserved at the functional level only. Future approaches could benefit from genome-wide data of tissue specific enhancers. Notably, a recent study has identified candidate limb enhancers in the upstream and intronic regions of the *Tbx15* and *Tbx18* loci, respectively (supplementary data in Visel et al., 2009), elements that could be tested for limb specific reporter-gene activity.

Molecular function of Tbx15 and Tbx18 during limb development.

Our finding that one allele of either *Tbx15* or *Tbx18* is sufficient to rescue the development of the proximal limb skeleton clearly demonstrates functional redundancy of both proteins and confirms our previous results that Tbx15/18 share similar molecular functions *in vitro* (Farin et al., 2007; Farin et al., 2008). A puzzling question, however, is why Tbx18 misexpression in the distal mesenchyme resulted in a proximal recruitment of cells, whereas Tbx15, which is endogenously expressed in the distal region, does apparently not cause a similar effect? Possibly, expression of Tbx15 protein is insufficient to initiate this cellular migration program. This hypothesis is supported by the fact that a dose reduction of Tbx15 on a *Tbx18* mutant background caused a mild reduction in the humeral length and a thickening of radius and ulna (Supplemental Fig. 2, E). Similar changes were not observed in *Tbx15*$^{-/-}$, *Tbx18*$^{+/GFP}$ forelimbs, assigning Tbx18 a more critical role in the compartmentalization of the limb mesenchyme. Alternatively, functional differences between both proteins could result in a selective inhibition of the Tbx15 transcriptional activity in the distal region, e.g. by posttranslational regulation or by association with distinct co-factors. Misexpression experiments could reveal if Tbx15, similar to the Tbx18 protein, is also sufficient to specify the proximal limb identity.

We have previously suggested that Tbx15/18 act as transcriptional repressors *in vitro* (Farin et al., 2007). In our present study we demonstrate that Tbx18 and Tbx18-VP16 mediate opposite cellular phenotypes *in vivo*. Indeed, the distal localization of Tbx18-VP16-expressing cells mimics the Tbx18^{GFP}-expansion that was observed in *Tbx15/18 DM* limbs, and shows that the activator fusion-protein acts in a dominant negative fashion. A repressor function for Tbx18 (and Tbx15) is compatible with direct repression of proximal *Efna5* and *Efnb1* expression. One way of testing this hypothesis is to study *Efna5*/*Efnb1* expression in Tbx18-VP16 mosaic limb buds. As direct transcriptional targets, expression of both genes should be up-regulated in clones expressing the transgene.

Phenotypic characterization of *Tbx18* mutant mice has revealed functions of Tbx18 in the development of the inner ear and the ureter. In the inner ear, Tbx18 is required to maintain the separation of the otic mesenchyme in an inner compartment destined to differentiate into otic fibrocytes and an outer compartment from which the otic capsule will develop (Trowe et al., 2008). Ureter defects were traced back to the mis-separation of ureteric and metanephric mesenchyme in the early metanephric cell field and the subsequent failure of the ureteric mesenchyme to coherently condense (Airik et al., 2006). Considering the fact that the *Tbx15/Tbx18/Tbx22* subgroup of T-box genes is specific to chordates, this gene function may have been employed to subdivide homogenous mesenchymal cell fields into distinct compartments that subsequently can acquire new fates supporting an increase in evolutionary complexity.

ABBREVIATIONS

The abbreviations used are: AER, apical ectodermal ridge; AP, anterior-posterior; BrdU, bromodeoxyuridine; BSA, bovine serum albumin; CAG, CMV early enhancer/chicken β actin promoter; E, embryonic day; Hprt, hypoxanthine guanine phosphoribosyl transferase; IRES, internal ribosomal entry site; RA, retinoic acid; PD, proximal-distal; TUNEL, TdT-mediated dUTP-biotin nick end labeling; ZPA; zone of polarizing activity.

ACKNOWLEDGMENTS

We thank YiPing Chen (New Orleans), Denis Duboule (Lausanne), Achim Gossler (Hannover), Brigid Hogan (Durham), Alexandra Joyner (New York), Anders Linde (Göteborg), Malcolm Logan (London), Andrew McMahon (Cambridge), Cathy Mendelsohn (New York), Pier Paolo Pandolfi (Boston), Virginia Papaiannou (New York) and Deepak Srivastava (San Francisco) for providing plasmids. In addition we thank Rannar Airik (Hannover) for providing the *Pax3::cre*, *Sox9*$^{fl/fl}$ skeletons and Aravind Sekar (Hannover) for kind support with *Hprt* gene-targeting. This work was supported by grants to AK from the Deutsche Forschungsgemeinschaft.

REFERENCES

Agarwal, P., Wylie, J. N., Galceran, J., Arkhitko, O., Li, C., Deng, C., Grosschedl, R. and Bruneau, B. G. (2003). Tbx5 is essential for forelimb bud initiation following patterning of the limb field in the mouse embryo. *Development* **130,** 623-633.

Airik, R., Bussen, M., Singh, M. K., Petry, M. and Kispert, A. (2006). Tbx18 regulates the development of the ureteral mesenchyme. *J. Clin. Invest.* **116,** 663-674.

Akiyama, H., Lyons, J. P., Mori-Akiyama, Y., Yang, X., Zhang, R., Zhang, Z., Deng, J. M., Taketo, M. M., Nakamura, T., Behringer, R. R., McCrea, P. D. and de Crombrugghe, B. (2004). Interactions between Sox9 and beta-catenin control chondrocyte differentiation. *Genes Dev.* **18,** 1072-1087.

Akiyama, H., Stadler, H. S., Martin, J. F., Ishii, T. M., Beachy, P. A., Nakamura, T. and de Crombrugghe, B.. (2007). Misexpression of Sox9 in mouse limb bud mesenchyme induces polydactyly and rescues hypodactyly mice. *Matrix Biol.* **26,** 224-233.

Arques, C. G., Doohan, R., Sharpe, J. and Torres, M. (2007). Cell tracing reveals a dorsoventral lineage restriction plane in the mouse limb bud mesenchyme. *Development* **134,** 3713-3722.

Bandyopadhyay, A., Tsuji, K., Cox, K., Harfe, B. D., Rosen, V. and Tabin, C. J. (2006). Genetic analysis of the roles of BMP2, BMP4, and BMP7 in limb patterning and skeletogenesis. *PLoS Genet.* **2,** e216.

Barna, M. and Niswander, L. (2007). Visualization of cartilage formation, insight into cellular properties of skeletal progenitors and chondrodysplasia syndromes. *Dev. Cell.* **12,** 931-941.

Barna, M., Pandolfi, P. P. and Niswander, L. (2005). Gli3 and Plzf cooperate in proximal limb patterning at early stages of limb development. *Nature* **436,** 277-281.

Barrow, J. R., Thomas, K. R., Boussadia-Zahui, O., Moore, R., Kemler, R., Capecchi, M. R. and McMahon, A. P. (2003). Ectodermal Wnt3/beta-catenin signaling is required for the establishment and maintenance of the apical ectodermal ridge. *Genes Dev.* **17,** 394-409.

Begemann, G., Gibert, Y., Meyer, A. and Ingham, P. W. (2002). Cloning of zebrafish T-box genes tbx15 and tbx18 and their expression during embryonic development. *Mech. Dev.* **114,** 137-141.

ten Berge, D., Brugmann, S. A., Helms, J. A. and Nusse, R. (2008). Wnt and FGF signals interact to coordinate growth with cell fate specification during limb development. *Development* **135,** 3247-3257.

Bi, W., Deng, J. M., Zhang, Z., Behringer, R. R. and de Crombrugghe, B. (1999). Sox9 is required for cartilage formation. *Nat. Genet.* **22,** 85-89.

Boulet, A. M. and Capecchi, M. R. (2004). Multiple roles of Hoxa11 and Hoxd11 in the formation of the mammalian forelimb zeugopod. *Development* **131,** 299-309.

Bussen, M., Petry, M., Schuster-Gossler, K., Leitges, M., Gossler, A. and Kispert, A. (2004). The T-box transcription factor Tbx18 maintains the separation of anterior and posterior somite compartments. *Genes Dev.* **18,** 1209-1221.

Candille, S. I., Van Raamsdonk, C. D., Chen, C., Kuijper, S., Chen-Tsai, Y., Russ, A., Meijlink, F. and Barsh, G. S. (2004). Dorsoventral patterning of the mouse coat by Tbx15. *PLoS Biol.* **2,** E3.

Capdevila, J., Tsukui, T., Rodríquez Esteban, C., Zappavigna, V. and Izpisúa Belmonte, J. C. (1999). Control of vertebrate limb outgrowth by the proximal factor Meis2 and distal antagonism of BMPs by Gremlin. *Mol. Cell* **4,** 839-849.

Charité, J., McFadden, D. G. and Olson, E. N. (2000). The bHLH transcription factor dHAND controls Sonic hedgehog expression and establishment of the zone of polarizing activity during limb development. *Development* **127,** 2461-2670.

Christoffels, V. M., Mommersteeg, M. T., Trowe, M. O., Prall, O. W., de Gier-de Vries, C., Soufan, A. T., Bussen, M., Schuster-Gossler, K., Harvey, R. P., Moorman, A. F. and Kispert, A. (2006). Formation of the venous pole of the heart from an Nkx2-5-negative precursor population requires Tbx18. *Circ. Res.* **98,** 1555-1563.

Cobb, J., Dierich, A., Huss-Garcia, Y. and Duboule, D. (2006). A mouse model for human short-stature syndromes identifies Shox2 as an upstream regulator of Runx2 during long-bone development. *Proc. Natl. Acad. Sci. U. S. A.* **103,** 4511-4515.

Compagni, A., Logan, M., Klein, R. and Adams, R. H. (2003). Control of skeletal patterning by ephrinB1-EphB interactions. *Dev. Cell* **5,** 217-230.

Davenport, T. G., Jerome-Majewska, L. A. and Papaioannou, V. E. (2003). Mammary gland, limb and yolk sac defects in mice lacking Tbx3, the gene mutated in human ulnar mammary syndrome. *Development* **130,** 2263-2273.

Dollé, P., Izpisúa-Belmonte, J. C., Falkenstein, H., Renucci, A. and Duboule, D. (1989). Coordinate expression of the murine Hox-5 complex homoeobox-containing genes during limb pattern formation. *Nature* **342,** 767-772.

Echelard, Y., Vassileva, G. and McMahon, A. P. (1994). Cis-acting regulatory sequences governing Wnt-1 expression in the developing mouse CNS. *Development* **120,** 2213-24.

Farin, H. F., Bussen, M., Schmidt, M. K., Singh, M. K., Schuster-Gossler, K. and Kispert, A. (2007). Transcriptional repression by the T-box proteins Tbx18 and Tbx15 depends on Groucho corepressors. *J. Biol. Chem.* **282,** 25748-25759.

Farin, H. F., Mansouri, A., Petry, M. and Kispert, A. (2008). T-box protein Tbx18 interacts with the paired box protein Pax3 in the development of the paraxial mesoderm. *J. Biol. Chem.* **283,** 25372-25380.

Gale, N. W., Holland, S. J., Valenzuela, D. M., Flenniken, A., Pan, L., Ryan, T. E., Henkemeyer, M., Strebhardt, K., Hirai, H., Wilkinson, D. G., Pawson, T., Davis, S. and Yancopoulos, G. D. (1996). Eph receptors and ligands comprise two major specificity

Yancopoulos, G. D. (1996). Eph receptors and ligands comprise two major specificity subclasses and are reciprocally compartmentalized during embryogenesis. *Neuron* **17,** 9-19.

Habets, P. E., Moorman, A. F., Clout, D. E., van Roon, M. A., Lingbeek, M., van Lohuizen, M., Campione, M. and Christoffels, V. M. (2002). Cooperative action of Tbx2 and Nkx2.5 inhibits ANF expression in the atrioventricular canal, implications for cardiac chamber formation. *Genes Dev.* **16,** 1234-1246.

Harrelson, Z., Kelly, R. G., Goldin, S. N., Gibson-Brown, J. J., Bollag, R. J., Silver, L. M. and Papaioannou, V. E. (2004). Tbx2 is essential for patterning the atrioventricular canal and for morphogenesis of the outflow tract during heart development. *Development* **131,** 5041-5052.

Karaulanov, E., Knöchel, W. and Niehrs, C. (2004). Transcriptional regulation of BMP4 synexpression in transgenic Xenopus. *EMBO J.* **23,** 844-856.

Khokha, M. K., Hsu, D., Brunet, L. J., Dionne, M. S. and Harland, R. M. (2003). Gremlin is the BMP antagonist required for maintenance of Shh and Fgf signals during limb patterning. *Nat. Genet.* **34,** 303-307.

Kispert, A., Vainio, S. and McMahon, A. P. (1998). Wnt-4 is a mesenchymal signal for epithelial transformation of metanephric mesenchyme in the developing kidney. *Development* **125,** 4225-4234.

Klein, R. (2004). Eph/ephrin signaling in morphogenesis, neural development and plasticity. *Curr. Opin. Cell. Biol.* **16,** 580-589.

Lausch, E., Hermanns, P., Farin, H. F., Alanay, Y., Unger, S., Nikkel, S., Steinwender, C., Scherer, G., Spranger, J., Zabel, B., Kispert, A. and Superti-Furga, A. (2008). TBX15 mutations cause craniofacial dysmorphism, hypoplasia of scapula and pelvis, and short stature in Cousin syndrome. *Am. J. Hum. Genet.* **83,** 649-655.

Lewandoski, M., Sun, X. and Martin, G. R. (2000). Fgf8 signalling from the AER is essential for normal limb development. *Nat. Genet.* **26,** 460-463.

Li, J., Chen, F. and Epstein, J. A. (2000). Neural crest expression of Cre recombinase directed by the proximal Pax3 promoter in transgenic mice. *Genesis* **26,** 162-164.

Lingbeek, M. E., Jacobs, J. J. and van Lohuizen, M. (2002). The T-box repressors TBX2 and TBX3 specifically regulate the tumor suppressor gene p14ARF via a variant T-site in the initiator. *J. Biol. Chem.* **277,** 26120-26127.

Luche, H., Weber, O., Nageswara Rao, T., Blum, C. and Fehling, H. J. (2007). Faithful activation of an extra-bright red fluorescent protein in "knock-in" Cre-reporter mice ideally suited for lineage tracing studies. *Eur. J. Immunol.* **37,** 43-53.

Ma, L., Lu, M. F., Schwartz, R. J. and Martin, J. F. (2005). Bmp2 is essential for cardiac cushion epithelial-mesenchymal transition and myocardial patterning. *Development* **132,** 5601-5611.

Mariani, F. V., Ahn, C. P. and Martin, G. R. (2008). Genetic evidence that FGFs have an instructive role in limb proximal-distal patterning. *Nature* **453,** 401-405.

Marigo, V., Scott, M. P., Johnson, R. L., Goodrich, L. V. and Tabin, C. J. (1996). Conservation in hedgehog signaling, induction of a chicken patched homolog by Sonic hedgehog in the developing limb. *Development* **122,** 1225-1233.

Matsuda, T., Nomi, M., Ikeya, M., Kani, S., Oishi, I., Terashima, T., Takada, S. and Minami, Y. (2001). Expression of the receptor tyrosine kinase genes, Ror1 and Ror2, during mouse development. *Mech. Dev.* **105,** 153-156.

Mendelsohn, C., Ruberte, E., LeMeur, M., Morriss-Kay, G. and Chambon, P. (1991). Developmental analysis of the retinoic acid-inducible RAR-beta 2 promoter in transgenic animals. *Development* **113,** 723-734.

Mercader, N., Leonardo, E., Azpiazu, N., Serrano, A., Morata, G., Martínez, C. and Torres, M. (1999). Conserved regulation of proximodistal limb axis development by Meis1/Hth. *Nature* **402,** 425-429.

Mercader, N., Leonardo, E., Piedra, M. E., Martínez, A. C., Ros, M. A. and Torres, M. (2000). Opposing RA and FGF signals control proximodistal vertebrate limb development through regulation of Meis genes. *Development* **127,** 3961-3970.

Mercader, N., Tanaka, E. M. and Torres, M. (2005). Proximodistal identity during vertebrate limb regeneration is regulated by Meis homeodomain proteins. *Development* **132,** 4131-4142.

Moorman, A. F., Houweling, A. C., de Boer, P. A. and Christoffels, V. M. (2001). Sensitive nonradioactive detection of mRNA in tissue sections, novel application of the whole-mount in situ hybridization protocol. *J. Histochem. Cytochem.* **49,** 1-8.

Naiche, L. A., Harrelson, Z., Kelly, R. G. and Papaioannou, V. E. (2005). T-box genes in vertebrate development. *Annu. Rev. Genet.* **39,** 219-239.

Naiche, L. A. and Papaioannou, V. E. (2003). Loss of Tbx4 blocks hindlimb development and affects vascularization and fusion of the allantois. *Development* **130,** 2681-2893.

Nomi, M., Oishi, I., Kani, S., Suzuki, H., Matsuda, T., Yoda, A., Kitamura, M., Itoh, K., Takeuchi, S., Takeda, K., Akira, S., Ikeya, M., Takada, S. and Minami, Y. (2001). Loss of mRor1 enhances the heart and skeletal abnormalities in mRor2-deficient mice, redundant and pleiotropic functions of mRor1 and mRor2 receptor tyrosine kinases. *Mol. Cell. Biol.* **21,** 8329-8335.

Ohuchi, H., Nakagawa, T., Yamamoto, A., Araga, A., Ohata, T., Ishimaru, Y., Yoshioka, H., Kuwana, T., Nohno, T., Yamasaki, M., Itoh, N. and Noji, S. (1997). The mesenchymal factor, FGF10, initiates and maintains the outgrowth of the chick limb bud through interaction with FGF8, an apical ectodermal factor. *Development* **124,** 2235-2244.

Packham, E. A. and Brook, J. D. (2003). T-box genes in human disorders. *Hum. Mol. Genet.* **12,** R37-44.

Parr, B. A., Shea, M. J., Vassileva, G. and McMahon, A. P. (1993). Mouse Wnt genes exhibit discrete domains of expression in the early embryonic CNS and limb buds. *Development* **119,** 247-261.

Pearse, R. V. 2nd, Scherz, P. J., Campbell, J. K. and Tabin, C. J. (2007). A cellular lineage analysis of the chick limb bud. *Dev. Biol.* **310,** 388-400.

Roehl, H. and Nüsslein-Volhard, C. (2001). Zebrafish pea3 and erm are general targets of FGF8 signaling. *Curr. Biol.* **11,** 503-507.

Sato, K., Koizumi, Y., Takahashi, M., Kuroiwa, A. and Tamura, K. (2007). Specification of cell fate along the proximal-distal axis in the developing chick limb bud. *Development* **134,** 1397-1406.

Saunders, J. W. Jr. (1948). The proximo-distal sequence of origin of the parts of the chick wing and the role of the ectoderm. *J. Exp. Zool.* **108,** 363-403.

Selever, J., Liu, W., Lu, M. F., Behringer, R. R. and Martin, J. F. (2004). Bmp4 in limb bud mesoderm regulates digit pattern by controlling AER development. *Dev. Biol.* **276,** 268-279.

Singh, M. K., Petry, M., Haenig, B., Lescher, B., Leitges, M. and Kispert, A. (2005). The T-box transcription factor Tbx15 is required for skeletal development. *Mech. Dev.* **122,** 131-144.

Soriano, P. (1999). Generalized lacZ expression with the ROSA26 Cre reporter strain. *Nat. Genet.* **21,** 70-71.

Storm, E. E. and Kingsley, D. M. (1999). GDF5 coordinates bone and joint formation during digit development. *Dev. Biol.* **209,** 11-27.

Sun, X., Mariani, F. V. and Martin, G. R. (2002). Functions of FGF signalling from the apical ectodermal ridge in limb development. *Nature* **418,** 501-508.

Suzuki, T., Takeuchi, J., Koshiba-Takeuchi, K. and Ogura, T. (2004). Tbx Genes Specify Posterior Digit Identity through Shh and BMP Signaling. *Dev. Cell* **6,** 43-53.

Tabin, C. and Wolpert, L. (2007). Rethinking the proximodistal axis of the vertebrate limb in the molecular era. *Genes Dev.* **21,** 1433-1442.

Towers, M. and Tickle, C. (2009). Growing models of vertebrate limb development. *Development* **136,** 179-190.

Trowe, M. O., Maier, H., Schweizer, M. and Kispert, A. (2008). Deafness in mice lacking the T-box transcription factor Tbx18 in otic fibrocytes. *Development* **135,** 1725-1734.

Tümpel, S., Sanz-Ezquerro, J. J., Isaac, A., Eblaghie, M. C., Dobson, J. and Tickle, C. (2002). Regulation of Tbx3 expression by anteroposterior signalling in vertebrate limb development. *Dev. Biol.* **250,** 251-262.

Vance, K. W., Carreira, S., Brosch, G. and Goding, C. R. (2005). Tbx2 is overexpressed and plays an important role in maintaining proliferation and suppression of senescence in melanomas. *Cancer Res.* **65,** 2260-2268.

Visel, A., Blow, M. J., Li, Z., Zhang, T., Akiyama, J. A., Holt, A., Plajzer-Frick, I., Shoukry, M., Wright, C., Chen, F., Afzal, V., Ren, B., Rubin, E. M. and Pennacchio, L. A. (2009). ChIP-seq accurately predicts tissue-specific activity of enhancers. *Nature* **457,** 854-858.

Wada, N. and Ide, H. (1994). Sorting out of limb bud cells in monolayer culture. *Int. J. Dev. Biol.* **38,** 351-356.

Wada, N., Kimura, I., Tanaka, H., Ide, H. and Nohno, T. (1998). Glycosylphosphatidylinositol-anchored cell surface proteins regulate position-specific cell affinity in the limb bud. *Dev. Biol.* **202,** 244-252.

Wada, N., Tanaka, H., Ide, H. and Nohno, T. (2003). Ephrin-A2 regulates position-specific cell affinity and is involved in cartilage morphogenesis in the chick limb bud. *Dev. Biol.* **264,** 550-563.

Wilkinson, D. G. and Nieto, M. A. (1993). Detection of messenger RNA by in situ hybridization to tissue sections and whole mounts. *Methods Enzymol.* **225,** 361-373.

Yang, L., Cai, C. L., Lin, L., Qyang, Y., Chung, C., Monteiro, R. M., Mummery, C. L., Fishman, G. I., Cogen, A. and Evans, S. (2006). Isl1Cre reveals a common Bmp pathway in heart and limb development. *Development* **133,** 1575-1585.

Yashiro, K., Zhao, X., Uehara, M., Yamashita, K., Nishijima, M., Nishino, J., Saijoh, Y., Sakai, Y. and Hamada, H. (2004). Regulation of retinoic acid distribution is required for proximodistal patterning and outgrowth of the developing mouse limb. *Dev. Cell* **6,** 411-422.

Yu, L., Liu, H., Yan, M., Yang, J., Long, F., Muneoka, K. and Chen, Y. (2007). Shox2 is required for chondrocyte proliferation and maturation in proximal limb skeleton. *Dev. Biol.* **306,** 549-559.

Yu, P. B., Hong, C. C., Sachidanandan, C., Babitt, J. L., Deng, D. Y., Hoyng, S. A., Lin, H. Y., Bloch, K. D. and Peterson, R. T. (2008). Dorsomorphin inhibits BMP signals required for embryogenesis and iron metabolism. *Nat. Chem. Biol.* **4,** 33-41.

SUPPLEMENTAL FIGURES

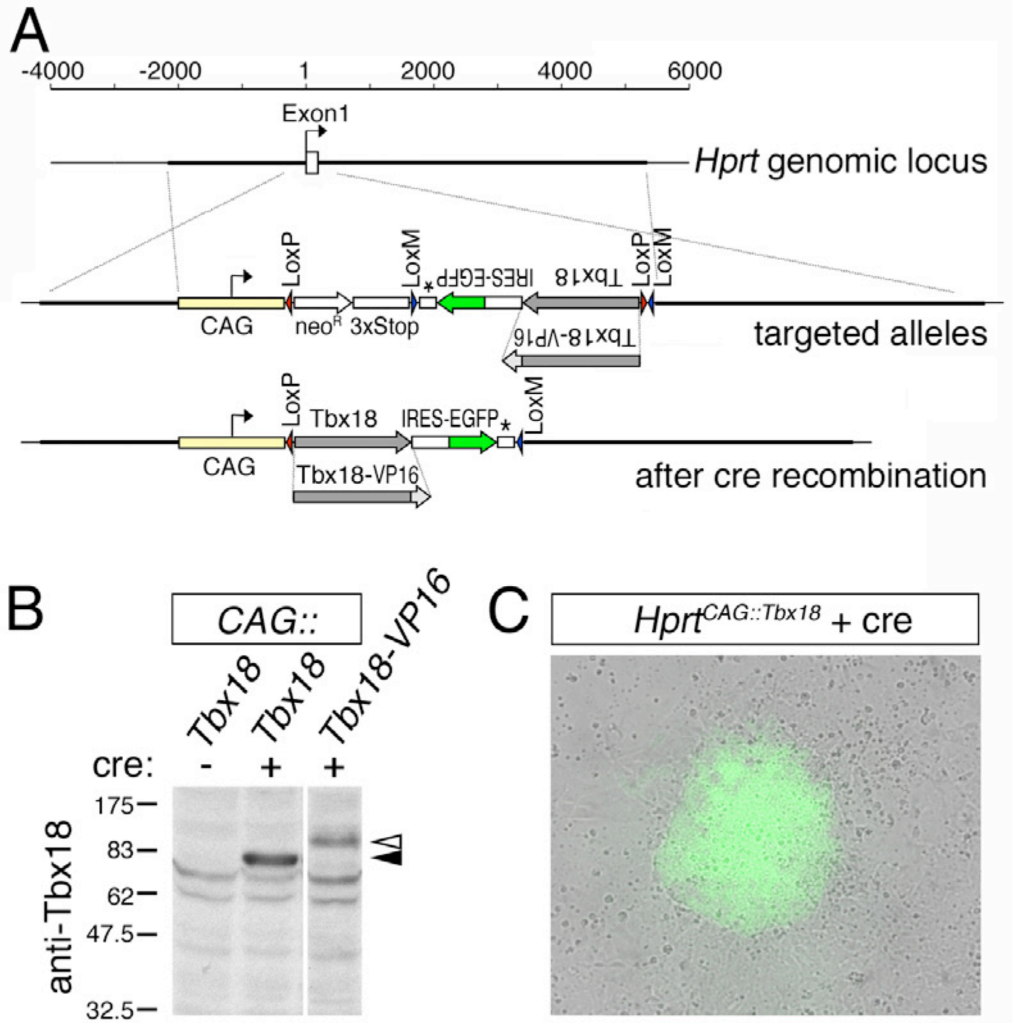
A
-4000
-2000
1
2000
4000
6000
Exon1
Hprt genomic locus
LoxP
LoxM
IRES-EGFP
Tbx18
LoxP
LoxM
CAG
neoR
3xStop
Tbx18-VP16
targeted alleles
LoxP
Tbx18
IRES-EGFP
LoxM
CAG
Tbx18-VP16
after cre recombination
B
CAG::
Tbx18
Tbx18
Tbx18-VP16
cre:
-
+
+
anti-Tbx18
175
83
62
47.5
32.5
C
HprtCAG::Tbx18 + cre

Supplemental Fig. 1. **Generation of $Hprt^{CAG::Tbx18}$ and $Hprt^{CAG::Tbx18\text{-}VP16}$ 'knock-in' alleles.**

A, targeting strategy depicting the *Hypoxanthine guanine phosphoribosyl transferase* (*Hprt*) genomic locus in the *wild type* (top), after homologous recombination in ES cells (middle) and after cre-mediated recombination (bottom), respectively The scale bar shows distances (in base pairs) relative to the *HPRT* transcription start site; homology regions included in the targeting vectors are labeled with thick lines; asterisks mark a SV40 polyadenylation signal. B, Test of protein expression from targeting vectors after cre-mediated recombination in HeLa cells. The circular targeting vectors were transfected either alone or in combination with a cre expression plasmid. Cell lysates were analyzed by Western blot using anti-Tbx18 antibody. Specific bands for Tbx18 (black arrowhead) and Tbx18-VP16 (white arrowhead) were detected only after co-transfection with cre-recombinase. Left, molecular weight standard in kilodaltons. C, inducibility of transgene expression was tested in the ES clones used for blastocyst injection. As an example the GFP-epifluorescence of a $Hprt^{CAG::Tbx18}$ ES clone is shown 6 days after electroporation of cre-recombinase expression plasmid. Image was merged to a brightfield image. Abbreviations are: 3xStop, tree successive polyadenylation sequences from the bovine growth hormone gene; CAG, CMV early enhancer/chicken β actin promoter; IRES, internal ribosomal entry site; neo^R, neomycin resistance.

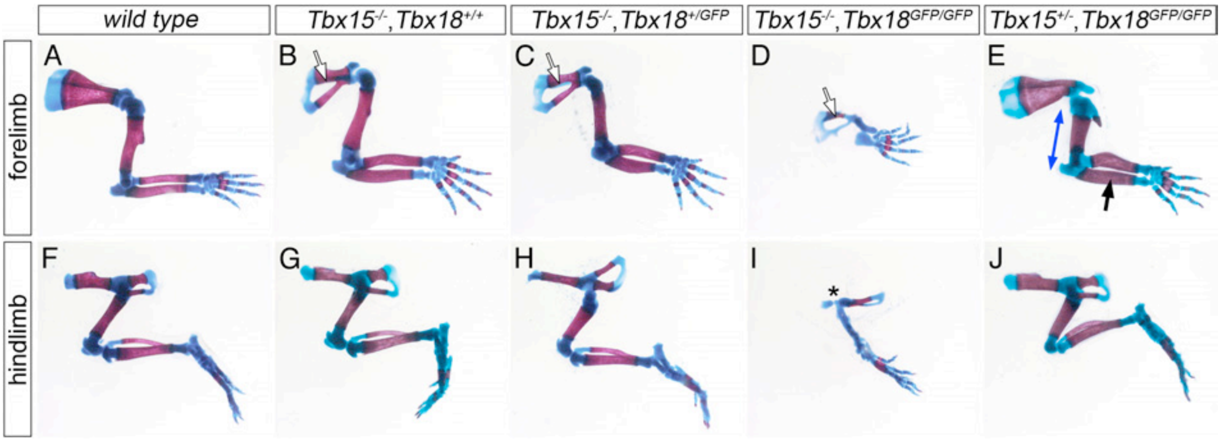
wild type
$Tbx15^{-/-}$,$Tbx18^{+/+}$
$Tbx15^{-/-}$,$Tbx18^{+/GFP}$
$Tbx15^{-/-}$,$Tbx18^{GFP/GFP}$
$Tbx15^{+/-}$,$Tbx18^{GFP/GFP}$
forelimb
hindlimb
A
B
C
D
E
F
G
H
I
*
J

Supplemental Fig. 2. **One functional copy of *Tbx15* or *Tbx18* is sufficient to allow the development of the proximal limb skeleton.**

Skeletal preparations of E18.5 fore- (A-E) and hindlimbs (F-J) in an allelic series of *Tbx15* and *Tbx18* compound mutant embryos. Genotypes are as indicated. A major reduction of the proximal limb skeleton (stylopod and zeugopod) is only observed after removal of all functional alleles of *Tbx15* and *Tbx18* (D and I). A mild reduction in the relative length of the stylopod and a thickening of the zeugopod is observed in *Tbx15*$^{+/-}$, *Tbx18*$^{GFP/GFP}$ forelimbs (E, blue and black arrow, respectively), whereas *Tbx15*$^{+/+}$, *Tbx18*$^{GFP/GFP}$ limbs appear phenotypically normal (not shown). Mice homozygous mutant for *Tbx15* feature a reduced scapula with a central hole in its blade (B, C, D, white arrows). Hypoplasia of the ilium is exclusively found in the *DM* (I, asterisk).

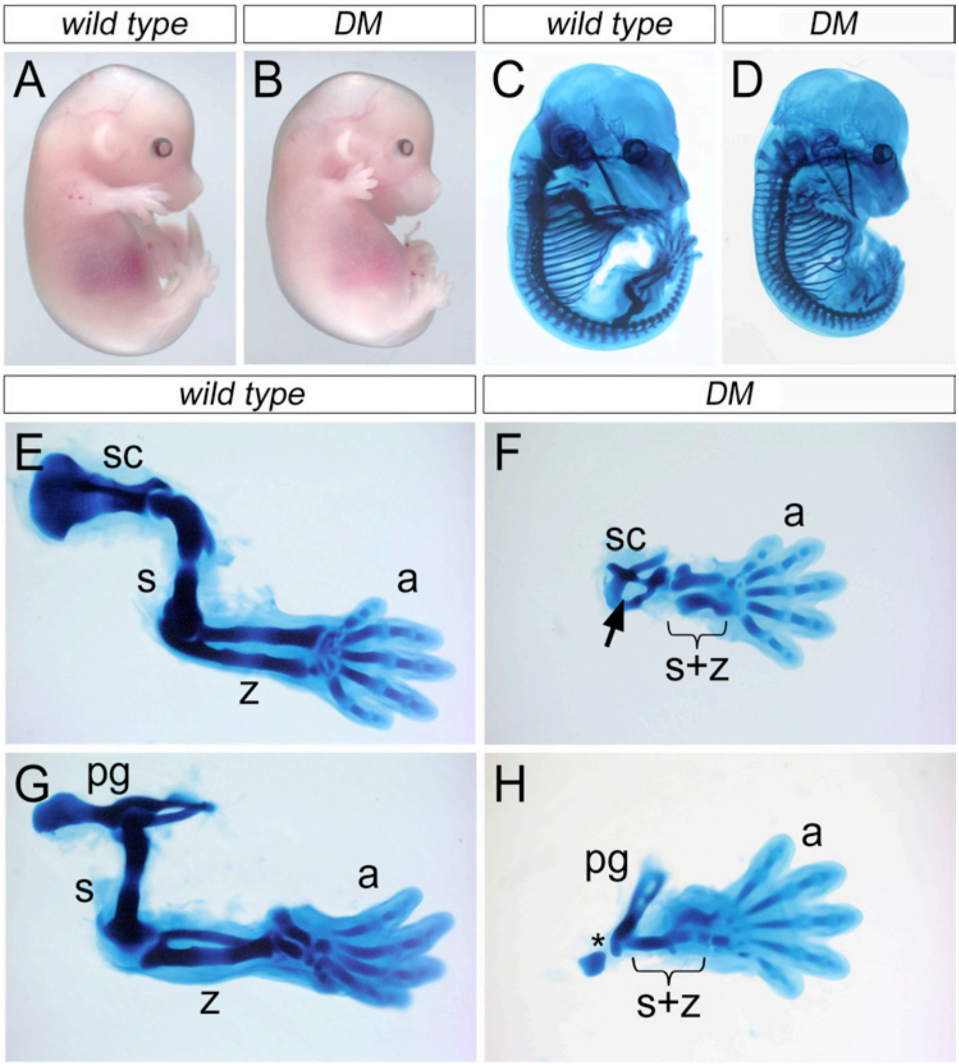
wild type
DM
wild type
DM
A
B
C
D
wild type
DM
E
sc
s
a
z
F
sc
a
s+z
G
pg
s
a
z
H
pg
a
*
s+z

Supplemental Fig. 3. **Skeletal phenotype of *Tbx18*/*Tbx15* double mutants at E14.5.**

Morphology (A, B) and skeletal preparations of E14.5 *wild type* and *Tbx15/Tbx18* double mutant embryos (C, D) and of forelimb (E, F) and hindlimb skeletons (G, H). Severe reduction of stylopod and zeugopod elements in the *DM* embryos; fusions between stylopod and zeugopod are indicated by brackets. Reduced size of pectoral and pelvic girdles of *DM* embryos; the central hole in the scapula (F, black arrow) and the hypoplastic ilium (H, asterisk) are marked. Abbreviations as in Figure 3.

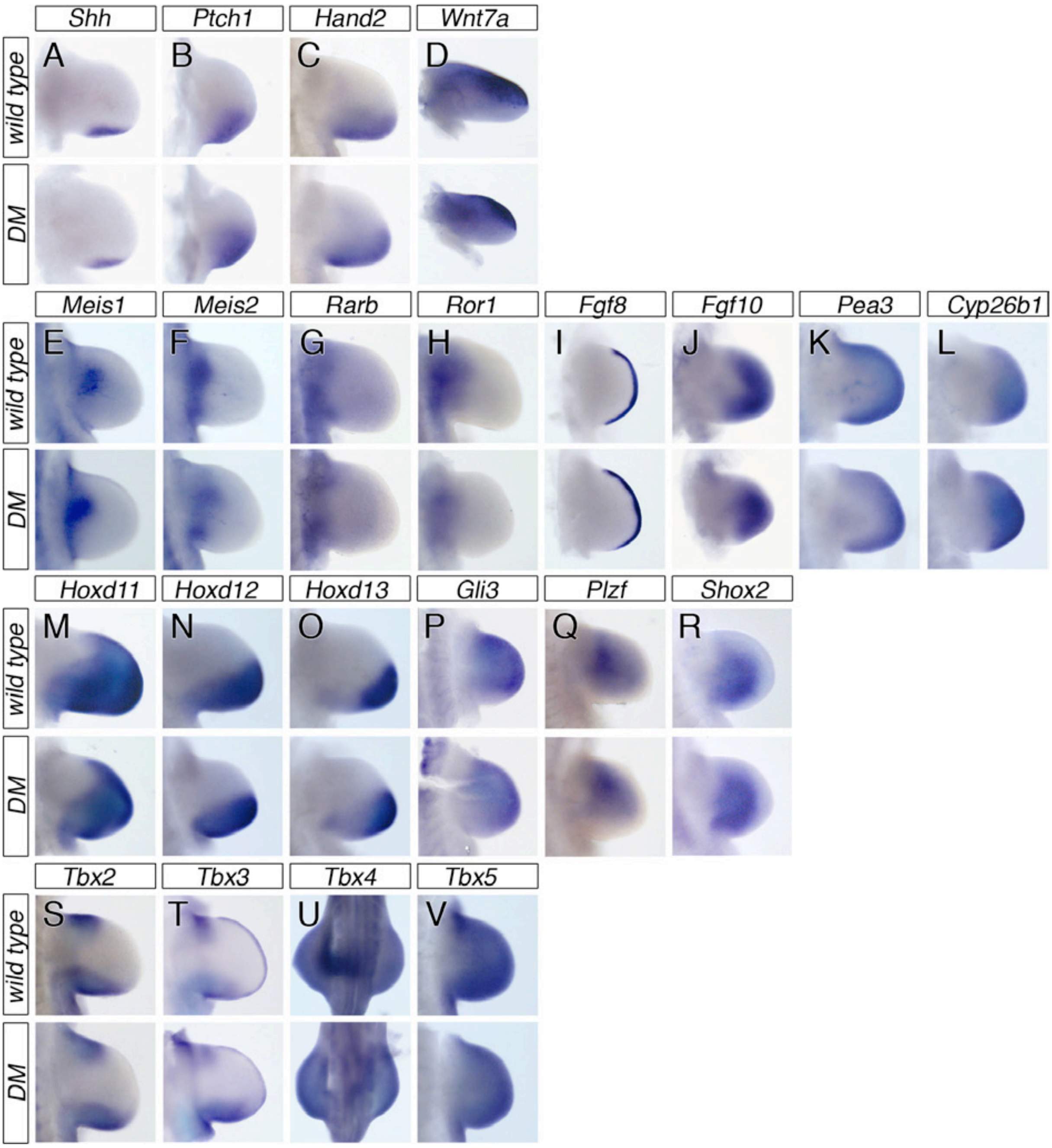
Shh
Ptch1
Hand2
Wnt7a
A
B
C
D
wild type
DM
Meis1
Meis2
Rarb
Ror1
Fgf8
Fgf10
Pea3
Cyp26b1
E
F
G
H
I
J
K
L
wild type
DM
Hoxd11
Hoxd12
Hoxd13
Gli3
Plzf
Shox2
M
N
O
P
Q
R
wild type
DM
Tbx2
Tbx3
Tbx4
Tbx5
S
T
U
V
wild type
DM

Supplemental Fig. 4. **Patterning of *Tbx18/Tbx15* double mutant limb buds is unaffected at E10.5.**

Whole mount *in situ* hybridization of E10.5 *wild type* and *DM* limb buds. All images show dorsal views of the forelimb, except D (lateral view) and U (hindlimbs). A-C, expression analysis of marker genes of anterior-posterior patterning using probes specific for *Shh* (A), *Ptch1* (B) and *Hand2* (C). Study of dorso-ventral patterning by expression analysis of *Wnt7a* (D). E-L, expression of marker genes of proximal-distal patterning using probes specific for *Meis1* (E), *Meis2* (F), *Rarb* (G), *Ror1* (H), and the distal marker genes *Fgf8* (I), *Fgf10* (J), *Pea3* (K), *Cyp26b1* (L). M-R, expression analysis of candidate transcription factors with a known function in proximal-distal limb patterning, *Hoxd11* (M), *Hoxd12* (N), *Hoxd13* (O), *Gli3* (P), *Plzf* (Q) and *Shox2* (R). S-V, the expression of other *T-box* genes involved in limb development is unchanged. Images show the expression of *Tbx2* (S), *Tbx3* (T), *Tbx4* (U) and *Tbx5* (V), respectively.

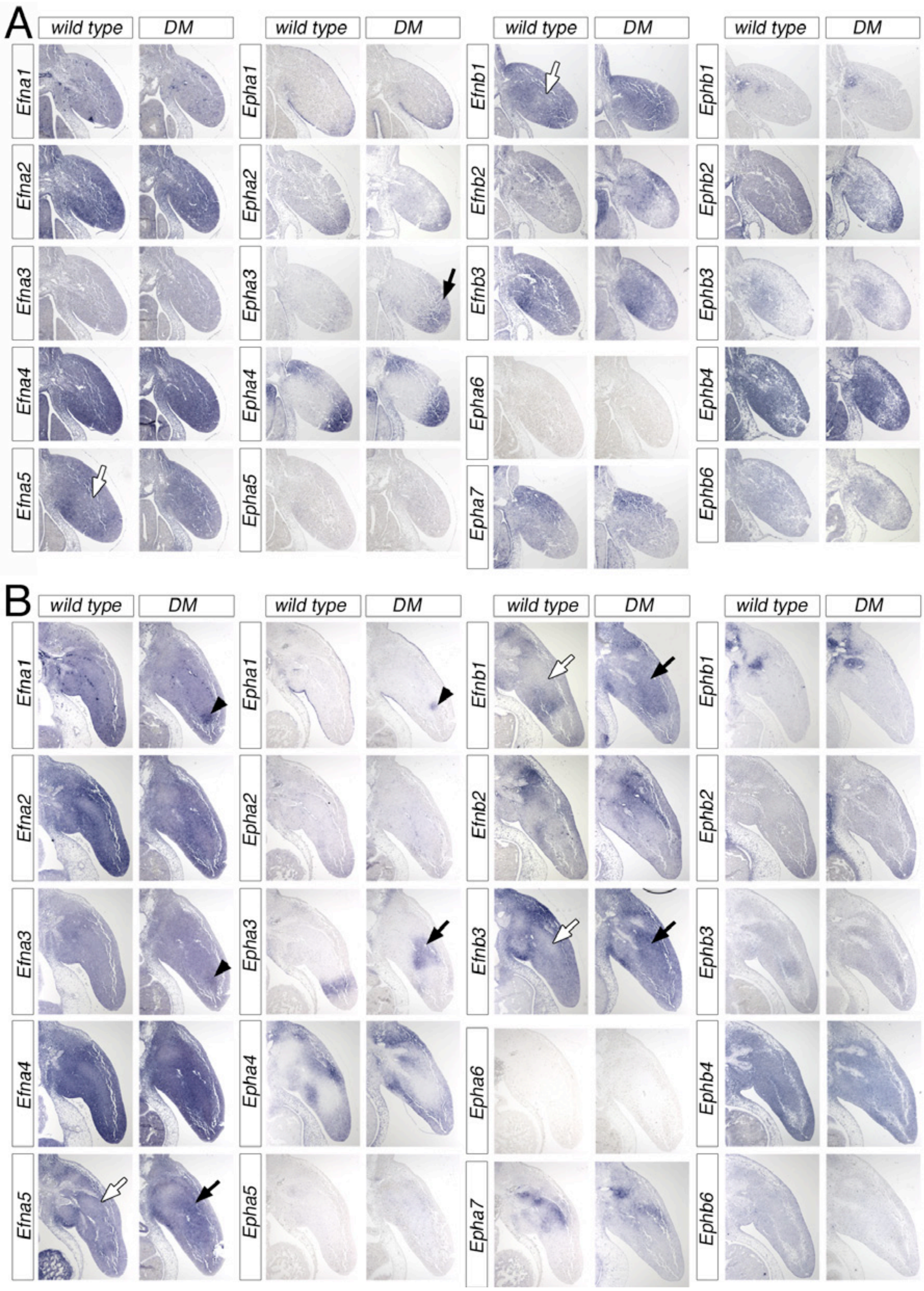
A
wild type
DM
wild type
DM
wild type
DM
wild type
DM
Efna1
Efna2
Efna3
Efna4
Efna5
Epha1
Epha2
Epha3
Epha4
Epha5
Efnb1
Efnb2
Efnb3
Epha6
Epha7
Ephb1
Ephb2
Ephb3
Ephb4
Ephb6
B
wild type
DM
wild type
DM
wild type
DM
wild type
DM
Efna1
Efna2
Efna3
Efna4
Efna5
Epha1
Epha2
Epha3
Epha4
Epha5
Efnb1
Efnb2
Efnb3
Epha6
Epha7
Ephb1
Ephb2
Ephb3
Ephb4
Ephb6

Supplemental Fig. 5. **Expression of *Eph/Ephrin* genes in *Tbx18/Tbx15 DM* limb buds.**

Section *in situ* hybridization on transverse forelimb sections of E10.5 (A) and E11.5 (B) embryos. The analysis includes all described *Eph*/*Ephrin* genes, except *Epha8* and *Epha1*, for which no probes could be generated. Images were grouped according to the family nomenclature; adjacent images compare the expression in the *wild type* and *DM* limb buds. White arrows were used to label domains where a lower expression was observed in the *wild type* compared to the *DM* limb sections. Black arrows indicate ectopic expression in the *DM*. The distal mesenchyme of E11.5 *DM* forelimbs additionally showed a small region of up-regulated *Efna1*, *Efna3* and *Epha1* expression (black arrowheads).

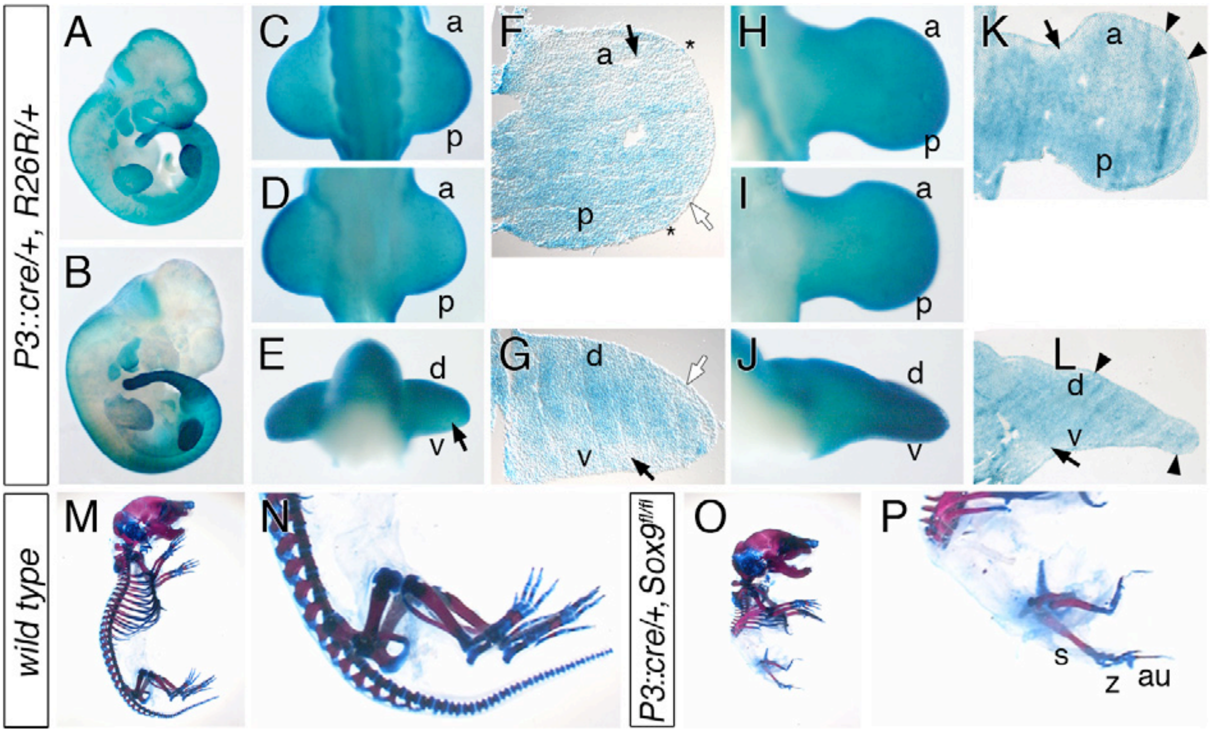

Supplemental Fig. 6. **Analysis of *Pax3::cre* mediated recombination in hindlimbs**.

β-galactosidase staining of *Pax3::cre*/+, *R26R*/+ embryos at E10.5 (A and C-G) and E12.0 (B and H-L) demonstrates an efficient recombination in the posterior trunk region including the hindlimbs. Shown are whole embryos (A, B) and hindlimbs in dorsal (C, H), ventral (D, I) and anterior (E, J) views. β-galactosidase staining on tangential (F, K) and transverse (G, L) cryosections shows a broad recombination pattern in the posterior (p) and dorsal (d) regions of the mesenchyme, while the signal is weaker in anterior (a) and ventral (v) regions (black arrows). The ectoderm is negative for β-galactosidase activity at E10.5 (white arrows, sporadic recombination is labeled by asterisks), but patches of ectodermal expression are evident at E12.0 (black arrowheads). M-P, skeletal preparations of E18.5 *wild type* (M, N) and *Pax3::cre*/+, *Sox9*$^{fl/fl}$ (O, P) embryos. The *Pax3::cre* mediated deletion of *Sox9* causes severe skeletal defects in the posterior body (O) and a strong reduction of all hindlimb elements (P). Abbreviations: au, autopod; s, stylopod; z, zeugopod.

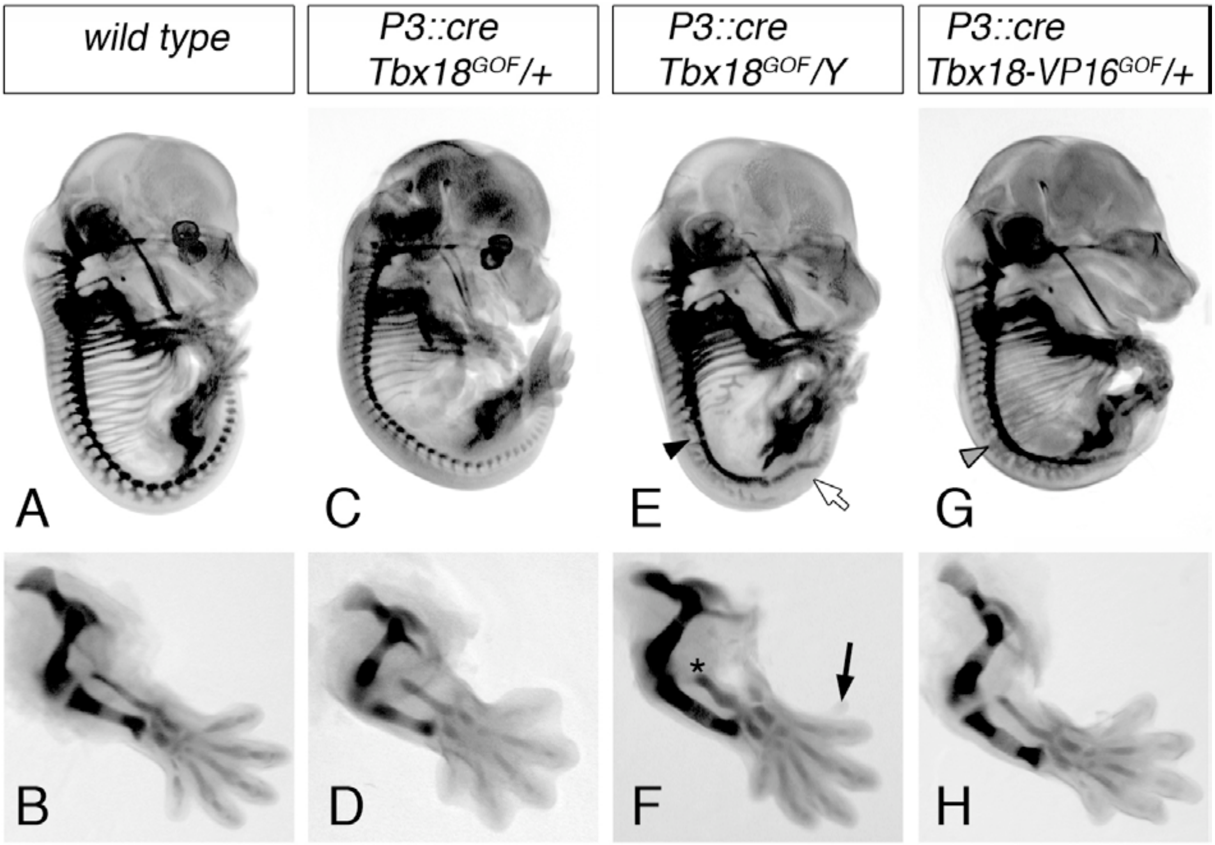

Supplemental Fig. 7. **Skeletal analysis of Tbx18 and Tbx18-VP16 misexpressing embryos at E14.5.**

Skeletal preparations of E14.5 *wild type* (A, B) and transgene expressing embryos (C-H); lower panels show details of the hindlimb skeleton. *P3::cre*, *Tbx18*^{GOF}/+ females have a normal axial and appendicular skeleton (C, D). In *P3::cre*, *Tbx18*^{GOF}*/Y* male embryos (E, F) a shortened tail (white arrow) and reduced pedicles (black arrowhead) are observed. Except slight reductions of fibula (asterisk) the hindlimb skeleton is relatively normal at this stage. The black arrow highlights an ectopic postaxial digit that lacks skeletal structures. Female *P3::cre*, *Tbx18-VP16*^{GOF}/+ embryos (G, H) have a normal hindlimb skeleton, but show irregular pedicles that are partly fused (grey arrowhead).

Concluding remarks

As a significant contribution to the functional understanding of Tbx15 and Tbx18, the present study demonstrates that both proteins have a role as transcriptional repressors (part 1 & 4 of this thesis) that may achieve target specificity by interaction with other classes of transcription factors (part 1 & 2). A cellular adhesion/migration mechanism was proposed that explains Tbx15/18 function during limb development (part 4). In a more general manner these findings may help to understand the role of T-box proteins in other developmental contexts but also their involvement in human pathologies (part 3).

Recruitment of groucho corepressors represents a novel mechanism how T-box proteins mediate transcriptional repression. The classical T-box repressors Tbx2 and Tbx3 were shown to directly associate with histone deacetylases (4), causing chromatin condensation and transcriptional silencing of target genes. In comparison, repression by Tbx15 and Tbx18 involves an additional step as the recruitment of histone deacetylases occurs indirectly via groucho proteins. This could explain the weaker repression activity of Tbx18 compared to Tbx2 (page 21, Fig. 7, F), but also implies that repression by Tbx15/18 could be subject to an additional level of regulation, by signaling pathways that control the activity of groucho proteins (34). In this context it is interesting to note that Ripply proteins have recently been identified as specific interaction partners of Tbx1 and Tbx6 that mediate an activator-to-repressor conversion (35 and Takada research communication). Ripply proteins themselves recruit groucho corepressors, demonstrating a third and even more indirect mode of transcriptional repression. Repression by T-box proteins thus appears to be graded and highly context dependent, which argues that the two proteins may exert additional molecular functions.

Future research avenues will require genome- and proteome-wide approaches to identify transcriptional targets and physiological binding partners of Tbx15 and Tbx18, respectively. ChIP-Chip and ChIP-Seq represent powerful techniques for genome-wide identification of transcriptional targets (36). However, their successful application strongly relies on the presence of suitable antibodies that are currently not available for Tbx18. To circumvent this problem another *Hprt-Tbx18* allele was generated that allows the conditional expression of epitope-tagged Tbx18 protein (unpublished). I employed the TAP (tandem affinity purification)-tag, which is a state of the art tool suited for the isolation of protein complexes under physiological conditions (37). Conditional expression of this construct, using a recently generated *Tbx18*^{cre} mouse line (38), should be highly suitable for the identification of target DNA-binding sites but also of protein interaction partners of Tbx18 *in vivo*.

Importantly, this study demonstrated that Tbx18 regulates cell-affinity properties in the proximal limb mesenchyme. Since analyses of other *Tbx18* phenotypes have pinpointed to a role in tissue compartmentalization (19-21; see introduction), regulation of cell adhesion/cell repulsion may represent a general theme of the cellular function of Tbx18. Future experiments shall, e.g. address if misexpression of Tbx18 in the entire metanephric field or the entire otic mesenchyme is sufficient to impose compartment-specific adhesion properties. Preliminary results indicate that the role of Tbx18 during somitogenesis indeed involves the regulation of cell adhesion. Homogenous misexpression of Tbx18 in entire somites (*P3::cre, Hprt::Tbx18*^{GOF}*/Y*) caused massive defects of the axial skeleton, whereas chimeric expression in female embryos did not interfere with normal development of the vertebral column (page 65, Fig. 7, F, J). In this mosaic condition, Tbx18-expressing cells preferentially localized to the anterior somite halves (unpublished data), indicative of a cellular sorting process. Similar to the situation during limb development, transgene expressing cells are thus recruited into the compartment of endogenous *Tbx18* expression, either by active migration or by a passive adhesion mechanism.

Regulation of cell adhesion and migration may represent a common developmental function of T-box proteins in mesenchymal tissues. Chimeric analyses have shown a role of Brachyury for migration of mesodermal cells through the primitive streak during gastrulation (39) and of Tbx6 for cell migration in the paraxial mesoderm (40). Loss-of-function studies in zebrafish embryos revealed a role for Tbx5 in the coherent movement of lateral plate mesenchymal cells into the prospective limb field, as a prerequisite for the initiation of forelimb bud formation (41). Finally, the sharp expression borders of many T-box genes (e.g. *Tbx2* and *Tbx3*; 42) are suggestive for functions in maintenance of compartment boundaries. Collectively, T-box genes may exert important roles in migration and/or adhesion of mesenchymal cells to achieve tissue complexity.

References

1. **Kispert, A. and Hermann, B. G.** (1993). The Brachyury gene encodes a novel DNA binding protein. *EMBO J.* **12,** 3211-3220.
2. **Kispert, A., Koschorz, B., Herrmann B. G.** (1995). The T protein encoded by Brachyury is a tissue-specific transcription factor. *EMBO J.* **14,** 4763-4772.
3. **Stennard, F. A., Costa, M. W., Elliott, D. A., Rankin, S., Haast, S. J., Lai, D., McDonald, L. P., Niederreither, K., Dolle, P., Bruneau, B. G., Zorn, A. M. and Harvey, R. P.** (2003). Cardiac T-box factor Tbx20 directly interacts with Nkx2-5, GATA4, and GATA5 in regulation of gene expression in the developing heart. *Dev. Biol.* **262,** 206-224.
4. **Vance, K. W., Carreira, S., Brosch, G. and Goding, C. R.** (2005). Tbx2 is overexpressed and plays an important role in maintaining proliferation and suppression of senescence in melanomas. *Cancer Res.* **65,** 2260-2268.
5. **Paxton, C., Zhao, H., Chin, Y., Langner, K. and Reecy, J.** (2002). Murine Tbx2 contains domains that activate and repress gene transcription. *Gene* **23,** 117-124.
6. **Agarwal, P., Wylie, J. N., Galceran, J., Arkhitko, O., Li, C., Deng, C., Grosschedl, R. and Bruneau, B. G.** (2003). Tbx5 is essential for forelimb bud initiation following patterning of the limb field in the mouse embryo. *Development* **130,** 623-633.
7. **Hofmann, M., Schuster-Gossler, K., Watabe-Rudolph, M., Aulehla, A., Herrmann, B. G. and Gossler, A.** (2004). WNT signaling, in synergy with T/TBX6, controls Notch signaling by regulating Dll1 expression in the presomitic mesoderm of mouse embryos. *Genes Dev.* **18,** 2712-2717.
8. **Yasuhiko, Y., Haraguchi, S., Kitajima, S., Takahashi, Y., Kanno, J. and Saga, Y.** (2006). Tbx6-mediated Notch signaling controls somite-specific Mesp2 expression. *Proc. Natl. Acad. Sci. U. S. A.* **103,** 3651-3656.
9. **Wittler, L., Shin, E. H., Grote, P., Kispert, A., Beckers, A., Gossler, A., Werber, M. and Herrmann, B. G.** (2007). Expression of Msgn1 in the presomitic mesoderm is controlled by synergism of WNT signalling and Tbx6. *EMBO Rep.* **8,** 784-789.
10. **Yasuhiko, Y., Kitajima, S., Takahashi, Y., Oginuma, M., Kagiwada, H., Kanno, J. and Saga, Y.** (2008). Functional importance of evolutionally conserved Tbx6 binding sites in the presomitic mesoderm-specific enhancer of Mesp2. *Development* **135,** 3511-3519.
11. **Hiroi, Y., Kudoh, S., Monzen, K., Ikeda, Y., Yazaki, Y., Nagai, R. and Komuro, I.** (2001). Tbx5 associates with Nkx2-5 and synergistically promotes cardiomyocyte differentiation. *Nat. Genet.* **28,** 276-280.
12. **Bruneau, B. G., Nemer, G., Schmitt, J. P., Charron, F., Robitaille, L., Caron, S., Conner, D. A., Gessler, M., Nemer, M., Seidman, C. E. and Seidman, J. G.** (2001). A murine model of Holt-Oram syndrome defines roles of the T-box transcription factor Tbx5 in cardiogenesis and disease. *Cell* **106,** 709-721.
13. **Habets, P. E., Moorman, A. F., Clout, D. E., van Roon, M. A., Lingbeek, M., van Lohuizen, M., Campione, M. and Christoffels, V. M.** (2002). Cooperative action of Tbx2 and Nkx2.5 inhibits ANF expression in the atrioventricular canal: implications for cardiac chamber formation. *Genes Dev.* **16,** 1234-1246.
14. **Garg, V., Kathiriya, I. S., Barnes, R., Schluterman, M. K., King, I. N., Butler, C. A., Rothrock, C. R., Eapen, R. S., Hirayama-Yamada, K., Joo, K., Matsuoka, R., Cohen, J. C. and Srivastava, D.** (2003). GATA4 mutations cause human congenital heart defects and reveal an interaction with TBX5. *Nature* **424,** 443-447.
15. **Nowotschin, S., Liao, J., Gage, P. J., Epstein, J. A., Campione, M. and Morrow, B. E.** (2006). Tbx1 affects asymmetric cardiac morphogenesis by regulating Pitx2 in the secondary heart field. *Development* **133,** 1565-1573.

16. **Naiche, L. A., Harrelson, Z., Kelly, R. G. and Papaioannou, V. E.** (2005). T-box genes in vertebrate development. *Annu. Rev. Genet.* **39,** 219-239.
17. **Packham, E. A. and Brook, J. D.** (2003). T-box genes in human disorders. *Hum. Mol. Genet.* **12,** R37-44.
18. **Kraus, F., Haenig, B. and Kispert, A.** (2001). Cloning and expression analysis of the mouse T-box gene Tbx18. *Mech. Dev.* **100,** 83-86.
19. **Airik, R., Bussen, M., Singh, M. K., Petry, M. and Kispert, A.** (2006). Tbx18 regulates the development of the ureteral mesenchyme. *J. Clin. Invest.* **116,** 663-674.
20. **Trowe, M. O., Maier, H., Schweizer, M. and Kispert, A.** (2008). Deafness in mice lacking the T-box transcription factor Tbx18 in otic fibrocytes. *Development* **135,** 1725-1734.
21. **Bussen, M., Petry, M., Schuster-Gossler, K., Leitges, M., Gossler, A. and Kispert, A.** (2004). The T-box transcription factor Tbx18 maintains the separation of anterior and posterior somite compartments. *Genes Dev.* **18,** 1209-1221.
22. **Barrantes, I. B., Elia, A. J., Wünsch, K., Hrabe de Angelis, M. H., Mak, T. W., Rossant, J., Conlon, R. A., Gossler, A. and de la Pompa, J. L.** (1999). Interaction between Notch signalling and Lunatic fringe during somite boundary formation in the mouse. *Curr. Biol.* **9,** 470-480.
23. **Morimoto, M., Takahashi, Y., Endo, M. and Saga, Y.** (2005). The Mesp2 transcription factor establishes segmental borders by suppressing Notch activity. *Nature* **435,** 354-359.
24. **Huang, R., Zhi, Q., Brand-Saberi, B. and Christ, B.** (2000). New experimental evidence for somite resegmentation. Anat. Embryol. (Berl) **202,** 195-200
25. **Neidhardt, L. M., Kispert, A., and Herrmann, B. G.** (1997). A mouse gene of the paired-related homeobox class expressed in the caudal somite compartment and in the developing vertebral collumn, kidney and nervous system. *Dev. Genes Evol.* **207,** 330 –339.
26. **Leitges, M., Neidhardt, L., Haenig, B., Herrmann, B. G. and Kispert, A.** (2000). The paired homeobox gene Uncx4.1 specifies pedicles, transverse processes and proximal ribs of the vertebral column. *Development* **127,** 2259-2267.
27. **Christoffels, V. M., Mommersteeg, M. T., Trowe, M. O., Prall, O. W., de Gier-de Vries, C., Soufan, A. T., Bussen, M., Schuster-Gossler, K., Harvey, R. P., Moorman, A. F. and Kispert, A.** (2006). Formation of the venous pole of the heart from an Nkx2-5-negative precursor population requires Tbx18. *Circ. Res.* **98,** 1555-1563.
28. **Agulnik, S. I., Papaioannou, V. E. and Silver, L. M.** (1998). Cloning, mapping, and expression analysis of TBX15, a new member of the T-Box gene family. *Genomics* **51,** 68-75.
29. **Singh, M. K., Petry, M., Haenig, B., Lescher, B., Leitges, M. and Kispert, A.** (2005). The T-box transcription factor Tbx15 is required for skeletal development. *Mech. Dev.* **122,** 131-144.
30. **Candille, S. I., Van Raamsdonk, C. D., Chen, C., Kuijper, S., Chen-Tsai, Y., Russ, A., Meijlink, F. and Barsh, G. S.** (2004). Dorsoventral patterning of the mouse coat by Tbx15. *PLoS Biol.* **2,** E3.
31. **Begemann, G., Gibert, Y., Meyer, A. and Ingham, P. W.** (2002). Cloning of zebrafish T-box genes tbx15 and tbx18 and their expression during embryonic development. *Mech. Dev.* **114,** 137-141.
32. **Beaster-Jones, L., Horton, A. C., Gibson-Brown, J. J., Holland, N. D. and Holland, L. Z.** (2006). The amphioxus T-box gene, AmphiTbx15/18/22, illuminates the origins of chordate segmentation. *Evol. Dev.* **8,** 119-129.
33. **Tanaka, M. and Tickle, C.** (2004). Tbx18 and boundary formation in chick somite and wing development. *Dev. Biol.* **268,** 470-480.
34. **Cinnamon, E. and Paroush, Z.** (2008). Context-dependent regulation of Groucho/TLE-mediated repression. *Curr. Opin. Genet. Dev.* **18,** 435-440.

35. **Kawamura, A., Koshida, S. and Takada, S.** (2008). Activator-to-repressor conversion of T-box transcription factors by the Ripply family of Groucho/TLE-associated mediators. *Mol. Cell Biol*. **28,** 3236-3244.
36. **Massie, C. E. and Mills, I. G.** (2008). ChIPping away at gene regulation. *EMBO Rep*. **9,** 337-343.
37. **Tsai, A. and Carstens, R. P.** (2006). An optimized protocol for protein purification in cultured mammalian cells using a tandem affinity purification approach. *Nat. Protoc.* **1,** 2820-2827.
38. **Wiese, C., Grieskamp, T., Airik, R., Mommersteeg, M. T. M., Gardiwal, A., de Gier-de Vries, C., Schuster-Gossler, K., Moorman, A. F. M., Kispert, A. and Christoffels V. M.** (2009). Formation of the sinus node head and differentiation of sinus node myocardium are independently regulated by Tbx18 and Tbx3. *Circ Res*. **104,** 388-397.
39. **Wilson, V., Rashbass, P. and Beddington, R. S.** (1993). Chimeric analysis of T (Brachyury) gene function. *Development* **117,** 1321-1331.
40. **Chapman, D. L., Cooper-Morgan, A., Harrelson, Z. and Papaioannou, V. E.** (2003). Critical role for Tbx6 in mesoderm specification in the mouse embryo. *Mech. Dev*. **120,** 837-847.
41. **Ahn, D. G., Kourakis, M. J., Rohde, L. A., Silver, L. M. and Ho, R. K.** (2002). T-box gene tbx5 is essential for formation of the pectoral limb bud. *Nature* **417,** 754-758.
42. **Chapman, D. L., Garvey, N., Hancock, S., Alexiou, M., Agulnik, S. I., Gibson-Brown, J. J., Cebra-Thomas, J., Bollag, R. J., Silver, L. M. and Papaioannou, V. E.** (1996). Expression of the T-box family genes, Tbxl-Tbx5, during early mouse development. *Dev. Dyn.* **206,** 379-390.

Acknowledgements

I would like to thank my supervisor Prof. Dr. Andreas Kispert for this fascinating project and the great opportunity to take part in his research group. I am thankful for his enthusiastic and constant support.

Thanks also to all other members of the lab and the IfM for discussions and fantastic teamwork. In particular I would like to thank Mark-Oliver Trowe und Rannar Airik, Ph.D. for accompanying my research project by sharing ideas and concepts.

Kindly acknowledged are Dr. Karin Schuster-Gossler (IfM, Hannover) for her enormous efforts in mouse transgenesis, Prof. Dr. Andrea Superti-Furga for offering collaboration and Prof. Dr. Ahmed Mansouri for providing the $Pax3^{lacZ}$ mice.

I would like to thank Ferenc Müller, Ph.D. (Karlsruhe, new address Birmingham) as well as Prof. Dr. Silke Sperling (Berlin), for the generous permission to conduct experiments in their laboratories.

And finally, I would like to thank Prof. Dr. Achim Gossler for facilitating the IfM as a great institution that allows students to start their work as independent scientists.

Curriculum vitae

Name:	Henner Friedhelm Farin
Date of birth:	26/09/1978
Place of birth:	Nordhorn
Citizenship:	German
Marital status:	single

Contact information:

Address:	Schneiderberg 29 30167 Hannover
Phone:	0511 3949688
Email:	farin.henner@mh-hannover.de; hfarin@gmx.de

School education:

1987 - 1990	Grundschule Waldschule (Nordhorn)
1990 - 1992	Orientierungsstufe Freiherr vom Stein (Nordhorn)
1992 - 1998	Gymnasium Nordhorn

Alternative civilian service:

1998 - 1999	Ambulatory geriatric care (Nordhorn)

University studies:

1999 - 2001	Undergraduate studies of Biology ("Vordiplom") at the University of Hannover.
2001 - 2002	"Licence de Biologie Cellulaire et Physiologie" at the University Paul Sabatier (Toulouse, France).
2002	Scholarship of the "Studienstiftung des Deutschen Volkes".
2002 - 2004	Graduate studies of Biology ("Diplom") at the University of Hannover.
2004 - 2005	Diploma thesis at the Institute for Molecular Biology, Hannover Medical School, under supervision of Prof. Dr. A. Kispert. Title of the diploma thesis: "Functional analysis of homeobox gene *Uncx4.1*"
2005 - 2008	Research assistant in the laboratory of Prof. Dr. A. Kispert at the Institute for Molecular Biology, Hannover Medical School. Dissertation with the title: "Function und regulation of the murine T-box genes *Tbx15* and *Tbx18*"

Declaration

"I hereby declare and confirm that this thesis is entirely the result of my own work except where otherwise indicated. This thesis has not been used as part of any other examination."

Henner Farin
Hannover, 10/07/2009

____
(Signature)